

THESIS FOR THE DEGREE OF DOCTOR OF PHILOSOPHY

Satellite-borne L-band Interferometric
Coherence for Forestry Applications in
the Boreal Zone

LEIF E. B. ERIKSSON

Faculty of Chemistry and Geosciences
Institute of Geography
Department of Geoinformatics and Remote Sensing
FRIEDRICH-SCHILLER-UNIVERSITY JENA
Jena, Germany 2004

Satellite-borne L-band Interferometric Coherence for Forestry Applications in the Boreal Zone

LEIF E.B. ERIKSSON

Faculty of Chemistry and Geosciences
Institute of Geography
Department of Geoinformatics and Remote Sensing
FRIEDRICH-SCHILLER-UNIVERSITY JENA
Jena, Germany

© LEIF E.B. ERIKSSON, 2004

Printed by Chalmers Reproservice
Göteborg, Sweden

Satellite-borne L-band interferometric coherence for forestry applications in the boreal zone

Dissertation

Zur Erlangung des akademischen Grades doctor rerum naturalium
(Dr. rer. nat.)

vorgelegt dem Rat der Chemisch-Geowissenschaftlichen Fakultät der
Friedrich-Schiller-Universität Jena

von Dipl.-Ing. Leif Eriksson
geboren am 11. Juni 1970 in Bolstad, Schweden

Gutachter:

1. Prof. Dr. C. Schullius, FSU Jena, Germany
2. Prof. Dr. J. Askne, Chalmers University of Technology, Sweden

Tag der öffentlichen Verteidigung: 14.07.2004

Satellite-borne L-band interferometric coherence
for forestry applications in the boreal zone

LEIF ERIKSSON

Institute of Geography, Department of Geoinformatics and Remote Sensing
Friedrich-Schiller-University Jena

Abstract

About one third of all forests in the world are found in the boreal zone. It has become increasingly important to have the possibility to map the extent and state of the forests, and to identify and monitor changes. One way to do this is to use satellite remote sensing. In this thesis the possibilities to use L-band interferometric coherence for forestry applications are evaluated. Repeat-pass coherence from the JERS-1 satellite has been used to study the forest in six test areas located on the Central Siberian Plateau in Russia. Five ERS-1/2 tandem pairs were included in the study to allow a comparison between L-band and C-band coherence.

Repeat-pass coherence is influenced by differences between the acquisitions. Based on the available meteorological information it was found that freeze and thaw cause strong decorrelation and the corresponding coherence was not suitable for forestry applications. The largest contrast in coherence between sparse and dense forest was observed when both acquisitions were done under frozen winter conditions. No image pairs from dry unfrozen conditions were available. Coherence from winter images with up to two years between the acquisitions still allowed separation between sparse and dense forest. No clear correlation could be identified between perpendicular baseline and coherence. Under frozen conditions, baselines up to 2 km were found to give high coherence for sparse forest.

To investigate if L-band repeat-pass coherence can be used for retrieval of forest parameters, a study on growing stock volume estimation was conducted. An exponential regression model was used to describe the relationship between the coherence and growing stock volume. Compared with the Russian forest inventory data, the estimated growing stock volumes in most cases showed RMS errors in the range 60 to 100 m³/ha. The same model was used for growing stock volume retrieval from ERS-1/2 tandem coherence. The obtained retrieval accuracy for JERS-1 coherence was in some cases even higher than for the ERS-1/2 coherence. This indicates that under frozen winter conditions L-band repeat-pass coherence can be an alternative to C-band coherence for growing stock volume retrieval.

Two applications were selected for evaluation of the potential of JERS-1 repeat-pass coherence for forest mapping and forest monitoring. To test the mapping potential a simple growing stock volume classification was done. The results show high classification accuracy for the class with growing stock volumes above 80 m³/ha, but an overestimation of the growing stock volume for sparse forest. The possibility to detect clear-cutting was demonstrated with a time series of JERS-1 and ERS-1/2 coherence images.

Keywords: SAR, boreal forest, JERS, ERS, interferometry, coherence, growing stock volume, change detection.

Zusammenfassung

Die in dieser Doktorarbeit vorgestellte Arbeit konzentriert sich auf den Wald der Borealen Zone. Der Boreale Wald ist die nördlichste Waldzone der Erde und umfasst den ganzen Globus. Etwa 33 % aller Waldgebiete befinden sich in dieser Zone. Jedes Jahr sind große Waldgebiete durch Schäden natürlichen oder anthropogenen Ursprungs betroffen. Die Möglichkeit, Ausdehnung und Zustand von Wäldern zu kartieren sowie Veränderungen zu erfassen, gewinnt zunehmend an Bedeutung. In der gesamten Borealen Zone ist der Wald eine der größten natürlichen Ressourcen und Quelle von Einkommen, was ihn auf regionaler und nationaler Ebene bedeutsam macht. Ein Wald kann sowohl als Quelle als auch als Senke von Kohlenstoffdioxid dienen, und enorme Mengen Kohlenstoff sind in über- und unterirdischer Biomasse gespeichert. Boreale Wälder sind deshalb für die „United Nations Framework Convention on Climate Change“ (UNFCCC) und Kyoto-Protokoll von Bedeutung. Darüber hinaus ist das Ökosystem des Borealen Waldes der einzige natürliche Lebensraum für viele Pflanzen und Tiere. Klimaveränderungen und starke Zerstörungen können zu einem Aussterben von seltenen Arten führen. Die Erhaltung der biologischen Vielfalt wird durch die „United Nations Convention on Biological Diversity“ thematisiert.

Für forstwirtschaftliche Anwendungen hat Fernerkundung den Vorteil, dass große Gebiete preiswert, verglichen mit konventionellen Feldstudien, abgedeckt werden können. Satelliten-getragenes Radar hat nicht die hohe räumliche Auflösung vieler optischer Satellitensensoren, aber Radar ist in der Lage, Bilder unabhängig von Bewölkungsgrad und Sonneneinstrahlung aufzunehmen. Es führt daher zu einer höheren Wahrscheinlichkeit, Informationen regelmäßig bereitzustellen. Viele Arbeiten haben gezeigt, dass Synthetic Aperture Radar (SAR) des Japanese Earth Resources Satellite (JERS-1) und der beiden European Remote sensing Satellites (ERS-1 und ERS-2) Informationen über den Wald liefern können. Für den Borealen Wald wurden die L-Band-Rückstreuung des JERS-1 und die interferometrische Kohärenz des ERS-1/2 (C-Band) für die Bestimmung des Stammvolumen benutzt. Bisher wurden nur wenige Arbeiten veröffentlicht, die interferometrische Kohärenz aus Satelliten-getragendem L-Band SAR mit Wald verknüpfen. Diese Doktorarbeit versucht, einige der offenen Fragen bezüglich Charakteristik und Anwendbarkeit von L-Band Kohärenz für forstwirtschaftliche Anwendungen zu beantworten. Dazu wurden 19 JERS-1 Bildpaare analysiert, die Sibirischen Wald abdecken.

Auf der Grundlage der Verfügbarkeit von Bodendaten, Satellitendaten und meteorologischen Daten wurden sechs Testgebiete ausgewählt. Sie befinden sich innerhalb der Bolshe Murtinsky und Chunsky Waldgebiete auf dem

Zentralsibirischen Plateau. Bolshe Murtinsky befindet sich beiderseits des Jenissej, etwa 90 km nördlich von Krasnojarsk, der Hauptstadt der Verwaltungseinheit Krasnojarsk Krai. Drei Testgebiete liegen innerhalb Bolshe Murtinsky. Die verbleibenden drei Testgebiete gehören zum Chunsky, welches sich circa 280 km nordöstlich von Krasnojarsk und südlich des Flusses Angara befindet. Jedes Testgebiet umfasst 200 bis 400 km² und beinhaltet 500 bis 1300 Waldbestände. Die durchschnittliche Bestandsgröße der ausgewählten Testgebiete schwankt zwischen 22 und 48 ha. Dominierende Arten sind Tanne (*Abies sibirica*), Fichte (*Picea sibirica*), sibirische Kiefer (*Pinus sibirica*), Kiefer (*Pinus sylvestris*), Lärche (*Larix dahurica* and *Larix sibirica*), Birke (*Betula pendula*), und Espe (*Populus tremula*). Prinzipiell sind die meisten Waldbestände gemischte Wälder natürlichen Ursprungs.

Informationen über Fläche, Land-Kategorie, Stammvolumen, Alter, Höhe, Durchmesser und Zusammensetzung standen für jeden Waldbestand zur Verfügung. Von diesen konnten nur Fläche, Land-Kategorie, Stammvolumen und Zusammensetzung für die Auswertung benutzt werden. Zusätzlich zu den Forstdaten waren topographische Karten mit Maßstab 1:200000 verfügbar, und Digitale Höhenmodelle wurden aus interferometrischen ERS-1/2-SAR Daten gewonnen. Meteorologische Daten einzelner Wetterstationen wurden durch die World Meteorological Organization bereitgestellt. Diese beinhalten Lufttemperatur, Windgeschwindigkeit, Niederschlag, Schneehöhe, Taupunkt und Bewölkungsgrad. Mindestens vier Beobachtungen pro Tag wurden angegeben.

Zur Auswertung standen JERS-1 Daten des Zeitraums 1993-1998 zur Verfügung. Für den westlichen Teil von Bolshe Murtinsky, der zwei Testgebiete beinhaltet, war eine Zeitreihe mit fünf aufeinander folgenden Akquisitionen von Oktober 1996 bis April 1997 verfügbar, und für das östlichste Testgebiet innerhalb des selben Waldgebiets fünf aufeinander folgende Akquisitionen von Februar 1997 bis August 1997. Für die beiden Testgebiete in Nord-Chunsky lagen alle vier Akquisitionen zwischen Oktober 1995 und Februar 1996 vor und für das restliche Testgebiet drei Akquisitionen innerhalb des selben Zeitraums. Alle diese Zeitreihen bieten Möglichkeiten, Bildpaare mit lediglich 44 Tagen Zeitdifferenz zwischen den Akquisitionen zu bilden. Der Hauptteil der Auswertung beruht auf der Kohärenz solcher 44-Tage-Paare. Zwei ERS-1/2 Paare von Bolshe Murtinsky und drei von Chunsky wurden in die Arbeit zusätzlich eingefügt, um einen Vergleich zwischen L-Band und C-Band Kohärenz zu erlauben. Alle Bilder stammen aus den Jahren 1996 bis 1998, als die beiden ERS-Satelliten in einer Tandem-Mission flogen. Lediglich ein Tag liegt zwischen den Akquisitionen dieser Paare.

Die Kohärenz ist ein Maß für den Grad der Korrelation zweier Bilder. Ihre Werte liegen zwischen null und eins. Es gibt verschiedene mögliche Gründe für eine Reduzierung der Kohärenz. Einige dieser können vernachlässigt werden, oder ihr Einfluss ist abschätzbar und kann berücksichtigt werden. Nachdem diese beseitigt wurden, bleiben zwei Hauptgründe für Dekorrelation übrig: die zeitliche oder die Volumendekorrelation. Die zeitliche Dekorrelation ist auf Änderungen der Eigenschaften oder Lage der beobachteten Objekte zwischen den Aufnahmezeitpunkten zurückzuführen. Volumendekorrelation tritt auf, wenn das Signal in einem Volumen gestreut wird, z. B. innerhalb von Baumkronen oder Schneeschicht.

Der erste Teil der Auswertung konzentriert sich darauf, die Hauptgründe für eine Dekorrelation der verfügbaren JERS-1 Kohärenz zu finden. Der Einfluss von verschiedenen Umweltbedingungen zu oder zwischen den Aufnahmen wurde mit Hilfe von meteorologischen Daten studiert. Es stellte sich heraus, dass Gefrier- und Tauprozesse eine Dekorrelation stark bedingen. Diese Reduktion der Kohärenz ist wahrscheinlich ein gemeinsames Ergebnis einer veränderten dielektrischen Konstante und dem Auftreten oder Verschwinden einer Schneeschicht. Wenn man den eingeschränkten Einfluss der Schneeschicht auf L-Band-Signale berücksichtigt, kann die Änderung der dielektrischen Konstante als der Hauptgrund für die Dekorrelation angenommen werden. Regen verursachte auch Dekorrelation, aber für die verfügbaren Bildpaare war sein Einfluss auf die Kohärenz nicht so stark wie Tau- oder Gefrierprozesse. Die höchste Kohärenz wurde bei lichtem Wald erreicht wenn beide Akquisitionen bei gefrorenen Winterbedingungen statt fanden. Diese Bedingungen ergaben außerdem den größten Kohärenz-Unterschied zwischen lichtem und dichtem Wald. Schneefall schien die Kohärenz im Winter nicht zu beeinflussen. Aufgrund von ungenauen Messungen konnten keine Rückschlüsse auf den Einfluss von Wind gemacht werden.

Eine Anzahl an Bildpaaren mit mehr als 44 Tagen Differenz zwischen den Aufnahmen wurde ausgesucht, um zu untersuchen, wie die Kohärenz von der Zeitdifferenz zwischen den Akquisitionen abhängt. Der Evaluierung von Umwelteinflüssen folgend, wurden nur Winterpaare berücksichtigt. Die zur Verfügung stehenden Daten erlaubten die Bildung von Paaren mit einer Zeitdifferenz von 88 Tagen sowie zwei und drei Jahren. Die Auswertung zeigte, dass bei günstigen Bedingungen die 88-Tage-Kohärenz lichten Waldes bis zu 0.5 ergeben kann, was im oberen Bereich der 44-Tage-Kohärenz liegt. Bei Bildern, die mehr als ein Jahr auseinander lagen, war die Kohärenz wesentlich niedriger, aber in einigen Testgebieten zeigte sie die Möglichkeit, lichten und dichten Wald zu unterscheiden.

Bei aufeinander folgenden Aufnahmen sind die Positionen der SAR-Antenne nicht exakt gleich. Die Entfernung zwischen diesen Positionen nennt man räumliche Basislinie. Diese Basislinie kann in Komponenten, die parallel und senkrecht zur Beobachtungsrichtung sind, aufgeteilt werden. Bei Erhöhung der senkrechten Basislinie wird eine Länge erreicht, ab der vollständige Dekorrelation auftritt. Diese Länge wird kritische Basislinie bezeichnet. Für JERS-1 liegt die kritische Basislinie bei etwa 5700 m. Nur ein Paar hatte eine senkrechte Basislinie, die diesen Wert überstieg. Mit Hilfe der verfügbaren Daten konnte keine klare Korrelation zwischen senkrechter Basislinie und Kohärenz gefunden werden. Dichter Wald zeigt eine geringe Tendenz zu höherer Kohärenz für Basislinien kleiner als 500 m. Basislinien bis zu 2 km ergaben hohe Kohärenz für lichten Wald.

Der Vergleich mit Tandem-Kohärenz von ERS-1/2 machte deutlich, dass die aus JERS-1 ermittelte Winter-Kohärenz Niveaus erreicht, die mit denen aus ERS-1/2 Akquisitionen bei ungefrorenen Bedingungen vergleichbar sind, obwohl die Wiederholrate von JERS-1 beträchtlich länger ist. ERS-1/2 Kohärenz zeigte im Winter höhere Kohärenz.

Das Ziel im zweiten Teil der Arbeit bestand darin, zu ermitteln, ob JERS-1 Kohärenz für die Bestimmung von Waldparametern benutzt werden kann. Eines der bedeutendsten Waldparameter ist Biomasse. Eine Möglichkeit, die überirdische Biomasse zu quantifizieren, stellt die Bestimmung von Stammvolumen dar, das pro

Flächeneinheit definiert ist. Die Evaluierung wurde deshalb auf die Bestimmung von Stammvolumen konzentriert. Der Erfassungsprozess kann in vier Schritte unterteilt werden: Auswahl des Modells, Modelltraining, Erfassung und Fehleranalyse. Aufgrund der Ergebnisse der Auswertung der zeitlichen Dekorrelation wurde nur 44-Tage-Kohärenz aus der Wintersaison berücksichtigt.

In einem ersten Schritt wurde die Korrelation zwischen Kohärenz und Stammvolumen getestet. Für Winterpaare lag der Pearson-Koeffizient zwischen -0.60 und -0.87 . Er war bei der Hälfte dieser Fälle kleiner als -0.8 . Das beweist, dass es eine Korrelation zwischen JERS-1 repeat-pass Kohärenz und Stammvolumen gibt. Ein exponentielles Modell wurde ausgewählt, um die Beziehung zu beschreiben. Nach dem Training des Modells durch Kurvenanpassung wurden die Regressionskurven mit Testreihen verglichen, und in allen Fällen ergab sich, dass die Kurven in guter Übereinstimmung mit den Testdaten waren.

Als Indikatoren für die Genauigkeit der Bestimmung wurden die mittlere quadratische Abweichung (Root Mean Square Error, RMSE), die relative RMSE und das Bestimmtheitsmaß (R^2) gewählt. Als kleinste mittlere quadratische Abweichung wurde $60 \text{ m}^3/\text{ha}$ erhalten, und in den meisten Fällen lag RMSE unter $100 \text{ m}^3/\text{ha}$. Abgesehen von einer Ausnahme lag die relative RMSE zwischen 43 und 76% . R^2 zeigte starke Schwankungen, zum Teil wegen der Verteilung von Stammvolumen innerhalb der jeweiligen Testgebiete. Der höchste Wert für R^2 war 0.75 .

Das gleiche Modell wurde für die Stammvolumenbestimmung aus ERS-1/2 Tandem-Kohärenz benutzt. Die am besten ermittelten Werte für RMSE, relative RMSE und R^2 waren jeweils $57 \text{ m}^3/\text{ha}$, 37% und 0.73 . Dennoch lag RMSE für über 70% der betrachteten Bildpaare über $100 \text{ m}^3/\text{ha}$. Die Ergebnisse sind weit entfernt von den besten, die andere Autoren für Testgebiete in Nordeuropa veröffentlichten. Das könnte sowohl durch die unterschiedliche Struktur der Wälder mit höherem Anteil an gemischten, unbewirtschafteten Wäldern in Sibirien, als auch durch größere Ungenauigkeit der Bodendaten erklärt werden. Die erhaltene Genauigkeit der Stammvolumenbestimmung aus JERS-1 Kohärenz ist in vielen Fällen so gut oder besser als die aus ERS-1/2 Kohärenz. Das deutet darauf hin, dass unter gefrorenen Winterbedingungen L-Band Kohärenz eine Alternative zu C-Band Kohärenz für die Bestimmung von Stammvolumen sein kann.

Der letzte Teil der Arbeit verfolgt das Ziel, potentielle forstwirtschaftlichen Anwendungen der JERS-1 Kohärenz zu evaluieren. Zwei Anwendungen wurden für die Evaluierung ausgewählt, die Kartierung und Überwachung von Wald repräsentieren. Eine einfache Klassifikation von Stammvolumen wurde gewählt, um das Potenzial der Kartierung zu überprüfen. Für die Klassifikation wurde eine Methode benutzt, die ein Kohärenz- und ein Rückstreubild benötigt. Die Methode basiert auf einem Modell, dessen Parameter an den Informationsgehalt in den Bildern angepasst sind. Das begrenzt die Anforderung an Trainingsdaten. Die Methode wurde im Projekt SAR Imaging for Boreal Ecology and Radar Interferometry Applications (SIBERIA) für ERS-1/2 Tandem-Kohärenz- und JERS-Rückstreubilder entwickelt und erfolgreich angewendet. Die ERS-1/2 Kohärenz wurde in dieser Doktorarbeit durch JERS-1 Kohärenz ersetzt, um eine Klassifikation zu erhalten, die allein auf L-Band Daten basiert. Die Ergebnisse zeigen eine hohe Genauigkeit der Klasse mit Stammvolumen oberhalb von $80 \text{ m}^3/\text{ha}$, aber mit der derzeitigen Modellversion wird Stammvolumen von lichtigem und jungem Wald

überschätzt. Es wurden Hinweise für Verbesserungen der Methoden gegeben, aber in ihrer jetzigen Form können sie bereits für eine Wald-/Nichtwaldkartierung verwendet werden.

Als ein Beispiel des Waldmonitoring mit JERS-1 Kohärenz wurde eine einfache Methode für „change detection“ überprüft. Indem man Grenzwerte für Histogramme auf eine Zeitreihe von mindestens zwei Kohärenzbildern anwendet, ist es möglich, größere Änderungen wie Kahlschläge zu identifizieren, wenn diese Ereignisse in der Zeitspanne zwischen den Aufnahmen eintreten. Kleinere Änderungen, wie z. B. punktuelle Rodung oder Ausdünnung, können nur durch verfeinerte Methoden erkannt werden. Die Möglichkeit der Kombination von L-Band und C-Band Kohärenz wurde durch Zeitreihen von Kohärenzbildern von JERS-1 (1994 und 1996) und ERS-1/2 (1996 und 1997) demonstriert.

Die vorgestellten Ergebnisse zeigen, dass solange Aufnahmen unter gefrorenen Bedingungen gemacht werden, Satelliten-getragene L-Band Kohärenz Informationen für forstwirtschaftliche Anwendungen liefern kann. Alle Methoden, die für Bestimmung, Kartierung und Monitoring von Waldparametern vorgestellt wurden, können weiter verbessert werden, und mehr Untersuchungen sind notwendig, um zu entscheiden, ob die Genauigkeit für operationelle Anwendungen hoch genug sein kann. Das PALSAR Instrument an Bord des Japanese Advanced Land Observing Satellite (ALOS), der voraussichtlich in der zweiten Hälfte des Jahres 2005 gestartet werden soll, wird die Möglichkeit hinzufügen, Multi-Polarisationen zu verwenden. Mit einer kürzeren Bildwiederholrate, wie z. B. 14 Tage des vorgeschlagenen TerraSAR-L Satelliten, wird die Möglichkeit, Bildpaare mit höherer Kohärenz zu erhalten, beträchtlich erhöht.

Table of contents

Abstract	i
Zusammenfassung	iii
Table of contents	ix
Acronyms.....	xiii
Units	xiv
Symbols.....	xv
Chapter 1	1
Introduction.....	1
1.1 Boreal forest.....	1
1.2 The JERS-1 and ERS-1/2 missions.....	2
1.3 Radar remote sensing of forest.....	3
1.4 Scope of the thesis.....	4
1.5 Outline of the thesis	5
Chapter 2	7
SAR and InSAR theory	7
2.1 SAR system overview.....	7
2.2 Radar scattering.....	8
2.2.1 Scattering mechanisms.....	9
2.2.2 Scattering from forest.....	10
2.2.3 Scattering from snow	11
2.3 SAR interferometry.....	12
2.3.1 InSAR baselines.....	12
2.3.2 Coherence and interferometric phase.....	13
2.3.3 Spatial decorrelation.....	15
2.3.4 Temporal decorrelation	16

2.4	InSAR processing.....	18
2.4.1	Pre-processing.....	18
2.4.2	Coherence estimation.....	19
2.4.3	Post-processing.....	19
Chapter 3.....		21
Test sites and data		21
3.1	Test sites.....	21
3.1.1	Bolshe Murtinsky.....	21
3.1.2	Chunsky.....	22
3.2	Ground data.....	26
3.2.1	Russian forest inventory.....	26
3.2.2	Forest GIS parameters.....	26
3.2.3	Digital elevation models and topographic maps.....	27
3.3	Satellite image data.....	28
3.3.1	Bolshe Murtinsky.....	30
3.3.2	Chunsky.....	30
3.4	Meteorological data.....	30
3.4.1	Bolshe Murtinsky.....	31
3.4.2	Chunsky.....	31
Chapter 4.....		35
Decorrelation analysis		35
4.1	Environmental conditions.....	35
4.1.1	Temperature.....	35
4.1.2	Precipitation and moisture.....	38
4.1.3	Snow cover.....	39
4.1.4	Wind.....	40
4.1.5	Seasonal variations.....	41
4.1.6	Interannual consistency.....	44
4.2	Temporal baseline.....	45
4.2.1	Anthropogenic and natural forest change.....	45
4.2.2	Multiple repeat-cycles.....	46
4.3	Volume decorrelation.....	47
4.4	Comparison with C-band.....	49
4.5	Conclusions.....	53

Chapter 5	55
Forest parameter retrieval	55
5.1 Growing stock volume retrieval	55
5.1.1 Model selection	56
5.1.2 Model training	58
5.1.3 Retrieval method	61
5.1.4 Retrieval results	61
5.2 Comparison with C-band	64
5.3 Conclusions	68
Chapter 6	69
Forest mapping and monitoring	69
6.1 Growing stock volume mapping	69
6.2 Change detection	73
6.3 Conclusions	74
Chapter 7	75
Conclusions	75
7.1 Summary of results	75
7.2 Discussion	76
7.3 Future outlook	77
Chapter 8	79
Acknowledgements	79
References	83
Appendix A	A1
Table of space-borne L-band SAR sensors	A1
Appendix B	B1
Results from the model fitting and growing stock volume retrieval	B1

Acronyms

ALOS	Advanced Land Observing Satellite
AMI	Active Microwave Instrument (on ERS)
ASAR	Advanced Synthetic Aperture Radar
BMBF	Bundesministeriums für Bildung und Forschung (German Ministry for Education and Research)
BOREAS	Boreal Ecosystem-Atmosphere Study
CEH	Centre for Ecology and Hydrology
CESBIO	Centre d'Etudes Spatiales de la Biosphere
CNR	Clutter to Noise Ratio
DEM	Digital Elevation Model
DIFF	Differential Interferometry and Geocoding Software (from Gamma RS)
DLR	Deutsches Zentrum für Luft- und Raumfahrt (German Aerospace Center)
DWD	Deutsche Wetter Dienst (German Weather Service)
EORC	Earth Observation Research and application Centre
ERS	European Remote sensing Satellite
ESA	European Space Agency
EU	European Union
FAO	Food and Agriculture Organization of the United Nations
FIP	Forest Inventory and Planning
FSU	Friedrich Schiller University
Gamma RS	Gamma Remote Sensing Research and Consulting AG
GBFM	Global Boreal Forest Mapping
GIS	Geographical Information System
GTOPO30	Global DEM with a horizontal grid spacing of 30 arc seconds
GRS	Ground Reference System (used by JAXA)
HH	Horizontal Horizontal polarization
HV	Horizontal Vertical polarization
IIASA	International Institute for Applied Systems Analysis
InSAR	Interferometric Synthetic Aperture Radar
ISP	Interferometric SAR Processor (from Gamma RS)
IWCM	Interferometric Water Cloud Model
JAXA	Japan Aerospace Exploration Agency
JERS-1	Japanese Earth Resources Satellite-1
JPL	Jet Propulsion Laboratory
JRC	Joint Research Centre of the European Commission
LAT	Land Application Tools (from Gamma RS)
MITI	Japanese Ministry of International Trade and Industry

ML	Maximum Likelihood
MSP	Modular SAR Processor (from Gamma RS)
NASA	National Aeronautics and Space Administration
NASDA	National Space Development Agency of Japan
NE	North East
NOPEX	Northern Hemisphere Climate-Processes Land-Surface Experiment
NW	North West
OPS	Optical Sensor (on JERS-1)
PALSAR	Phased Array type L-band Synthetic Aperture Radar
RMSE	Root Mean Square Error
SAR	Synthetic Aperture Radar
SCEOS	Sheffield Centre for Earth Observation Science
SIBERIA	SAR Imaging for Boreal Ecology and Radar Interferometry Applications
SE	South East
SW	South West
SIR	Shuttle Imaging Radar
SLC	Single Look Complex
SNR	Signal to Noise Ratio
SRTM	Shuttle Radar Topography Mission
SWE	Snow Water Equivalent
UN	United Nations
UNEP	United Nations Environment Programme
UNFCCC	United Nations Framework Convention on Climate Change
USGS	United States Geological Survey
UTC	Coordinated Universal Time
VH	Vertical Horizontal polarization
VV	Vertical Vertical polarization
WARC	World Administrative Radio Conference
WMO	World Meteorological Organization

Units

cm	centimetre
dB	decibel
°C	degree Celsius
GHz	gigahertz
ha	hectare
km	kilometre
m	metre
MHz	megahertz
s	second
W	watt

Symbols

a	signal amplitude
A	parameter in regression model for stock volume retrieval
B	parameter in regression model for stock volume retrieval
B_n	perpendicular spatial baseline
B_{nc}	critical baseline
B_p	parallel spatial baseline
B_{tot}	total spatial baseline
c	speed of light
C	parameter in regression model for stock volume retrieval
$E\{\}$	expected value
g	complex SAR image
G_r	gain of the receiving antenna
G_t	gain of the transmitting antenna
h	surface height
L_s	system loss factor
L_r	range resolution
n	amplitude of the thermal noise
N	total amplitude of the thermal noise
N_{est}	number of pixels in estimation window
N_{test}	number of samples in test set
P	position number in sorted test area data base
P_b	power scattered back towards the antenna
P_r	power received by the radar
P_t	output power from transmitter
R	slant range distance
R^2	coefficient of determination
s	interferogram
SE	sampling error
V	growing stock volume
\hat{V}	estimated growing stock volume
V^{gt}	growing stock volume in ground truth database
W	system bandwidth
z	elevation
α	local terrain slope in range direction
γ	interferometric coherence
$\hat{\gamma}$	estimated interferometric coherence
$\Delta\eta$	coherent terrain displacement
θ_i	incidence angle
θ_l	local incidence angle
θ_{look}	look angle of the antenna
λ	wavelength
ρ	atmospheric path delay
σ	radar cross section
σ^0	normalized radar cross section or backscatter coefficient
φ	signal phase
Φ	phase of the complex coherence
ψ	phase of the thermal noise
Ψ	total phase of the thermal noise

Chapter 1

Introduction

1.1 Boreal forest

The work that will be presented in this thesis is focused on forest in the boreal zone. The word boreal originates from the Greek word boreios, which means northern, or “coming from the north”. Boreas was also the name of the Greek god of the northern wind. Consequently, the boreal forest is the northernmost forest zone on Earth and stretches all around the globe at latitudes 60°-70° N in Alaska and northern Europe, 55°-70° in western Canada, 45°-60° in eastern Canada, and all the way from 45° to above 70° N in Siberia (TRETER, 1993). The extent of the boreal forests and the limits of the regions affected by permafrost are shown in Figure 1.1. The permafrost has a great influence on the tree species composition in different parts of the boreal zone.

According to the “Global Forest Resources Assessment 2000” that was published by the Food and Agriculture Organization of the United Nations (FAO) (FAO, 2001), about 13 million km² of the Earth’s surface is covered with boreal forests. This corresponds to 33 % of all forests in the world. Each year large areas in the boreal forest are affected by disturbances of natural (fire, insect infestation, wind throw) or anthropogenic (logging, fire, pollution) origin. Having the possibility to map the extent and state of the forests, and to identify and monitor changes, has become increasingly important for several reasons:

Economy: Throughout the boreal zone the forest has always been one of the main natural resources. Forest products like wood, paper and pulp, are important for the trading balance for most of the countries in this region, and for many people the forest or the local forest industry are the main sources of income.

Climate: During the last 20 years there has been an increasing awareness concerning the influence human activities have on climate. The United Nations Framework Convention on Climate Change (UNFCCC) and the Kyoto Protocol are two high-level international initiatives that address this problem. Studies of the global carbon balance are components in this work and here the boreal forests play an important role. A forest can serve both as a source and a sink for carbon dioxide and vast amounts of carbon are stored in the above ground and below ground biomass.

Biodiversity: The forest ecosystem does not only contain a large number of different tree species, it is also the only natural environment for many types of plants, moss, lichen, and mushrooms, and many species of mammals, birds, insects and other types of animals. Naturally there are differences between the species found in Eurasia and in North America, but also within the continents big differences can be found, and many species are only found in certain regions. Climate changes or large disturbances can lead to the extinction of sensitive species that are not so widespread. The United Nations Convention on Biological Diversity has been initiated to work for the conservation of biological diversity and for sustainable use and fair sharing of its components (UNEP - WWW.BIODIV.ORG).

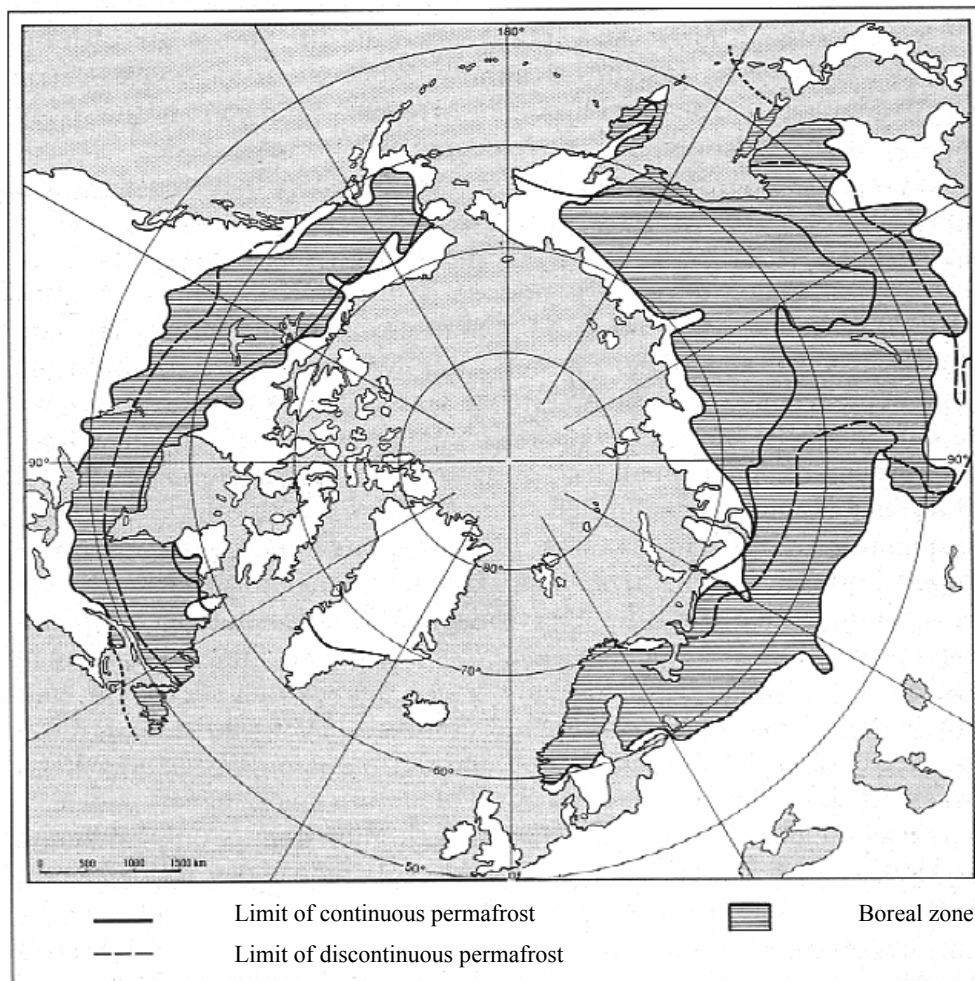


Figure 1.1 Extent of the boreal forests and limits of the regions affected by permafrost (from (TRETER, 1993)).

1.2 The JERS-1 and ERS-1/2 missions

The main focus of the work has been on L-band SAR data from the Japanese Earth Resources Satellite-1 (JERS-1). JERS-1 was developed by the National Space Development Agency of Japan (NASDA) and the Ministry of International Trade and Industry (MITI). It was launched with a H-I launch vehicle on 11 February 1992 from NASDA's Tanegashima Space Centre. JERS-1 carried two instruments, the

Synthetic Aperture Radar (SAR) and the Optical Sensor (OPS) (YONEYAMA *et al.*, 1990). After the initial commissioning phase the satellite was operational from the beginning of June 1992 until 12 October 1998.

Data from the European Remote sensing Satellite 1 and 2 (ERS-1 and ERS-2) have been considered in this thesis to give a possibility to compare the L-band data with the more commonly used C-band data. ERS-1 was launched by the European Space Agency (ESA) on 17 July 1991, and was operational from December 1991 (end of commissioning phase) to March 2000. ERS-2 was launched on 21 April 1995 and is still delivering data. A comparison between the JERS-1 and ERS-1/2 mission characteristics is given in Table 1.1. The characteristics for previous, upcoming and planned L-band SAR sensors are given in Appendix A.

Table 1.1 Characteristics of the JERS-1 and ERS-1/2 missions. Sources: (YONEYAMA, *et al.*, 1990; OLMSTED, 1993; ESA, 1997; KRAMER, 2002).

Mission	JERS-1	ERS-1 and ERS-2
Duration	Feb. 1992 – Oct. 1998	ERS-1: July 1991 – March 2000 ERS-2: April 1995 -
Altitude [km]	568	770 – 785 (depending on phase)
Repeat cycle [days]	44	3 (commissioning and ice phase) 35 (multi-disciplinary phase) 168 (geodetic phase) 1 (tandem ERS-1 and ERS-2)
Frequency [MHz] (band)	1275 (L-band)	5300 (C-band)
Wavelength [cm]	23.5	5.66
Band width [MHz]	15	15.5
Polarization	HH	VV
Look angle	35.21° (right looking)	20.355° (right looking)
Swath width [km]	75	100
Spatial resolution [m]:		
range	18	26
azimuth	18 (3 looks)	30 (4 looks)

1.3 Radar remote sensing of forest

For forestry applications, remote sensing has the advantage that large areas can be covered to a relatively low cost compared to conventional field surveys. Spaceborne SAR does not have the high spatial resolution that many optical satellite sensors have, but a radar can acquire images independent of cloud cover and thereby give a higher probability that information can be provided on a regular basis. For boreal forest the backscatter from JERS-1 SAR has been used for the estimation of growing stock volume (HARRELL *et al.*, 1995; ISRAELSSON *et al.*, 1995; KURVONEN *et al.*, 1999; PULLIAINEN *et al.*, 1999; HYYPPÄ *et al.*, 2000; SANTORO *et al.*, 2002a; ASKNE *et al.*, 2003a; SANTORO *et al.*, 2003; WAGNER *et al.*, 2003).

Interferometric coherence from ERS-1/2 has also proved to provide valuable information about growing stock volume in boreal forests (ASKNE *et al.*, 1997b; SMITH *et al.*, 1998; HYYPPÄ, *et al.*, 2000; FRANSSON *et al.*, 2001; KOSKINEN *et al.*, 2001; SANTORO *et al.*, 2002b; ASKNE *et al.*, 2003b; WAGNER, *et al.*, 2003). For spaceborne L-band interferometric coherence only few results related to forest have been published.

The multi-frequency capability of the Shuttle Imaging Radar C (SIR-C) missions in 1994 made it possible to compare the coherence levels from simultaneous acquisitions at C-band and L-band. It was found that with the one-day repeat-cycle of the Shuttle, the coherence from tropical and temperate forests is higher at L-band than at C-band, and that the difference in coherence levels between forest and open areas is larger for C-band than for L-band (RIGNOT, 1996; WEGMÜLLER *et al.*, 1997). The temporal decorrelation that forested areas experience in L-band coherence was first reported for SEASAT data from a temperate forest in Oregon (ZEBKER & VILLASENOR, 1992). The repeat-cycle of SEASAT was 3 days. The 44-day repeat-cycle of JERS-1 gives larger temporal decorrelation, but the coherence is in many cases still high enough to allow analysis of forest. One application that has been studied with JERS-1 repeat-pass coherence is the possibility to detect deforestation. These studies have been done for tropical forest in the Amazon (ROSEN *et al.*, 1999; LUCKMAN *et al.*, 2000) and on Sumatra (SUGA & TAKEUCHI, 2000; TAKEUCHI & OGURO, 2003) and all show good results. Other studies have indicated that it is possible to separate temperate forest from other land cover types (TAKEUCHI *et al.*, 1998), to detect areas damaged by forest fire (TAKEUCHI & YAMADA, 2002) and that for forest type discrimination the JERS-1 coherence is superior to the backscatter coefficient (TAKEUCHI & YONEZAWA, 1997).

The first study on JERS-1 interferometry for boreal forests showed that under favourable conditions it is possible to get coherence levels that are comparable with those from ERS-1/2, but also pointed out difficulties in separating forest from some of the other landcover classes (ASKNE *et al.*, 1999). Preliminary results from boreal forest in Siberia indicated that a combination of JERS-1 intensity and coherence could provide information about forest cover (WIESMANN *et al.*, 2000b). None of these two studies reported any quantitative results.

The first analysis of the relationship between JERS-1 repeat-pass coherence and biomass was done for tropical forest and showed a strong correlation between increasing biomass and decreasing coherence (LUCKMAN, *et al.*, 2000). The relation was described by a simple saturating exponential model. Similar results have been reported for boreal forest (ERIKSSON *et al.*, 2002b; ERIKSSON *et al.*, 2003). The only published attempt to retrieve growing stock volume was done with a JERS-1 pair covering a test area in Southern Sweden (ASKNE, *et al.*, 2003b). A combination between JERS-1 backscatter and coherence was found to increase the retrieval accuracy.

1.4 Scope of the thesis

Although the main principles for SAR interferometry are well known and have been successfully implemented for a wide range of applications, the literature review reported in Section 1.3 showed that very little work has been done to study the

characteristics and applications of spaceborne L-band interferometry for forest. The scarcity of information on this topic combined with the fact that new L-band SAR satellites will be launched, or are under evaluation (see Appendix A), was the main motivation for the work presented in this thesis.

The overall goal of the work was to answer two questions:

1. **“Which are the characteristics of spaceborne L-band interferometric coherence from forest?”**
2. **“Can spaceborne L-band interferometric coherence provide accurate and consistent information about forest?”**

Based on the availability of ground and satellite data the work had to be limited to the study of boreal forest with JERS-1 repeat-pass coherence.

To answer the first question the following tasks were formulated:

- Analysis of variations in the coherence due to
environmental conditions
length of period between acquisitions
spatial distance between the acquisitions
- Investigation of seasonal dynamics.

The results of these tasks also show if there are limitations that are relevant for the second question. Three forest applications were tested to answer the second question:

- Retrieval of growing stock volume.
- Creation of a growing stock volume map.
- Creation of a forest change map.

It has not been the scope of the thesis to develop new methods for forest parameter retrieval, forest mapping, or forest monitoring.

1.5 Outline of the thesis

In Chapter 2 the theoretical background on SAR and interferometric SAR (InSAR) is given and terms and expressions that will be used in the analysis are defined. An overview of the processing of the data is also included.

Chapter 3 gives a detailed description of the test areas that have been used and the available data. The data are divided into three sections. The first section describes ground data, including forest inventory, digital elevation models (DEMs) and topographic maps. In the two following sections meteorological data are characterised and available satellite scenes are listed.

The following three chapters present the results. An analysis of potential causes for decorrelation of the interferometric SAR is given in Chapter 4. This corresponds to the tasks that were defined to answer the first question in Section 1.4. Chapter 5 reports on model selection, model training, retrieval and error analysis that were conducted for the estimation of growing stock volume. Finally two examples of

potential forestry applications for JERS-1 repeat-pass coherence, one for mapping and one for monitoring, are presented in Chapter 6.

An outlook and a summary of the results conclude the thesis. In the outlook, topics that need further investigation are discussed and some promising new techniques and future missions are mentioned.

Chapter 2

SAR and InSAR theory

In this chapter theoretical background will be given and terms and expressions that will be used in the analysis in coming chapters will be defined.

2.1 SAR system overview

A radar is an active sensor that sends out microwave pulses and records the echo. Compared with passive sensors that rely on electromagnetic waves that have been transmitted by another source, e.g. sunlight or thermal radiation, a radar has its own transmitter. At the cost of higher power consumption and more complex hardware and signal processing, this gives a radar system the advantage that it can collect data also during night. A radar can be mounted on different types of platforms, like air traffic towers, ships, planes and satellites, but in this thesis only airborne and spaceborne platforms, with a strong emphasis on the JERS-1, ERS-1 and ERS-2 satellites, will be considered.

To allow derivation of the location of the scattering elements, an imaging radar is mounted in a side-looking configuration on the platform. The area that is observed along the flight path is called the swath. The look angle of the radar decides how far to the side of the flight path the swath will be acquired, and the shape of the transmitted beam how wide the swath will be. Some radar systems have the possibility to mechanically or electronically steer the look angle and the shape of the beam, but both JERS-1 and the ERS satellites have fixed look angle and swath width (see Table 1.1).

The signal transmitted by a SAR system is characterized by its signal power, carrier frequency, frequency modulation, pulse length, and polarization. If the transmitter has a peak output power P_t [W], the power that is re-radiated towards the antenna by an object is

$$P_b = \frac{P_t G_t \sigma}{4\pi R^2} \quad [\text{W}] \quad (2.1)$$

where G_t is the gain of the transmitting antenna, σ is the radar cross section of the object and R is the distance between the antenna and the object. The power received by the radar from the object is then

$$P_r = \frac{P_t G_t G_r \sigma \lambda^2 L_s}{(4\pi)^3 R^4} \quad [\text{W}] \quad (2.2)$$

where G_r is the gain of the receiving antenna, λ is the wavelength, and L_s is the system loss factor.

During World War II the microwave frequencies where a radar is operating were divided into frequency bands that for security reasons were given code letters (KINGSLEY & QUEGAN, 1992). These code letters are still in use and for remote sensing with SAR the most common bands are P (0.3 – 1.0 GHz), L (1.0 – 2.0 GHz), C (4.0 – 8.0 GHz), X (8.0 – 12.5 GHz), and in some cases S (2.0 – 4.0 GHz). In this thesis only SAR systems with frequencies in the L- and C-band will be considered. Theoretically the transmitted signal could be given a polarization that is elliptical, circular or linear, but normally only the horizontal (H) or vertical (V) linear polarizations are used. The polarization of the radar system is then given by one of the combinations HH, HV, VH, or VV, where the first letter is the polarization of the transmitted signal and the second letter gives the received polarization.

In the across-track (range) direction, the spatial resolution of the acquired image is determined by the length of the transmitted pulse. A shorter pulse allows smaller objects to be observed, but gives reduced signal to noise ratio (SNR) since less energy is transmitted (JENSEN, 2000). However, with a so called chirp pulse modulation it is possible to use longer pulses and still get a relatively high range resolution (CURLANDER & MCDONOUGH, 1991; KINGSLEY & QUEGAN, 1992; OLMSTED, 1993). In the along-track (azimuth) direction, the achievable resolution is proportional to the wavelength and to the distance between the antenna and the observed object and inversely proportional to the length of the antenna. For spaceborne radar sensors very large antennas are required to get high resolution. By recording all echoes returned by an object when the radar flies past it and then, after phase correction, coherently summing them, it is possible to synthesize an antenna with a length (aperture) much longer than the real length. These synthetic aperture radar systems get an azimuth resolution that is independent of both the wavelength and the distance to the object.

For airborne and spaceborne SAR systems, the size of a resolution cell is much larger than the individual scattering objects, so that the signal that is returned is made up of contributions from a large number of objects. These contributions have different phase, causing constructive or destructive interference giving the resolution cell a backscattered signal amplitude that can differ a lot from the neighbouring resolution cells. The result is an image with a grainy salt-and-pepper pattern called speckle. One way to reduce speckle is multilook averaging of the image. A larger number of looks gives a less noisy image, but at the same time degrades the resolution.

2.2 Radar scattering

This section gives an introduction to scattering mechanisms and the physical properties that govern scattering from surfaces and volumes. The basic characteristics of scattering from forests are explained in a separate sub-section. As will be shown in Chapter 3, the majority of the satellite data that will be analysed in

this thesis were acquired during the winter season. For this reason a sub-section on scattering from snow has also been included.

2.2.1 Scattering mechanisms

The amplitude, phase and polarization of the signal that is scattered back in the direction of the receiving antenna depend on the characteristics of the scattering objects. Important is the local incidence angle, the surface roughness, the size, shape and orientation of the objects, and the dielectric properties. The local incidence angle θ_l is the angle between the direction of the incoming wave and the normal to the surface. With a surface facing towards the antenna a large portion of the signal will be returned to the receiver. With a larger local incidence angle, a larger amount of the transmitted energy will be reflected away from the antenna.

The scattering mechanisms are usually divided into surface scattering, volume scattering and double bounce. For surface scattering the roughness of the surface is one of the parameters that determine how much of the signal that is scattered back towards the antenna. For a smooth surface most of the incoming signal is reflected in one direction, while for a rough surface the signal is scattered in many different directions. Thus, for surfaces with a local incidence angle larger than zero, a rough surface normally gives a stronger backscatter than a smooth surface. To determine if a surface is rough or not we need to know the wavelength λ of the observing radar. A surface with a standard deviation of the surface height h will look smooth at long wavelengths, but rough at short wavelength. Different modified versions of the Rayleigh criterion have been reported as practical criteria for when a surface can be considered smooth. In (ULABY *et al.*, 1986a) the following condition is given:

$$h < \frac{\lambda}{32 \cos \theta_l} \quad [\text{m}] \quad (2.3)$$

Volume scattering occurs when the signal is scattered multiple times within a diffuse media. The number of scattering objects and their size, shape, and orientation determine the portion of the signal that will be returned to the antenna. Also in this case different wavelengths will be affected by different object sizes. The third common scattering mechanism, double bounce, occurs when the signal is reflected by two surfaces that are oriented perpendicular to each other, so that it is directed back towards the antenna. The smoothness of the surfaces will determine how large portion of the signal that is returned. In addition to the mentioned scattering properties, all three scattering mechanisms are affected by the dielectric constant of the scattering objects. An object with high water content has a high dielectric constant, which gives a small penetration depth and a larger part of the signal is reflected. Dry or frozen materials give lower scattering.

In Section 2.1 the radar cross section σ was introduced. σ is defined as the equivalent of a perfectly reflecting area that reflects isotropically (JENSEN, 2000). Such areas are rare in a natural environment, and instead it is common to use the normalised radar cross section per unit area $\sigma^0 = \sigma/A$, where A represents the geometric surface giving rise to the scattering. σ^0 is also called “radar backscatter coefficient” or simply “sigma nought”. In this thesis σ^0 will be referred to as the backscatter coefficient.

2.2.2 Scattering from forest

For the analysis of the scattering from forest, it is convenient to think of a forest as a three dimensional collection of elements with different size, shape, orientation and water content. The smallest elements that are relevant for the wavelengths considered in this thesis are the leaves, needles and twigs. In the mid-size range we find branches, and the largest elements are the stems. In addition to this we have to consider the forest floor and the ground vegetation. The scattering from these elements can be related to the scattering mechanisms that were introduced in the previous section. In the tree canopy the main scattering mechanism is volume scattering. The wavelength of the incoming radar wave determines which elements contribute most to the volume scattering. At L-band the main scattering elements are the branches and at C-band it is the leaves, needles, twigs and small branches. In addition to the number of scattering elements within a resolution cell, the polarization and incidence angle of the transmitted signal, in relation to the orientation of the elements, strongly influence the strength of the volume scattering.

According to (ULABY, *et al.*, 1986a), the surface scattering from the boundary between air and vegetation canopy is usually unimportant, but the surface scattering from the ground has to be considered. The strength of this component not only depends on the roughness and moisture of the ground, but also on the density of the forest canopy. A dense canopy attenuates the signal and reduces the amount of energy that reaches the ground. The signal is then further attenuated on its return path. At L-band the attenuation is relatively low and a contribution from the ground can be expected to be present until a high number of branches is reached. The wavelength is in most cases long in comparison with the standard deviation of the ground surface height, giving a reduced ground contribution. At C-band the density of scattering elements is higher, which leads to a stronger attenuation. Only in sparse forest can surface scattering from the ground become the dominant scattering mechanism. At this wavelength the forest floor also appears rougher and gives a stronger backscatter. A larger incidence angle gives a longer path length through the canopy and thereby a larger attenuation.

Double bounce occurs when the incoming wave is reflected first by a trunk, branch, or stub and then by the ground back towards the antenna, or vice versa first by the ground and then by a trunk, branch or stub. As with the normal surface scattering from the ground, the soil moisture, surface roughness and the attenuation through the canopy determine the strength of the returned signal. In sparse forest with smooth forest floor, double bounce will reflect a large portion of the energy back to the antenna. However, in order to contribute significantly to the total backscatter, double bounce has to occur for a large number of trunks within a resolution cell. A special case occurs when the forest is flooded. Since water has a high dielectric constant and can be considered being a smooth surface, at least at L-band, this condition has been observed to produce a strong double bounce contribution even in comparatively dense forest (HESS *et al.*, 1990; ROSENQVIST *et al.*, 2002).

The dielectric constant in trees is closely related to the moisture content in the wood (LIN, 1967), which thereby affects the strength of the scattering. The tree water content follows the availability of water in the ground. A dry summer gives a water content that is lower than normal, but there are also natural seasonal variations (GATES, 1991). In addition to these variations the tree water content also varies with

the time of the day (SALAS *et al.*, 1994; MCDONALD *et al.*, 1999). These diurnal variations are of minor importance in this study, since all satellite images are acquired at approximately the same time of the day. For boreal forests it is important to remember that the temperature has a big influence on the dielectric constant. Even if the tree water content is high, the dielectric constant will be considerably reduced if the water is frozen (MCDONALD, *et al.*, 1999). The water content is usually not homogeneously distributed in the stem. The bark contains little free water, the sapwood beneath it has the highest water content, while the heartwood in the centre holds less water (KRAVKA *et al.*, 1999). The dielectric constant follows the same pattern (WAY *et al.*, 1990; SALAS, *et al.*, 1994; MCDONALD, *et al.*, 1999), which means we can expect the radar signal to be scattered in the sapwood of the tree.

2.2.3 Scattering from snow

The analysis of scattering mechanisms for snow is usually simplified by dividing the total backscatter in three components (ULABY *et al.*, 1986b): (1) backscattering from the snow-air interface, (2) backscattering from the snow volume, and (3) backscattering from the underlying ground surface. The numbers (1) and (3) represent surface scattering and (2) represents volume scattering. Dry snow is a mixture of air and ice. If water in liquid form is present in the snow it will be called wet snow. The backscatter from snow is influenced by snow layer thickness, volumetric liquid water content, surface roughness of the two boundary layers, snow grain size and shape, snow layer temperature profile, snow layer density profile and layer structure (KOSKINEN, 2001). The commonly used term snow water equivalent (SWE) is related to the density and thickness of the snow layer and represents the amount of water potentially available for runoff.

The backscatter at the boundary between air and snow is strongly dependent on the liquid water content. The dielectric constant of dry snow is low enough that this backscattering contribution can be neglected for side looking radar systems (ULABY, *et al.*, 1986b). The backscatter coefficient increases with the liquid water content, so that for wet snow the backscatter from the air-snow interface can be the dominant scattering mechanism at C-band. At L-band, the difference between the backscatter from dry and wet snow is marginal and in general the longer wavelength makes the backscatter from snow significantly lower than at C-band (ULABY & STILES, 1981).

The volume scattering increases with the snow layer thickness and density. For a fixed thickness and density the volume contribution depends on the size of the ice particles in relation to the radar wavelength. The snow layer also affects the incidence angle and wavelength of the electromagnetic wave. A higher snow density gives an increased dielectric constant. Refraction within the snow gives a smaller incidence angle, and the fact that snow is dielectrically thicker than air reduces the wavelength (SHI & DOZIER, 2000). However, even though the wavelength is reduced, at L-band it is still considerably larger than the size of the ice particles, and therefore no significant volume scattering occur.

The backscatter from the ground underneath the snow layer depends on the attenuation in the snow layer and the strength of the other two scattering mechanisms. In addition to this the dielectric contrast between snow and ground is smaller than between air and ground, which reduces the reflectivity at the snow-

ground interface (SHI & DOZIER, 2000). However, the reduction of the wavelength in the snow layer makes the ground surface appear rougher and together with the decreased incidence angle this gives an increase in the backscatter. At L-band this results in a backscattering coefficient that is higher for a snow covered surface than for a bare surface (SHI & DOZIER, 2000). At C-band the backscatter from the ground can be significant for dry snow, but the attenuation in the snow layer increases rapidly with increasing snow wetness so that for wet snow there is hardly any scattering contribution from the snow-ground interface (KOSKINEN, 2001).

In addition to the three scattering mechanisms mentioned above, indirect scattering occurs when two or more scattering mechanisms are combined before the signal is returned, e.g. when a part of the incoming wave is first scattered by ice particles in the snow layer and then by the ground. The indirect scattering also adds to the total scattering, but due to multiple scattering and attenuation this contribution is weak.

2.3 SAR interferometry

Radar interferometry was first used in earth-based observations of Venus (ROGERS & INGALLS, 1969; RUMSEY *et al.*, 1974) and the Moon (ZISK, 1972a; ZISK, 1972b). Measurements of topography on Earth with an airborne radar were conducted in the early seventies (GRAHAM, 1974). The first spaceborne SAR images were acquired by Seasat in 1978, but it took almost 10 years until the first InSAR results were published (GOLDSTEIN & ZEBKER, 1987; GOLDSTEIN *et al.*, 1988). At the same time the first InSAR results from the second Shuttle Imaging Radar mission (SIR-B) were published (GABRIEL & GOLDSTEIN, 1988). After that the development went fast and with the launch of ERS-1 in 1991 there were also a lot of suitable data available.

2.3.1 InSAR baselines

For the creation of an interferogram, a minimum of two acquisitions of the same object are needed. In order to provide any new information, the second image has to be acquired with a slightly different flight path or acquisition time (BAMLER & HARTL, 1998). We will refer to these differences as spatial and temporal baseline. In order to have a temporal baseline equal to zero, two receiving antennas can be mounted on the same platform. This is common for airborne SAR systems, but so far the Shuttle Radar Topography Mission (SRTM) is the only example of a spaceborne single-pass system. In most other cases we have to rely on repeat-pass acquisitions, which means that the second image is acquired with a time delay of one or more repeat cycles. The repeat cycle, also known as revisit time, is the shortest time between two overflights of the same area. Normally the two acquisitions have to be done with the same satellite, but in the case ERS-1 and ERS-2 both satellites had identical SAR systems, which made it possible to create interferograms from image pairs where one image was acquired by ERS-1 and the other by ERS-2. Recently it has been proven that, under special conditions, it is also possible to create an interferogram from an ERS-2/Envisat SAR-pair, even though Envisat ASAR operates at a frequency that is 31 MHz higher than the frequency of ERS-2 Active Microwave Instrument (AMI) (GATELLI *et al.*, 1994; ARNAUD *et al.*, 2003).

In theory it is possible to get a repeat pass pair with only temporal baseline, but in practise the two orbits are never exactly the same. Figure 2.1 shows a simple image of the spatial baseline (B_{tot}) between the positions of the two acquisitions and its parallel (B_p) and perpendicular (B_n) components. For our applications B_n is the most important component. B_n can vary from a few meters up to several kilometres. The effect of the baseline length on the interferometric products will be discussed in the next sections.

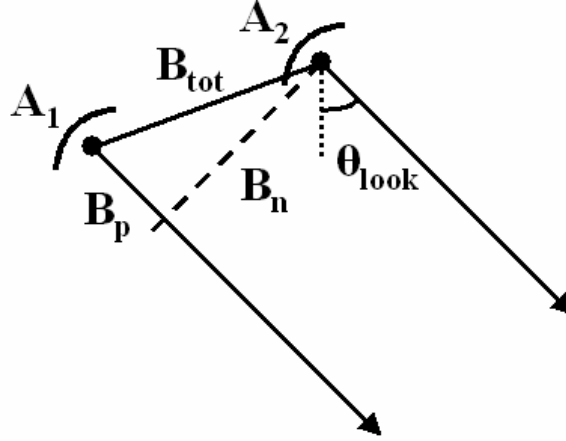


Figure 2.1 Spatial baseline B_{tot} between two antennas A_1 and A_2 . B_p is the parallel component, B_n is the perpendicular component and θ_{look} corresponds to the look angle of the antennas.

2.3.2 Coherence and interferometric phase

SAR interferograms are produced by forming the Hermitian product of the two complex images g_1 and g_2 . Both images need to be coregistered with sub-pixel accuracy. The signals from the radar system for pixel i are given by (LI & GOLDSTEIN, 1990; HAGBERG *et al.*, 1995)

$$g_{1,i} = a_{1,i} e^{-j\varphi_{1,i}} e^{-j\frac{4\pi}{\lambda} R_{1,i}} + n_{1,i} e^{-j\psi_{1,i}} \quad (2.4)$$

$$g_{2,i} = a_{2,i} e^{-j\varphi_{2,i}} e^{-j\frac{4\pi}{\lambda} R_{2,i}} + n_{2,i} e^{-j\psi_{2,i}} \quad (2.5)$$

where a is the signal amplitude, φ is the signal phase, and R is the slant range between the observed pixel and the antenna. The amplitude and phase of the thermal noise are given by n and ψ respectively. If we assume that we don't have any misregistration between the images, the value of pixel i in the interferogram can then be calculated as

$$s_i = g_{1,i} g_{2,i}^* = (a_{1,i} a_{2,i}) e^{j\Delta\varphi_i} e^{j\frac{4\pi}{\lambda} \Delta R_i} + N_i e^{-j\psi_i} \quad (2.6)$$

where $*$ gives the complex conjugate, $\Delta\varphi_i$ is the difference in phase contribution within the pixel, and ΔR is the path difference, which corresponds to B_p in Figure 2.1. The amplitude and phase of all parts of the product that are caused by the thermal

noise are denoted by N and Ψ . The complex coherence is defined as (BORN & WOLF, 1980)

$$\gamma = |\gamma|e^{j\Phi} = \frac{E\{g_1 g_2^*\}}{\sqrt{E\{|g_1|^2\}E\{|g_2|^2\}}} \quad (2.7)$$

where $E\{\}$ represents expected value, $|\cdot|$ denotes the magnitude, and Φ is the phase of the complex coherence. If we assume that there is no correlation between the thermal noise terms, or between the thermal noise and the signal, then the noise term in Equation (2.6) will not influence $E\{g_1 g_2^*\}$ (LI & GOLDSTEIN, 1990). Coherence estimation will be discussed in section 2.4.2.

In most literature the magnitude of the complex coherence is simply referred to as the coherence, so from now on, unless specifically stated, coherence will refer to $|\gamma|$. The coherence is a measure of the degree of correlation between the images and can take values between 0 and 1. To make it easier to analyse the coherence we can divide it in several components (ZEBKER & VILLASENOR, 1992; ULANDER & HAGBERG, 1995; SMITH *et al.*, 1996)

$$|\gamma| = |\gamma|_{processor} |\gamma|_{azimuth} |\gamma|_{noise} |\gamma|_{spatial} |\gamma|_{temporal} \quad (2.8)$$

The first two terms are independent of the observed object, the third and fourth are related to both the object and the system, and the fifth term is only related to the object properties.

$|\gamma|_{processor}$ accounts for distortions due to the SAR processor, e.g. misregistration, resampling, interpolation, and focus parameters. Nowadays most processors produce coherence images that hold a quality high enough that $|\gamma|_{processor}$ can be set to unity, and thereby do not reduce the total coherence.

$|\gamma|_{azimuth}$ is a result of different antenna squint angles, i.e. the orbits are not completely parallel. This leads to a misalignment of the azimuth spectra of the two images. With a proper azimuth band-pass filter this effect can be reduced (SCHWÄBISCH & GEUDTNER, 1995), so that $|\gamma|_{azimuth}$ normally can be set equal to one. It has also been shown by (ZEBKER & VILLASENOR, 1992) that L-band SAR systems are less sensitive to squint angle differences than C-band systems.

$|\gamma|_{noise}$ gives the coherence due to thermal noise in the receivers. According to (ZEBKER & VILLASENOR, 1992) we have

$$|\gamma|_{noise} = \frac{CNR}{CNR + 1} \quad (2.9)$$

where CNR is the clutter to noise ratio. If the system has a high CNR, the noise decorrelation will be negligible.

$|\gamma|_{spatial}$ is determined by volume decorrelation and decorrelation that originates from the spatial baseline. Spatial decorrelation will be discussed in more detail in 2.3.3.

$|\gamma|_{temporal}$ is caused by temporal decorrelation that occurs when the backscatter of the observed objects change between the acquisitions. In a single-pass system this term is equal to one, but for repeat-pass systems with long repeat cycles, this term can be equal to zero. Section 2.3.4 will give more information about temporal decorrelation.

When all decorrelation terms that are insignificant or can be compensated are removed the coherence expression is reduced to a product of spatial volume decorrelation and temporal decorrelation

$$|\gamma| = |\gamma|_{spatial} |\gamma|_{temporal} \quad (2.10)$$

The phase of the complex coherence is often called the interferometric phase. Like the coherence, the phase difference between two pixels in an interferogram can also be divided in several terms with different physical meaning (ULANDER & HAGBERG, 1995; DAMMERT, 1999)

$$\Delta\Phi = \frac{4\pi B_n}{\lambda R \tan \theta_i} \Delta R + \frac{4\pi B_n}{\lambda R \sin \theta_i} \Delta z + \frac{4\pi}{\lambda} \Delta \eta + \frac{4\pi}{\lambda} \Delta \rho + \Delta\Phi_{noise} + n2\pi \quad (2.11)$$

The first two terms are related to the geometry of the two SAR systems through the perpendicular baseline B_n , incidence angle θ_i , and slant range R . The first term also includes the slant range difference ΔR that gives rise to phase fringes related to the system geometry. These fringes occur in the across track direction and can be removed with so called flat earth removal. The second term contains the difference in elevation Δz , and thereby describes the phase fringes that are caused by ground topography.

The third phase term only applies when a coherent movement of all the scatterers within a resolution cell, given by $\Delta \eta$, has occurred between the acquisitions. Ground subsidence, earthquakes, and volcanic activity can cause such movements.

The fourth phase term has been included to account for differences in the atmospheric path $\Delta \rho$. If the electron density in the ionosphere or the water vapour content in the troposphere changes significantly between the acquisitions, this will reduce the quality of the interferogram. This effect is commonly referred to as atmospheric artefact.

The two last terms are the noise contribution and the phase ambiguity. In InSAR processing, the 2π ambiguity is resolved by the phase unwrapping.

A more thorough description of the phase, and an analysis of the possibilities to retrieve tree height from C-band interferometric phase is given in (SANTORO, 2003; SANTORO *et al.*, submitted).

2.3.3 Spatial decorrelation

If the two images used to produce the interferogram have been acquired from slightly different positions we obtain spatial baseline decorrelation. This means that we are measuring the backscattered signal from the observed objects with a slightly different

slant range and look angle and that the images therefore not are completely correlated. If we only have surface scattering, the spatial decorrelation can be reduced by wavenumber shift filtering (GATELLI, *et al.*, 1994). This technique works also if we have a slope in the range direction, but if there is a slope component in the azimuth direction, this will give residual decorrelation.

Volume scattering, e.g. from a forest canopy or a snow layer, will increase the spatial decorrelation and cannot be compensated by wavenumber shift filtering. If we consider the volume scattering being only a function of height above a plane surface, the total spatial decorrelation can be split in two components (ULANDER *et al.*, 1995):

$$|\gamma|_{spatial} = |\gamma|_{slanrange} |\gamma|_{volume} \quad (2.12)$$

where the first component depends only on system parameters and corresponds to the part that can be removed with wavenumber shift filtering.

If the baseline is increased a length will be reached where $|\gamma|_{spatial}$ becomes zero, or in other words, we have complete decorrelation. This length is called the critical baseline and is given by (ZEBKER & VILLASENOR, 1992)

$$B_{nc} = \frac{R\lambda}{2L_r \cos \theta_{look}} \quad [\text{m}] \quad (2.13)$$

where L_r is the ground resolution in the range direction. This expression can be rewritten so that the critical baseline is said to occur when the difference in look angle is large enough to give a frequency shift that equals the system bandwidth W (GATELLI, *et al.*, 1994). Including the local terrain slope in range direction, α , we get

$$|B_{nc}| = \left| \frac{WR\lambda \tan(\theta_{look} - \alpha)}{c} \right| \quad [\text{m}] \quad (2.14)$$

where c is the speed of light. With the system parameters given in Table 1.1, the critical baseline is about 5.7 km for JERS-1 and 950 km for ERS-1/2. For practical applications, baselines well below these values are recommended.

2.3.4 Temporal decorrelation

In a repeat-pass system the time between the acquisitions allows changes in the signal scattered back from the observed objects to occur. These changes can be caused by differences in the geometry or dielectric constant of the scatterers. A change in the dielectric constant affects the reflectivity, penetration depth and absorption of the incoming wave. As a result of changes in the backscattered signal, the coherence decreases and we talk about temporal decorrelation. Depending on (1) characteristics of the observed object, (2) properties of the observing system, (3) environmental conditions at the acquisitions, (4) time between the acquisitions and (5) time of the day and time of the year we can expect different causes and severity of the temporal decorrelation.

1) It is obvious that the temporal decorrelation for a forest canopy will be different from that of e.g. a water surface or exposed rock. Normally exposed rock will neither move nor change its dielectric properties and is thereby very stable and should not be affected by any temporal decorrelation. A water surface does not change its dielectric properties, but the surface is in constant motion and is characterized by strong decorrelation. A forest canopy is less predictable since it can be, but will not always be, affected by both motion and changing dielectric properties.

2) The most important system parameters determining temporal decorrelation are wavelength, incidence angle and polarization. It is important to note that when we talk about temporal correlation the system parameters do not change between the acquisitions. Systems with different system parameters observe the temporal changes differently, but contrary to spatial decorrelation, for a certain system configuration it is not changes in system characteristics that cause the decorrelation. For example, when scatterers move between the acquisitions, the decorrelation in these cases will be related to how large the movements are compared to the wavelength. For a forest the wind has to be stronger to give decorrelation at L-band than at C-band. In (ZEBKER & VILLASENOR, 1992) complete decorrelation is said to occur when the rms motion exceeds 10 cm at L-band and 2-3 cm at C-band. The incidence angle and polarization will affect what type of motion dominates the decorrelation. For incidence angles smaller than 45° we can expect a greater sensitivity to vertical displacement than to horizontal displacement (ZEBKER & VILLASENOR, 1992).

3) If the environmental conditions are different at the two acquisitions, this can cause severe decorrelation. Rainfall during, or shortly before one of the acquisitions will increase the dielectric constant, wind results in displacement of the scatterers, and freezing or thawing will dramatically change the dielectric constant. At C-band, occurrence of wet snow gives strong decorrelation (STROZZI *et al.*, 1999; GUNERIUSSEN *et al.*, 2001), but spatial variations in the depth of dry snow have also been observed to affect the coherence (LI & STURM, 2002). As mentioned in Section 2.2.3, at L-band a snow layer will affect the backscatter from the snow-ground surface and thereby lead to decorrelation if snow is only present at one of the acquisitions (SHI *et al.*, 1997). It is also likely that for forested areas a heavy snow cover on the branches will alter the geometry of the scatterers, but at the same time reduce their possibilities to move.

4) In general the longer the time between the acquisitions, the larger the decorrelation, simply because a longer repeat-pass allows more changes to occur. However, this is not always the case. If we have a time series of three images where the weather conditions at the first and the last acquisition were similar, but the second was affected by, e.g. rain or strong wind, it is likely that the coherence between the first and last image is higher than between the first and second or between the second and the third. In this case the decorrelation does not increase with increasing temporal interval between acquisitions, instead the observation conditions return to a “normal state” after a temporary disturbance. The stability of the observed objects determines the length of the interval between the acquisitions before we get complete decorrelation. Some objects, like buildings and exposed rock, will keep a high coherence over very long periods, even when the rest of the image is completely decorrelated.

5) To a certain extent the above mentioned normal state for the observations follow diurnal and annual cycles. As mentioned in Section 2.2.2, the water content in a tree can vary over the day. If acquisitions are done at different times of the day, a small temporal decorrelation due to the diurnal change in the backscatter coefficient of the forest canopy can occur. This is also the case for large diurnal differences in the temperature or soil moisture. More obvious is the decorrelation that is caused by seasonal changes in the observation conditions. In the sub-tropical zone the backscatter from an open surface or a forest will be different depending on if the observations are made during the dry or the rainy season. In the boreal zone, the average backscatter level from a scene acquired when the forest is frozen will be several dB lower than the backscatter coefficient from a summer scene (SANTORO, *et al.*, 2002a; SANTORO, *et al.*, 2003). If the images used for the coherence estimation are from different seasons, this can lead to significant decorrelation, whereas two scenes that are acquired with the same time span, but in the same season are likely to show less decorrelation (ERIKSSON, *et al.*, 2003).

2.4 InSAR processing

All JERS-1 scenes were processed from level 0 to single look complex (SLC) by Gamma Remote Sensing Research and Consulting AG (Gamma RS) in Switzerland. With the exception of the images from 1998, all processing of backscatter images, estimation of coherence, and geocoding was done at FSU-Jena using the Gamma Interferometric SAR Processor (ISP), Land Application Tools (LAT), and Differential Interferometry and Geocoding Software (DIFF) (WERNER *et al.*, 2000). For the images from 1998 this was done directly by Gamma RS for the project SIBERIA (SAR Imaging for Boreal Ecology and Radar Interferometry Applications) (WIESMANN *et al.*, 2000a). Several of the ERS-1/2 image pairs had been processed and geocoded by the German Aerospace Center (DLR) during the SIBERIA project, but to reduce possible error sources from the comparison with the JERS-1 data and with the new ERS-1/2 data, all ERS-1/2 data from SIBERIA were reprocessed with the Gamma software.

The definition of what should be called pre-processing and post-processing depends on what is considered being the main processing. In this thesis the focus is on the coherence, so consequently all processing steps conducted before the coherence estimation will be called pre-processing whereas everything done afterwards is post-processing.

2.4.1 Pre-processing

The first steps of the JERS-1 pre-processing were done with the Gamma Modular SAR Processor (MSP) in connection with the preparation of the SLC images. This included the radiometric calibration that accounts for sensitivity gain control, automatic gain control, and correction for the range antenna pattern. In addition the data were filtered for radio frequency interference. All ERS-1/2 data were delivered from ESA directly in SLC-format.

The SLC data have been registered to common slant range geometry. The quality of the coherence estimate depended on the co-registration accuracy. An automated approach based on the co-registration of many image chips has been used (WEGMÜLLER *et al.*, 2001). The standard deviation of the SLC registration in range and azimuth was between 0.1 and 0.3 pixels depending on image content. Common band filtering has also been applied.

2.4.2 Coherence estimation

The magnitude of the complex coherence defined in (2.7) can be estimated for example by means of a Maximum Likelihood (ML) estimator of the form (DAMMERT, 1996):

$$|\hat{\gamma}_{ML}| = \frac{\left| \sum_{i=1}^{N_{est}} g_{1,i} g_{2,i}^* e^{-j\varphi_i} \right|}{\sqrt{\sum_{i=1}^{N_{est}} |g_{1,i}|^2 \sum_{i=1}^{N_{est}} |g_{2,i}|^2}} \quad (2.15)$$

where N_{est} is the number of pixels in the estimation window. The term $e^{-j\varphi_i}$ has been added to correct for topography induced phase. If the ground is flat this term can be excluded, but this is rarely the case. The bias in the estimation will decrease with increasing window size, but at the same time the spatial resolution will decrease (SEYMOUR & CUMMING, 1994).

As a compromise between accurate estimation and high spatial resolution the coherence estimation was carried out with an adaptive window size. The size of the estimation window was determined by the coherence values from a rough first estimation with fixed window size (WEGMÜLLER & WERNER, 1996). The adaptive estimator was large when estimating low coherence values and small when estimating high coherence values. In addition to this the local phase plane and the backscatter texture were given as inputs to improve the coherence estimation. Without the phase plane the estimator would assume a constant phase within the estimation window, which would result in an underestimation of the degree of coherence in sloped terrain. The backscatter texture will affect the size of the adaptive window. For high texture areas the window size is reduced in order to get more homogeneous targets within the estimation window. The texture was defined as the standard deviation divided by the mean, and was calculated within 15x15 pixels large windows with a linearly decreasing weighting function. The lower and upper limits for the window size for the coherence estimation were set to 3x3 and 9x9 pixels. A Gaussian weighting function was applied to the estimation window.

2.4.3 Post-processing

Geocoding was used for the registration of the JERS with the ERS images and the available in-situ data. For Bolshe-Murtinsky an interferometric DEM was produced during the SIBERIA project (ROTH *et al.*, 1998; ROTH *et al.*, 1999). For Chunksky a new InSAR DEM had to be created from an ERS pair from 1996. These DEMs have

been used for the geocoding and terrain correction of all JERS and ERS data, except for the JERS summer pairs from 1998, which were processed before the InSAR-DEMs were available. In these cases the global DEM GTOPO30 from the United States Geological Survey (USGS) was used as geometric reference. GTOPO30 has a horizontal grid spacing of 30 arc seconds, which at these latitudes corresponds to approximately 1 km in latitude and 500 m in longitude. Quadratic spline interpolation algorithms were used for the data interpolation necessary in the resampling step. An additional fine registration with the ERS image was done to improve the data for analysis (WEGMÜLLER, 1999). The pixel spacing was chosen to 25 m. Coregistration accuracy on the order of 1-2 pixels was reached between the geocoded data sets.

Chapter 3

Test sites and data

3.1 Test sites

Two forest territories on the Central Siberian Plateau have been selected as test sites. The selected sites, Bolshe Murtinsky and Chunsky, are two of the 13 forest territories that were used in the European Union (EU) funded SIBERIA project (SCHMULLIUS *et al.*, 2001). These territories have been selected based on the availability of ground data, satellite data and meteorological data. They both belong to the southern taiga sub-zone of the boreal forest.

3.1.1 Bolshe Murtinsky

Bolshe Murtinsky is located on both sides of the river Yenisey, about 90 km north of Krasnoyarsk, the capital of the administrative region Krasnoyarsk Krai. Four test areas are situated within the Bolshe Murtinsky test territory. These four respectively belong to the Talovskoje, Krasnokluchevskoje, Predivinskoje and Ukseevskoje local forest districts, but for simplicity they will hereafter be referred to as Bolshe NW, Bolshe SW, Bolshe NE and Bolshe SE after their geographical location in the test territory. The coordinates for each test area, their extent and geographical location relative to each other are displayed in Figure 3.1.

The size of each test area is between 200 and 300 km² and based on the forest inventory, which will be discussed in more detail in Section 3.2, the number of forest stands ranges from 544 to 1605, which indicate large differences in the stand sizes. Bolshe NE is fractioned into a large number of smaller stands (mean size 17 ha), while Bolshe SW is more homogeneous and contains several stands larger than 200 ha, with a mean stand size of 48 ha. In this sense Bolshe NW and SE show more resemblance with Bolshe NE. More detailed information about number of forest stands, stand sizes and growing stock volume in the test areas is given in Table 3.1.

The main tree species are fir (*Abies sibirica*), spruce (*Picea sibirica*), cedar (*Pinus sibirica*), pine (*Pinus sylvestris*), birch (*Betula pendula*), and aspen (*Populus tremula*). Small amounts of larch (*Larix dahurica* and *Larix sibirica*) and willow (*Salix*) can also be found. In general it can be said that most forest stands are natural stands with mixed forest. Figure 3.2 gives two examples of the diversity in the forest composition of natural stands that can be found in the region. Forest plantations or

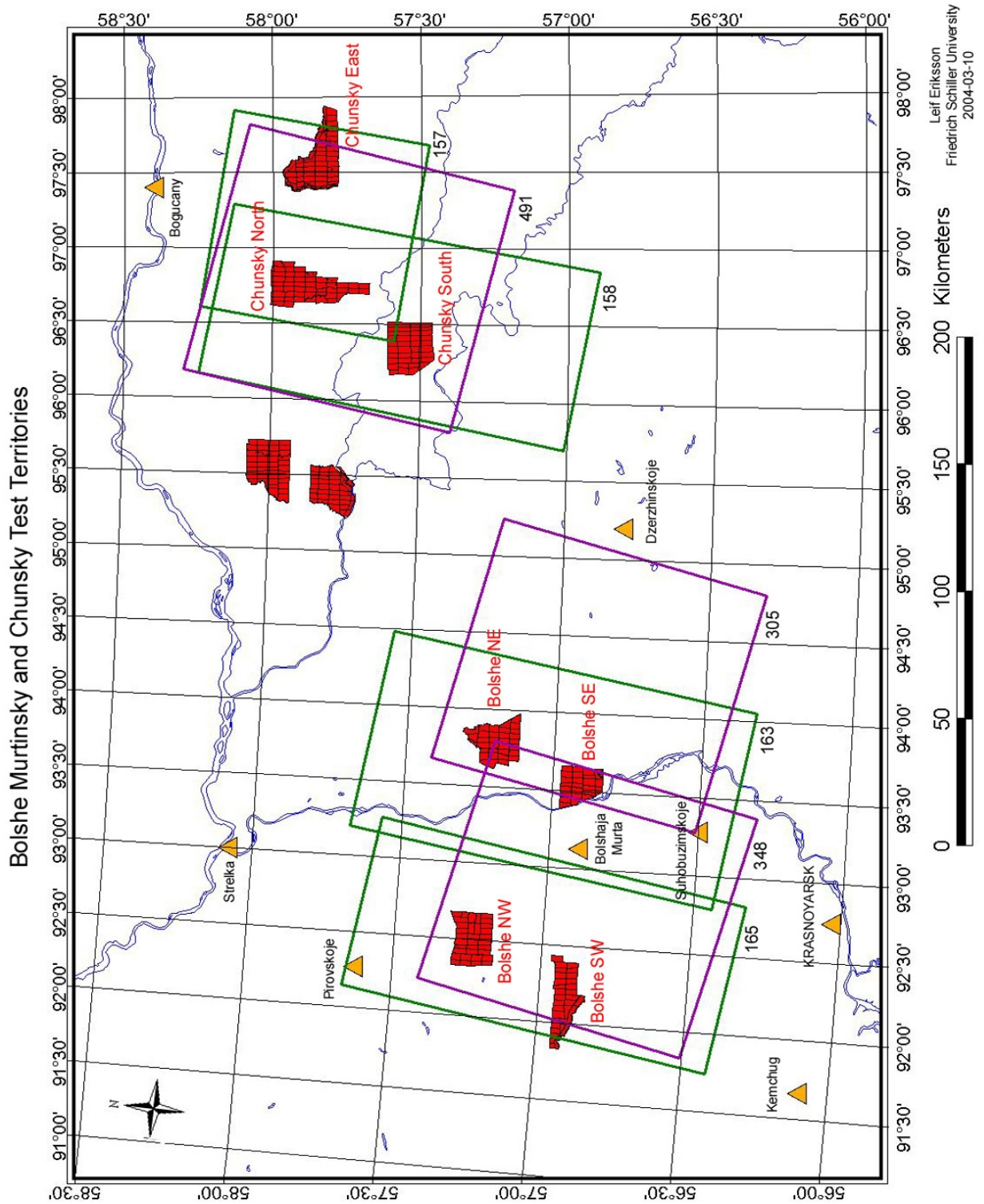
natural stands with only one tree species are not common in the test areas. A natural stand is here defined as a stand of growing trees resulting from natural regeneration following a forest disturbance like a stand replacing fire or clear cutting. The tree species composition differs somewhat between the four test areas, especially between the two areas west of Yenisey and the two on the eastern bank. Fir, spruce, cedar and birch are common in all test areas, but as shown in Figure 3.3 the coniferous species are more dominant in Bolshe NW and SW. The largest difference can be found for aspen, which is the second most common species east of Yenisey, but comparatively rare in the western areas. The same is true for pine, even though it only accounts for a smaller fraction of the total amount of trees.

In the Bolshe Murtinsky test territory the topography on the western and eastern sides of Yenisey are rather different. Except for a couple of steep slopes along the border of the Bolshe SW test area, the terrain on this side of the river is fairly gentle. At Bolshe NW the elevation varies between 220 and 260 m and at Bolshe SW between 300 and 330m. On the eastern side the topography is more varied, containing more hills and steeper slopes. The western parts of Bolshe SE are situated on a fairly steep slope down to the river. In a distance of 2-3 km from the river bank the elevation increase with up to 150 m. When moving further away from the river, the elevation reaches about 300 m above sea level at the centre of the test area and then decreases to around 200 m further to the east. With stream valleys at below 200 m and a peak at above 400 m above sea level, Bolshe NE is the test area with the largest topographical differences in the territory. This probably explains why Bolshe NE is fragmented into many small forest stands, and presents the smallest mean stand size of the available test areas.

3.1.2 Chunsky

The Chunsky forest territory is located about 280 km northeast of Krasnoyarsk, south of the river Angara. Chunsky contains five test areas spread over an area 160 km wide in east-west direction and 70 km in north-south direction. Only for three of these test areas a good time series of JERS scenes was available. The three areas will be referred to as Chunsky North, Chunsky South and Chunsky East. The coordinates for each test area, their extent and position relative to each other are displayed in Figure 3.1. Information about size, number of forest stands and growing stock volume of the test areas are given in Table 3.2. Compared to Bolshe Murtinsky the test areas are larger (between 300 and 400 km²), but the number of stands per test area is about the same (between 890 and 1226), resulting in considerably larger mean sizes of the stands.

As in the Bolshe Murtinsky territory, birch and aspen are the main broadleaf species, but the composition of coniferous species is radically different (see Figure 3.4). While pine and larch are comparatively rare in Bolshe Murtinsky, they are the dominant coniferous species in the three studied test areas in Chunsky. Fir, spruce and cedar, which are the main coniferous species in Bolshe Murtinsky, are less common in Chunsky. The majority of the forest stands are natural stands with mixed tree species composition, but the amount of stands with only one species seems to be slightly larger than in Bolshe Murtinsky. Most of these “single-species” stands contain either pine or birch. There are only small differences between the species composition in Chunsky South, North and East.



Leif Eriksson
Friedrich Schiller University
2004-03-10

Figure 3.1 Geographical location of the Bolshe Murtinsky and Chunskey test territories. The satellite frames have been indicated with boxes with the corresponding path/track numbers given at the lower right corner. 157, 158, 163 and 165 are JERS-1 paths and 305, 348 and 491 ERS tracks. The locations of the meteorological stations are marked with triangles.



Figure 3.2 Two examples of natural forest in the Bolshe Murtinsky territory. The left picture shows a dense mixed forest with trees of many different age classes. To the right a stand with mature pine and a few birches. The stems show clear marks of a ground fire.

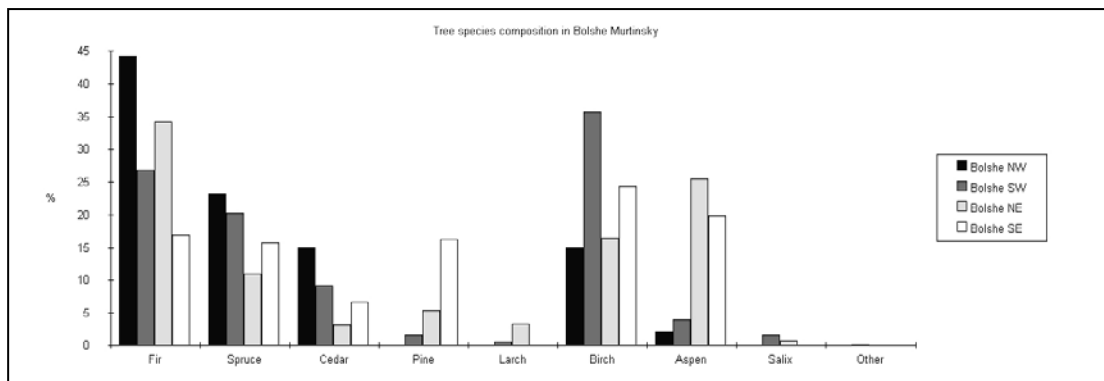


Figure 3.3 Tree species composition in Bolshe Murtinsky.

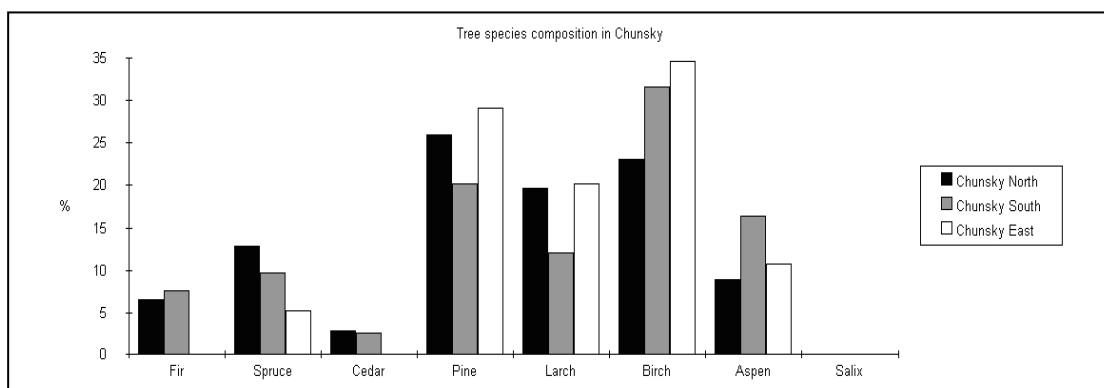


Figure 3.4 Tree species composition in Chunksy.

When the polygons of the Chunskey test territory are superimposed onto the DEM, it can be seen that the shapes of the three test areas have been influenced by the topography and the landscape. Chunskey South basically corresponds to the drainage area of two streams. A few peaks at elevation higher than 400 m can be found around the border of the test site. The average elevation varies between 300 and 350 m, with steep slopes down to a level of 200 m in the stream valleys. Chunskey North is situated between two streams. The range of elevations is similar to Chunskey South, with peaks above 400 m in the northwest corner and deep stream valleys, but the slopes down to the streams are less steep and the landscape is slightly gentler. The northern boarder of Chunskey East is the river Karabola and in the west it follows the railroad that crosses the landscape in north-south direction. The elevation of the test area slowly rises from 200 m along the river to almost 400 m in the south.

Table 3.1 Characteristics of the four test areas in the Bolshe Murtinsky test territory. The columns “Database” refer to all available stands in the ground truth database, and the columns “Used” to the stands that were used in the analysis, i.e. after removal of small stands. The total area and mean size for the stands in the column “Used” are the sizes before edge erosion.

	Bolshe-Murtinsky Northwest		Bolshe-Murtinsky Southwest		Bolshe-Murtinsky Northeast		Bolshe-Murtinsky Southeast	
	Database	Used	Database	Used	Database	Used	Database	Used
Area [km ²]	294	143	262	173	276		209	96
Stands	1259	242	544	156	1605	0	963	170
Mean size [ha]	23	59	48	111	17		22	56
Natural stands [%]	90	83	92	93	91		88	97
Min [m ³ /ha]	0	0	0	0	0		0	0
Max [m ³ /ha]	470	410	470	470	450		410	380
Mean [m ³ /ha]	236	234	175	143	188		185	192
Std. Dev [m ³ /ha]	102	103	104	115	98		78	77

Table 3.2 Characteristics of the three test areas in the Chunskey test territory. The columns “Database” refer to all available stands in the ground truth database, and the columns “Used” to the stands that were used in the analysis, i.e. after removal of small stands. The total area and mean size for the stands in the column “Used” are the sizes before edge erosion.

	Chunskey North		Chunskey South		Chunskey East	
	Database	Used	Database	Used	Database	Used
Area [km ²]	387	255	312	193	364	194
Stands	1226	396	890	290	1019	253
Mean size [ha]	32	64	35	67	36	77
Natural stands [%]	81	81	93	91	88	90
Min [m ³ /ha]	0	0	0	0	0	0
Max [m ³ /ha]	470	330	420	370	430	370
Mean [m ³ /ha]	163	150	207	209	141	119
Std. Dev [m ³ /ha]	101	107	77	73	112	113

3.2 Ground data

When methods for estimation of forest parameters with satellite data are developed, it is necessary to have reliable “ground truth” information for the validation of the results. The following sections describe the ground data that were available for the selected test areas.

3.2.1 Russian forest inventory

To identify individual forest stands the Russian forest has been divided in several geographical levels with decreasing spatial extent (SCHMULLIUS, *et al.*, 2001). The lowest level (largest extent) that is relevant in a test territory is the forest district. Each district is sub-divided in kvartals, which are administrative areas ranging in size from 50 to 4000 ha. The kvartal boundaries follow larger natural features like mountains and rivers, when such are available, and are otherwise made up of artificial lines that normally form rectangular boxes. Harvesting usually follows the kvartal boundaries. As a side effect, this allows identification of larger clear-cuts from their shape in remotely sensed imagery. Within a kvartal so called primary inventory units are formed. These should be relatively homogeneous in terms of tree species composition, age, vertical structure, quality and relative stocking. This is the highest level of sub-division, which hereafter, for forested areas, will be referred to as stands.

Depending on forest management requirements, two types of forest inventory are conducted in Russia (SCHMULLIUS, *et al.*, 2001). Remote unmanaged forests are surveyed with satellite images or a multi-stage sampling technique involving air photo transects and ground sample plots. However, about 70 % of the forests are inventoried with the second method, the “Forest Inventory and Planning” (FIP) method, that is used for managed forest. With the FIP method aerial photos at a scale of between 1:10000 and 1:25000 are used for the delineation of stand boundaries. Ground measurements are used to verify the photo interpretation and provide final estimates of the forest variables. Each Russian forest enterprise is supposed to update their FIP surveys every 10-20 years. All test territories from the SIBERIA project, were inventoried with the FIP method. The data from Bolshe Murtinsky and Chunsky were both updated in 1998.

3.2.2 Forest GIS parameters

Information about the forest stands was available in a geographical information system (GIS) database that was created by the International Institute for Applied Systems Analysis (IIASA) and their Russian partners in the SIBERIA project. For each stand there are parameters defining area, land category, relative stocking, growing stock volume, age of dominant species, tree species composition, tree height and diameter. Here follows a short description of each parameter:

Area – Vertical projection of the area as reported in the forest inventory.

Land category – All basic categories for the entire landscape, the most important being natural stand, forest plantation, burned forest, clear-cut areas, agriculture, and bog.

Relative stocking – A comparison of the stocking of a particular stand to the stocking achievable under perfect management conditions.

Growing stock volume – The stem volume for all trees greater than or equal to 6 cm at breast height (1.3 m). In young stands all stems are considered. Expressed in m³/ha.

Age – Age of the dominant species expressed in years.

Composition – Percent of the growing stock of the trees in the main canopy layer that belong to the specified tree species. Given separately for all main tree species.

Height – Estimate of the average tree height of the dominant species in a stand.

Diameter – Estimate of the average tree diameter of the dominant species. The diameter is measured at breast height.

Of these parameters only area, land category, growing stock volume and composition could be used. The relative stocking would require information about, e.g. site quality and yield table to make it possible to relate it to basal area, percent cover or density. The problem with the parameters age, height and diameter are that they are given for the dominant species and not for the entire stand. The dominant species is not dominant by number, but by economic value. Cedar has the highest value, followed by pine, and deciduous species have the lowest value. When cedar trees are present in a stand, the age of the stand is given for the cedars, regardless of their percentage in the stand (SCHMULLIUS, *et al.*, 2001).

As can be seen in Table 3.1 and 3.2, about 90% of all stands in the Bolshe Murtinsky and Chunsky test territories are classified as natural stands, i.e. “stands of growing trees resulting from natural regeneration following a forest disturbance”. This disturbance can, e.g. be a stand replacing fire or a clear-cut. These stands have relative stocking greater than or equal to 10 % for young age groups and greater than or equal to 30 % for all other age groups. The classes burned forest and clear-cut areas both have relative stockings of less than 10 %.

3.2.3 Digital elevation models and topographic maps

For the geometric and radiometric correction of the radar images a DEM is required. It is not possible to get DEMs directly from Russia since these are guarded by strict national security regulations. From the USGS the GTOPO30 is available. This is a DEM with global coverage, but the spatial resolution of 30 arc seconds corresponds to a grid size of only 1000 m in latitude and, at 60° N, 500 m in longitude. For correction of satellite images with 25 m pixel size this resolution is generally too coarse. During 11 days in February 2000 the US space shuttle flew the SRTM

mission, with the goal to collect single-pass interferometric SAR data that could be used to produce a DEM covering about 80% of the Earth landmass. Since the beginning of 2004 this DEM is available for Siberia (up to 60° N) at approximately 90 m resolution, but this was too late for the processing of the images that have been used in this study.

Instead of the above-mentioned alternatives, DEMs that were produced from repeat-pass interferometric SAR data from the ERS-1/2 tandem mission have been used. For Bolshe Murtinsky such DEMs were available from the SIBERIA project (SCHMULLIUS, *et al.*, 2001). They were produced by DLR and were available at 50 m horizontal resolution. However, InSAR DEMs could only be generated for 48 of the 122 ERS frames that were needed to cover the SIBERIA project area. Unfortunately the three test areas in Chunksky were not covered by InSAR DEMs, since the coherence between the available ERS scenes had been too low. A search in the ESA archives revealed that a tandem pair had been acquired over the area by the receiving station in Beijing in January 1996. This pair was ordered, delivered and processed to a DEM at FSU-Jena during 2001.

For the generation of InSAR DEMs, control points are needed to fix the unwrapped interferogram to real altitudes. These control points were taken from Russian topographic maps at 1:200000 scale that were available at DLR.

3.3 Satellite image data

Data from three different radar satellites have been used in the study. These three are the Japanese JERS-1 and the two European satellites ERS-1 and ERS-2. The main reason for focusing on the JERS-1 data was that less work has been done on L-band interferometry than on C-band interferometry, but the availability of suitable data was also an important factor. In 1997 and 1998 the Global Boreal Forest Mapping (GBFM) project and the SIBERIA project ensured that a large number of JERS-1, ERS-1 and ERS-2 images were acquired over central Siberia. These projects were the first efforts to get a complete and consistent coverage of this region. Before that, a few ERS-1/2 scenes had been acquired by the receiving station in Beijing during the tandem mission phase that lasted from August 1995 to June 1996. JERS-1 had the advantage of having an onboard data recorder that made it possible to record data from anywhere in the world and later download it to a receiving station. This might be one reason to why there exist more JERS-1 data than ERS-1/2 data from Bolshe Murtinsky and Chunksky. JERS-1 data are available as early as 1993. The ERS-1/2 data have been included in the study in order to allow a comparison between L-band and C-band coherence. To get comparable temporal baselines, 35-day repeat-pass pairs from either ERS-1 or ERS-2 would have been required, but unfortunately no 35-day pairs were available from the winter season. As will be shown in Chapter 4, the winter season is the most suitable for repeat-pass coherence with long temporal baselines.

A listing of the analysed JERS-1 and ERS-1/2 data is given in Table 3.3 and Table 3.4 respectively. Figure 3.1 shows the coverage of the satellite frames with respect to the test areas in Bolshe Murtinsky and Chunksky. A number of scenes from JERS-1 paths and ERS-1/2 tracks adjacent to those listed in Table 3.3 and Table 3.4 have been left out of the study, because i) they did not completely cover any test area, ii)

the image quality was too low, iii) the acquisition date duplicated acquisitions from the analysed tracks, and would thereby not add any additional information. The processing of the SAR data is described in Section 2.4.

Table 3.3 Available JERS-1 44-day pairs

First date	Second date	GRS Path	Baseline perpendicular [m]	Test site
1994-01-06	1994-02-19	165	1752	Bolshe Murtinsky
1996-10-14	1996-11-27	165	705	Bolshe Murtinsky
1996-11-27	1997-01-10	165	844	Bolshe Murtinsky
1997-01-10	1997-02-23	165	1875	Bolshe Murtinsky
1997-02-21	1997-04-06	163	2091	Bolshe Murtinsky
1997-02-23	1997-04-08	165	1212	Bolshe Murtinsky
1997-04-06	1997-05-20	163	374	Bolshe Murtinsky
1997-05-20	1997-07-03	163	>7000	Bolshe Murtinsky
1997-07-03	1997-08-16	163	970	Bolshe Murtinsky
1998-06-22	1998-08-05	165	208	Bolshe Murtinsky
1993-12-29	1994-02-11	157	550	Chunsky
1995-10-20	1995-12-03	157	1947	Chunsky
1995-12-03	1996-01-16	157	3	Chunsky
1995-12-04	1996-01-17	158	106	Chunsky
1996-01-16	1996-02-29	157	319	Chunsky
1996-01-17	1996-03-01	158	509	Chunsky
1997-04-01	1997-05-15	158	27	Chunsky
1998-06-14	1998-07-28	157	1108	Chunsky

Table 3.4 ERS pairs covering Bolshe Murtinsky and Chunsky.

First date	Second date	Track	Baseline perpendicular [m]	Test site
1996-01-01	1996-01-02	305	146	Bolshe Murtinsky
1997-09-22	1997-09-23	305	270	Bolshe Murtinsky
1997-09-25	1997-09-26	348	231	Bolshe Murtinsky
1997-10-27	1997-10-28	305	174	Bolshe Murtinsky
1998-05-28	1998-05-29	348	306	Bolshe Murtinsky
1996-01-14	1996-01-15	491	64	Chunsky
1997-10-05	1997-10-06	491	239	Chunsky
1998-06-07	1998-06-08	491	327	Chunsky

3.3.1 Bolshe Murtinsky

Bolshe NW and SW are covered by the JERS-1 ground reference system (GRS) path 165, row 204 and 205, and ERS-1/2 track 348, frame 2457. The two JERS-1 frames have been mosaicked together and will hereafter only be referred to as path 165. For this path a time series including five consecutive passes from October 1996 to April 1997 has been acquired. Together with the 44-day pair from the summer 1998, this provided good possibilities to study seasonal differences, which will be analysed in Section 4.1. In addition, a 44-day pair from January/February 1994 allowed an analysis of interannual differences. From track 348, two ERS-1/2 tandem pairs were available.

Bolshe NE and SE are covered by GRS-path 163, row 204 and 205, and these will be denoted path 163. Also in this case a time series containing five consecutive passes was available, but the covered period stretches from February to August 1997. The series could have been even longer, since the acquisition from November 1996 is also available, but unfortunately the pass from January 1997 is missing. The usefulness of the time series is also limited by the fact that a shift in the JERS-1 orbit occurred sometime between the acquisition in May and July, giving a spatial baseline of over 7 km. An additional problem is that the delivered August scenes show serious artefacts in the form of broad bands that cross the images. One of these bands passes over Bolshe NE, making it impossible to get any useful information from this test area.

As can be seen in Figure 3.1, the ERS-1/2 frames from track 348 and 305 are positioned so that Bolshe NE and SE are partly contained in the overlapping area between the frames. Bolshe SE is not 100 % covered by any of the two frames, and Bolshe NE is only fully covered by the frame from track 305.

3.3.2 Chunsky

Two JERS-1 paths have been used to cover the three test areas in the Chunsky territory. Chunsky South and North are situated within GRS-path 158. Row 203 and 204 have been mosaicked together and will be referred to as path 158. From path 157 it was enough to order row 203 to cover Chunsky North and about 90 % of Chunsky East. The data from path 157 included four consecutive passes from October 1995 to February 1996, and for path 158 three consecutive passes have been acquired in the period from December 1995 to February 1996. In addition a number of single 44-day pairs from different seasons were available. The ERS-1/2 coverage consisted of three tandem pairs from track 491, frame 2439. All three pairs were from different years and different seasons. Only about 70 % of Chunsky East was covered by this frame.

3.4 Meteorological data

For the interpretation of SAR images and derived products it is essential to have access to meteorological data. The World Meteorological Organization (WMO) has a network of weather stations all over the world that report a number of meteorological parameters on a regular basis. During the SIBERIA project data from all stations in

the project area were ordered from the German weather service (DWD) for September and October 1997 and May to August 1998. To cover the SAR acquisitions that were done before September 1997, additional data were ordered in 2002 for the stations that are located closest to Bolshe Murtinsky and Chunsky. The location of the stations in relation to the test areas can be seen in Figure 3.1. The meteorological data that were provided include air temperature, wind speed, precipitation, snow depth, dew point, and cloud cover.

3.4.1 Bolshe Murtinsky

Of the available WMO stations, seven are located within 100 km distance from at least one of the test areas in the Bolshe Murtinsky territory. Three of these, Pirovskoje, Bolshaja Murta and Suhobuzimskoje, are within 50 km from one of the test areas, but only Bolshaja Murta is within 50 km distance from all four test areas. The most important meteorological observations from the station in Bolshaja Murta are given in Table 3.5 for the dates with JERS acquisitions, and in Table 3.6 for the ERS dates. In general there are no big differences between the observations from Bolshaja Murta and the other six stations. From 1994 no observations were available from DWD for any of the seven stations. To fill this gap data from Bolshaja Murta were taken from the Weather Underground web site (www.wunderground.com). These data were only available on a daily basis.

For Bolshaja Murta DWD provided measurements from four daily observations, made at 0:00 Universal Time Coordinated (UTC), 6:00 UTC, 12:00 UTC and 18:00 UTC. The temperature and wind speed measurements that are reported in Table 3.5 and Table 3.6 are from the 6:00 measurement, since the JERS and ERS satellites passed over the studied region at approximately 4:30 UTC (11:30 official Russian time zone; 10:30 local solar time) for descending passes. No ascending passes have been used.

3.4.2 Chunsky

The network of WMO reporting stations was much sparser around Chunsky than around Bolshe Murtinsky. Only the station in Boguchany was located within 50 km distance from any of the test areas in the territory. The station in Dzerzhinskoje was situated approximately 100 km from Chunsky South, but from DWD observations from this station were only available after August 1996. The data set from Boguchany contained observations from the whole period between January 1993 and October 1997, and from May to August 1998. Until August 1996 four daily observations were recorded. After that the reporting frequency was doubled, giving observations every third hour. The observations from Boguchany are given in Table 3.7 for the dates with JERS acquisitions, and in Table 3.8 for the ERS dates. As explained in the previous section about Bolshe Murtinsky, all given temperature and wind speed measurements are from the 6:00 UTC observations. A more detailed analysis of the meteorological observations and their influence on the SAR acquisitions will be given in Section 4.1.

Table 3.5 Weather conditions at the JERS acquisitions over Bolshe Murtinsky.
Weather station: Bolshaja Murta.

Dates	Temp. [°C]	Wind speed [m/s]	Snow depth [cm]	Comments	Max/min temperature between acquisitions [°C]
1994-01-06 1994-02-19	-17 -17	2 2	39 49	Snowfall Light snowfall	1994-01-27: -3 1994-01-08: -36
1996-10-14 1996-11-27	+9 -22	2 2	0 27	Light snowfall	1996-10-14: +11 1996-11-11: -31
1996-11-27 1997-01-10	-22 -19	2 1	27 42	Light snowfall	1997-01-08: +2 1996-12-29: -39
1997-01-10 1997-02-23	-19 -16	1 3	42 54	Light snowfall	1997-02-20: +3 1997-01-12: -37
1997-02-21 1997-04-06	-1 +6	3 3	53 0	+3.5°C the day before Snowmelt	1997-04-04: +12 1997-02-26: -34
1997-02-23 1997-04-08	-16 +13	3 1	54 0	Light snowfall Snowmelt	1997-04-07: +15 1997-02-26: -34
1997-04-06 1997-05-20	+6 +26	3 2	0 0	Snowmelt	1997-05-07: +24 1997-05-03: -6
1997-05-20 1997-07-03	+26 +20	2 1	0 0		1997-05-21: +30 1997-06-04: 0
1997-07-03 1997-08-16	+20 +23	1 3	0 0	Heavy rain 2 days earlier	1997-07-12: +31 1997-08-14: +5
1998-06-22 1998-08-05	+10 +21	1 2	0 0	Rainfall Heavy rain the day before	1998-06-22: +2 1998-07-06: +28

Table 3.6 Weather conditions at the ERS acquisitions over Bolshe Murtinsky.
Weather station: Bolshaja Murta.

Dates	Temp. [°C]	Wind speed [m/s]	Snow depth [cm]	Comments
1996-01-01 1996-01-02	-22 -23	3 1	Unknown Unknown	Light snowfall Snowfall
1997-09-22 1997-09-23	+17 +19	1 1	0 0	Rain the day before
1997-09-25 1997-09-26	+19 +12	1 1	0 0	
1997-10-27 1997-10-28	+2 0	0 0	Unknown Unknown	Frozen at night Frozen at night
1998-05-28 1998-05-29	+26 +19	1 1	0 0	

Table 3.7 Weather conditions at the JERS acquisitions over Chunksy. Weather station: Boguchany.

Dates	Temp. [°C]	Wind speed [m/s]	Snow depth [cm]	Comments	Max/min temperature between acquisitions [°C]
1993-12-29 1994-02-11	-13 -13	3 4	27 45	Snowfall Light snowfall	1994-02-01: -4 1994-01-16: -44
1995-10-20 1995-12-03	0 -15	4 0	- 19	Freezing Light snowfall	1995-10-23: +10 1995-11-21: -22
1995-12-03 1996-01-16	-15 -23	0 0	19 27	Light snowfall Light snowfall	1995-12-18: -3 1996-01-11: -43
1995-12-04 1996-01-17	-17 -20	0 1	17 27		1995-12-18: -3 1996-01-11: -43
1996-01-16 1996-02-29	-23 -5	0 3	27 31	Light snowfall	1996-02-21: -4 1996-01-28: -37
1996-01-17 1996-03-01	-20 -3	1 4	27 31	Light snowfall	1996-03-17: -3 1996-01-28: -37
1997-04-01 1997-05-15	+7 +11	3 2	17 0	Rapid snowmelt	1997-05-07: +21 1997-04-19: -5
1998-06-14 1998-07-28	+16 +18	5 0	0 0	Rain Rain the day before	1998-07-01: +30 1998-06-19: +4

Table 3.8 Weather conditions at the ERS acquisitions over Chunksy. Weather station: Boguchany.

Dates	Temp. [°C]	Wind speed [m/s]	Snow depth [cm]	Comments
1996-01-14 1996-01-15	-19 -24	2 0	27 27	Snowfall Light snowfall
1997-10-05 1997-10-06	+6 +5	1 1	0 0	Rain between acquisitions
1998-06-07 1998-06-08	+15 +20	1 2	0 0	Rain the day before

Chapter 4

Decorrelation analysis

In Chapter 2 causes for decorrelation of the interferometric coherence were listed. In this chapter the main causes for decorrelation of the available JERS-1 repeat pass coherence will be analysed. Temporal decorrelation will be handled in two sections; one focused on the environmental conditions at and between the acquisition dates, and one on the temporal baseline. Spatial decorrelation will be examined in a separate section and finally a comparison with C-band data will be made.

4.1 Environmental conditions

In the following analysis we will only consider natural forest stands with a size of 5 ha (20 pixels) or more. As can be seen in Table 3.1 and Table 3.2, at least 80 % of all stands are classified as natural stands, and in four out of six test areas the percentage natural stands is at least 90%. For sparse forest a portion of the signal originates from the ground. To allow an evaluation of the effect canopy density has on the temporal decorrelation, coherence values will be given both for sparse and dense forest. Values for sparse forest represent stands with growing stock volumes in the range 5 to 25 m³/ha, and dense forest 280 to 470 m³/ha.

4.1.1 Temperature

The critical point when considering the influence of temperature is if the SAR data were acquired at temperatures above or below the freezing point. Since frozen water has a dielectric constant much lower than fluid water, the dielectric constant of trees and soil changes and thereby also the strength of the signal scattered back. At L-band it has been shown that the backscattering coefficient at HH-polarization is less affected by thawing/freezing than the VV- or HV-polarizations, but still gives a change of 0.4 to 2.5 dB for forest stands (WAY, *et al.*, 1990; RANSON & SUN, 2000).

When analysing repeat pass coherence it is necessary to consider the temperatures at both acquisitions. The temperatures between the acquisitions will only influence the coherence indirectly. In winter and spring composition and properties of the snow layer will be affected by the temperatures, especially thawing and freezing events, and the snow show a historical record for the temperatures during the whole winter. This will mainly affect volume scattering at shorter wavelengths, but as mentioned in

Section 2.2.3, L-band shows no significant volume scattering from snow. For coherence from the summer the temperatures between the acquisitions should have less influence, but during a period without rain higher temperatures will reduce the water content in ground and in forest canopy faster than lower temperatures.

Temperatures at the acquisitions and the temperature extremes in the period between the acquisitions are given in Table 3.5 and Table 3.7. To allow a more detailed analysis the complete temperature records for two periods covering the majority of the available JERS-1 acquisitions are displayed in Figure 4.1 (Bolshe Murtinsky) and Figure 4.2 (Chunsky). For Bolshe Murtinsky the acquisition in October was done during a period of frequent fluctuations around zero degrees. After that the temperatures stayed well below the freezing point, with a few short exceptions. It should be noted that the acquisitions on 25 November, 10 January and 21 February were done shortly after days with temperatures around zero. In the beginning of March 12 days of measurements are missing, and after that the thawing period has started. Both acquisitions from April were made during the thawing period. From mid May the temperatures are constantly above zero. The temperature curve from Boguchany, north of Chunsky, only displays values until March, since no more SAR acquisitions are available from that year. The trend is similar to the one recorded in Bolshaja Murta a year later. The temperatures fluctuate around the freezing point in October, then decrease to values constantly below zero from December to March when the average temperatures start rising again.

In Figure 4.3 the temperatures at the acquisitions have been plotted against the corresponding coherence values. Image pairs where one of the acquisitions was done at temperatures above zero and the other at temperatures below zero consistently show very low coherence values both for sparse and dense forest stands. In addition, three pairs where the lowest temperature is around 7° C have low coherence. A closer look at the data reveals that all these pairs are from April-May. For the February-April pair covering Bolshe NW and Bolshe SW the differences between the two SLC images were large enough that the normal coregistration procedure failed and no coherence estimation could be performed. This has been indicated with a zero coherence value in the figures. In sparse forest we find that for pairs where both acquisitions were done at temperatures below the freezing point the coherence in general is high. A single exception is found for the pair 27 November – 10 January where the coherence for Bolshe SW is as low as 0.21. The coherence for Bolshe NW from the same pair is considerably higher (0.38), and a visual inspection of the coherence image confirms that a large region in the south is affected by local decorrelation. The weather stations are too sparsely distributed to allow a study of local phenomena, but it is unlikely that the temperature should be 20 degrees higher in Bolshe SW than at the weather station in Bolshaja Murta. In the following sections it will be analysed if other environmental conditions can explain this discrepancy.

In Table 3.5 and 3.7 occurrence of snowmelt, rain and snowfall has been indicated in the comments column. The effect of freezing, thawing and precipitation on the coherence is illustrated in Figure 4.4. All JERS-1 pairs where thawing or freezing occurred between the acquisitions show very low coherence. The difference between sparse and dense forest becomes so low that no information about forest density can be derived from the coherence images. Thawing is the only environmental condition where the mean coherence from sparse forest is not higher than for dense forest. The effects of precipitation will be analysed in the following section.

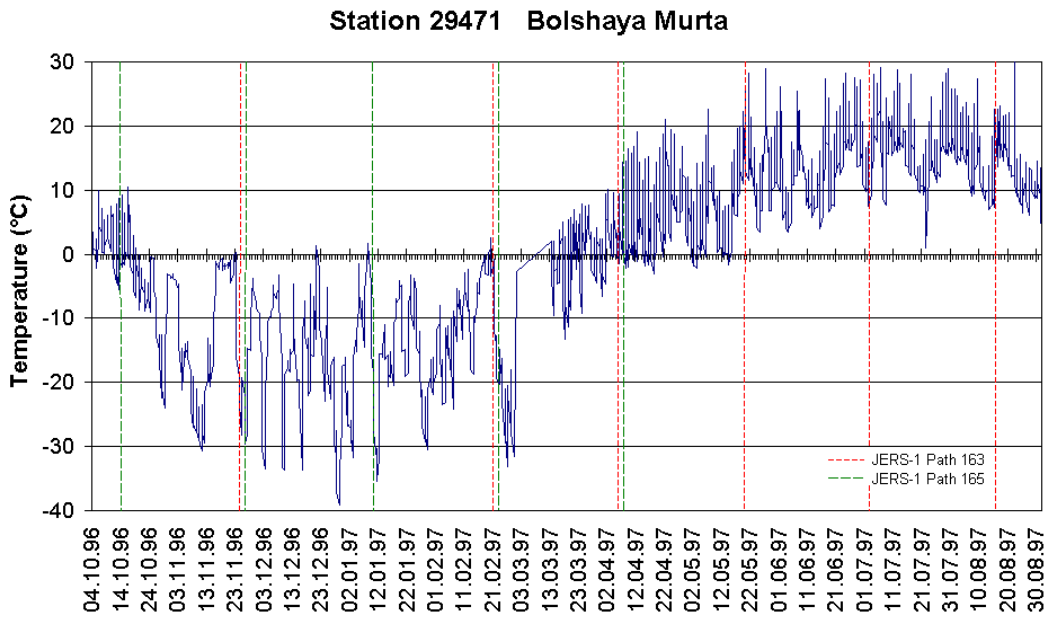


Figure 4.1 Temperatures registered between 4 October 1996 and 30 August 1997 at the weather station in Bolshaja Murta. No data was reported between 1 and 13 March 1997.

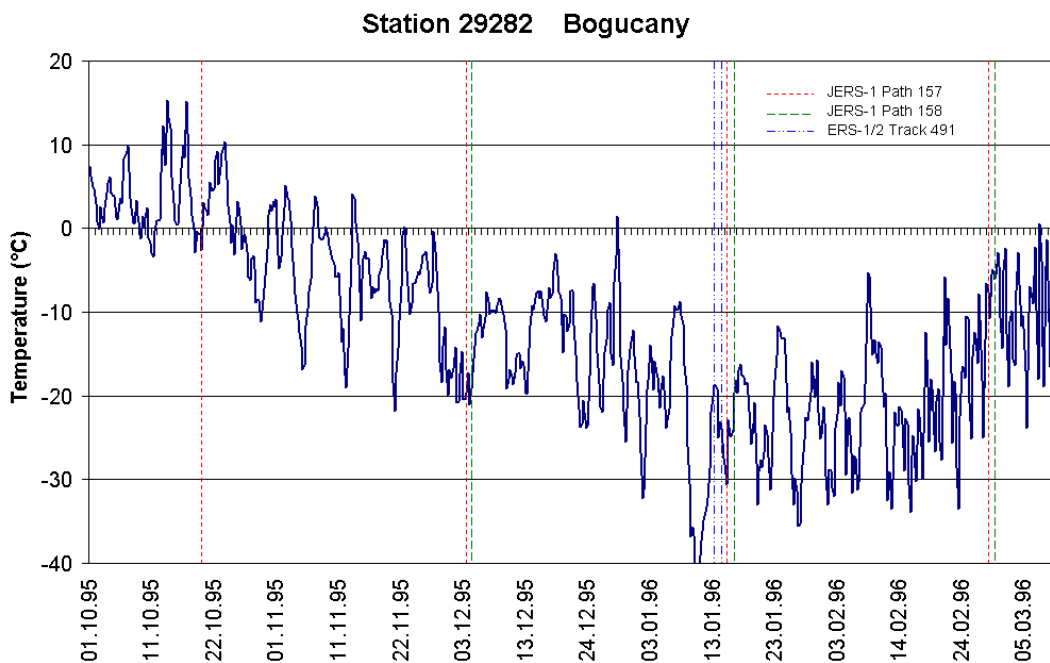


Figure 4.2 Temperatures registered between 4 October 1996 and 30 August 1997 at the weather station in Boguchany.

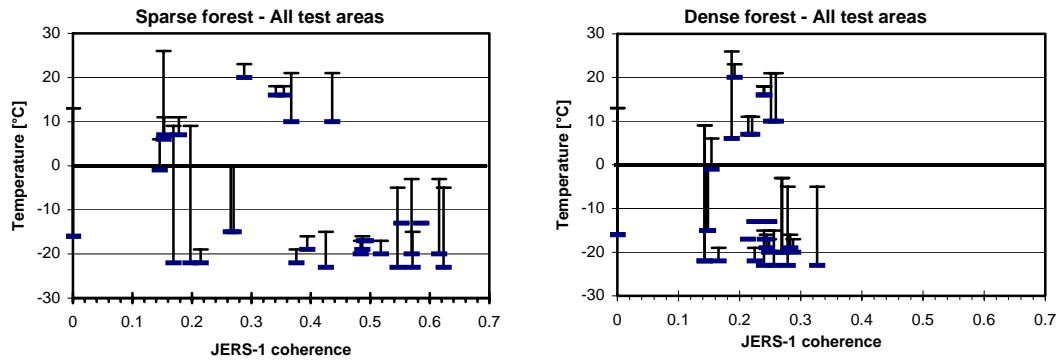


Figure 4.3 Coherence plotted against temperature. For each coherence pair the temperatures at both acquisition dates are given and connected with a vertical line.

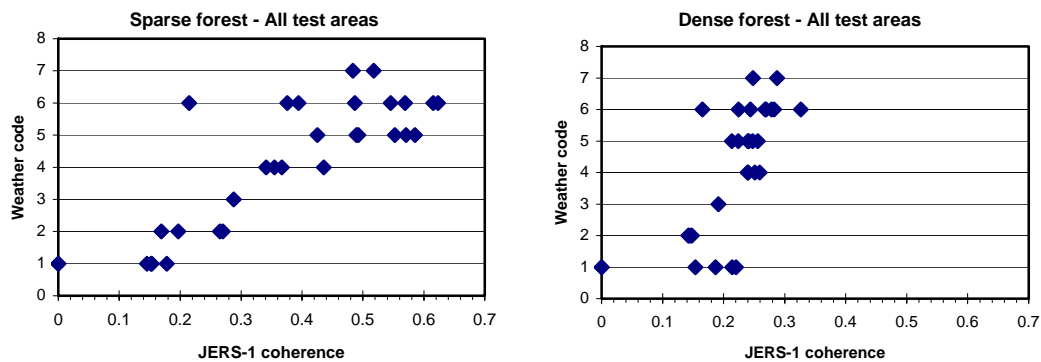


Figure 4.4 Coherence for different weather conditions. Weather code: 1 = thaw, 2 = freeze, 3 = rain at one of the acquisitions, 4 = rain at both acquisitions, 5 = snowfall at both acquisitions, 6 = snowfall at one acquisition, 7 = Frozen, but no precipitation, freezing, or thawing.

4.1.2 Precipitation and moisture

At temperatures above the freezing point precipitation will be in the form of rain, which affects the dielectric constant of the ground, and with some delay also of the forest canopy. At L-band and HH-polarization rain has been reported to give an increase in the backscattering coefficient from forest of 0-2 dB (BERGEN *et al.*, 1997). The coherence depends on the differences in soil moisture and tree water content between the two acquisitions. Similar conditions at both acquisitions will have little influence on the coherence, but if one acquisition was made under dry conditions and the other during or shortly after heavy rain this should have a decorrelating effect. To allow a detailed analysis of how rain affects the coherence it would be required to have measurements of soil moisture and the dielectric constant of the trees. Such measurements have been done in large multidisciplinary projects like the Boreal Ecosystem-Atmosphere Study (BOREAS) in Canada (SELLERS *et al.*, 1997; McDONALD, *et al.*, 1999) and the Northern Hemisphere Climate-Processes Land-Surface Experiment (NOPEX) in Sweden (HALLDIN *et al.*, 1999; KRAVKA, *et al.*, 1999), but are not available for the acquisitions that are analysed in this thesis.

Snow has a dielectric constant that is considerably lower than water. Snowfall will therefore influence the observed dielectric constant less than rain. For L-band the main backscatter contribution comes from the snow-ground interface. If small

amounts of dry snow fall on a surface already covered by snow, this should have little or no influence on the backscatter or coherence. However, if the ground is still not frozen and no snow layer is present, falling snow is likely to melt, which will give an increase in the dielectric constant. In the same way as with rain, the conditions at the other SAR acquisition will determine what effect this will have on the coherence.

Figure 4.4 shows that only one JERS-1 pair where one of the acquisitions had been affected by rain was available. The coherence for this pair is low both for sparse and dense forest. Four coherence images, from two pairs covering two test areas, were affected by rain at both acquisitions. The coherence in all these cases is higher than for the pair with one rainy day. For sparse forest the observed coherence is in the range between 0.3 and 0.45, so it is likely that also in this case the rain had a decorrelating effect. About half of all pairs were affected by snowfall. The coherence is in general high, and the only difference that can be observed between pairs where one or both of the acquisitions had snowfall is that the spread between the minimum and maximum coherence values is larger for pairs where only one acquisition had snowfall. In this group we also find the coherence from Bolshe SW from 27 November – 10 January that already in Section 4.1.1 was identified as a very low value that does not fit with the overall trend. Considering the long wavelength it is unlikely that even local heavy snowfall could cause the large difference in coherence between Bolshe NW and Bolshe SW. The coherence from Chunksy South and Chunksy North from the 4 December – 17 January pair are the only values that are not affected by rain, snowfall, freeze or thaw. It should be noted that several of the pairs that were affected by snow show higher coherence values. This indicates that there are other factors that have stronger decorrelating effects than snowfall.

The results can be summarized by rating the weather conditions after their decorrelating effect. For sparse forest thawing seems to give the most severe decorrelation, followed by freezing, rain at one of the acquisitions, rain at both acquisitions, and finally snowfall. For dense forest there are no significant differences between the groups, even though freezing appears to give the strongest decorrelation. It has to be noticed that for the group with rain at one of the acquisitions and for pairs without precipitation, freeze or thaw, the available measurements were too few to derive a general trend for the L-band coherence from stands with natural boreal forest.

4.1.3 Snow cover

As was mentioned in Section 2.3.4, a blanket of snow over the tree branches can alter the geometry of the scatterers, but at the same time reduce their possibilities to move. How strong this effect is depends on tree type and how wet and heavy the snow is. It should also be noted that dry snow is light and easily falls off the branches if they are moved by wind. It can therefore not be assumed that a snow cover on the ground automatically means there is snow on the trees. Wet snow that falls during the freezing period in October/November, or in periods of temporary warmer temperatures during the rest of the winter, should have a stronger decorrelating effect than dry snow that falls during cold periods.

The only information that was available about the snow conditions at the SAR acquisitions was the snow depth that was recorded at the weather stations. In Figure 4.5 the snow depth at both acquisitions in the JERS-1 pairs have been plotted against the corresponding coherence values. The pairs where one of the acquisitions was made without snow cover and the other with snow show the lowest coherence. These correspond to the freezing and thawing events discussed above. For sparse forest the pairs that had a significant snow cover at both acquisitions have coherence considerably higher than the ones where one acquisition was made without snow. Also in this case the November/January coherence from Bolshe SW does not follow the general trend, having a low coherence even though a thick snow layer was present at both acquisitions. It is not likely that local differences in the snow depth between Bolshe NW and Bolshe SW cause the big difference in coherence.

The plots in Figure 4.5 also make it possible to check if there exists a relationship between the degree of coherence and the difference in snow depth for the acquisitions. We find that the pairs with the smallest differences in snow depth all have high coherence, but apart from that no clear trends can be found.

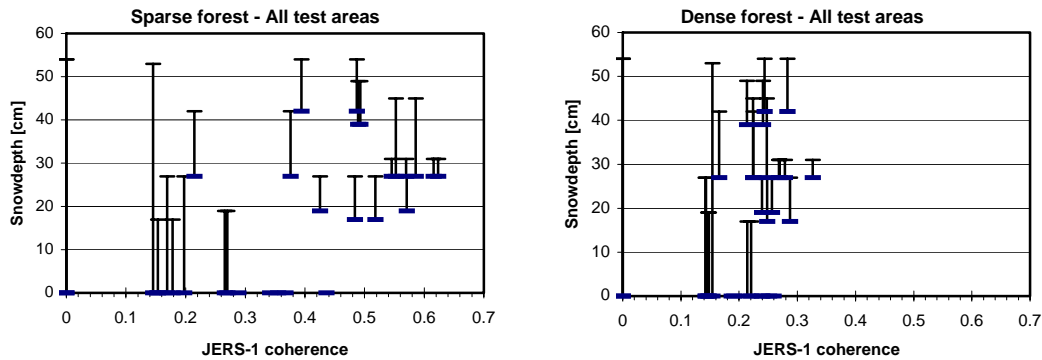


Figure 4.5 Coherence plotted against snow depth. For each coherence pair the snow depth at both acquisition dates are given and connected with a vertical line.

4.1.4 Wind

For repeat-pass coherence with short revisit times wind is assumed to be one of the main causes for temporal decorrelation. Wind will affect the orientation of the scatterers, and to some extent also their positions relative to each other. Assuming that the scatterers will return to their original orientations as soon as there is no wind, the decorrelating effect should neither increase nor decrease for SAR systems with a longer repeat cycle. Compared to C-band, the main scattering elements at L-band are larger and more stable. It can therefore be expected that L-band coherence is less sensitive to wind.

Wind speed is a parameter that can change rapidly both spatially and over time. The wind speed measurements that were available for our analysis were mean values over 10 minutes and even if we choose the measurement that was made closest in time to our SAR acquisition there will be at least one hour difference. It is also not possible to know if local wind gusts at the moment of the acquisition have affected the backscattered signal. This and the distance between the test areas and the meteorological stations make it questionable how relevant these wind measurements are. For completeness of the analysis the measured wind speeds have been plotted

against the coherence in Figure 4.6, but the mentioned uncertainties must be kept in mind when trying to interpret the data. It can be noted that none of the acquisitions experienced strong wind, but apart from this no clear trends can be found in the plots.

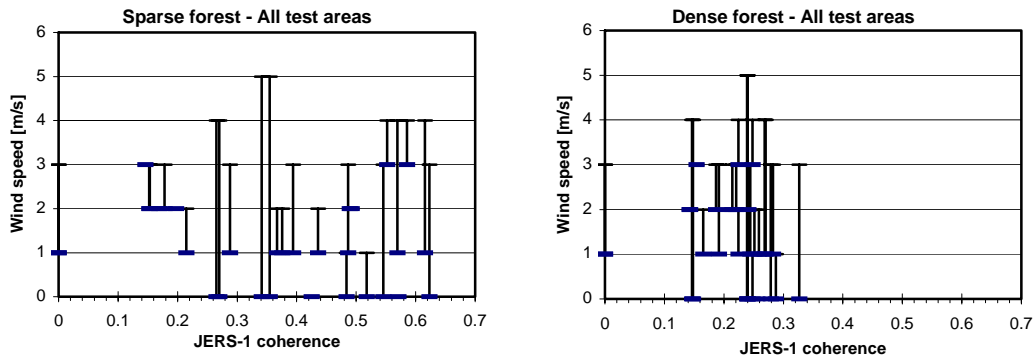


Figure 4.6 Coherence plotted against wind speed. For each coherence pair the wind speed at both acquisition dates are given and connected with a vertical line.

4.1.5 Seasonal variations

Some of the environmental parameters that have been described above vary with the season. To get an overview over how the level of coherence changes over the year, the coherence values and their standard deviations have been plotted against the corresponding acquisition dates. Figure 4.7 shows the values for sparse and dense forest in the three studied test areas in Bolshe Murtinsky and Figure 4.8 gives the values from Chunskey. The largest seasonal differences are found for sparse forest, where coherence values are found in the whole range between 0.15 and 0.62. The variations for dense forest are more moderate and, with one single exception, the values stay between 0.15 and 0.30. In Chunskey East the pair 16 January and 29 February 1996 reaches a mean coherence of 0.33 for dense forest.

Figure 4.4 shows that freezing give the lowest coherence for dense forest and thawing the lowest for sparse forest. These events occur for pairs where one of the acquisitions was made in October (freezing), or April (thawing). The observations are in correspondence with occurrence of freezing and thawing in the temperature curves in Figure 4.1 and 4.2. For all pairs with one acquisition in April the upper curves in Figure 4.7 and Figure 4.8 temporarily cross the lower ones. This indicates that the coherence during thawing is lower for sparse forest than for dense forest.

Five of the six test areas have been covered with JERS-1 pairs acquired in the summer. For dense forest the coherence values are at approximately the same level as for the winter pairs, but with larger standard deviations. For sparse forest the summer-pair from Chunskey show low coherence values in the range between those recorded for freezing and winter values. The standard deviations are comparable to the ones from all other seasons. The summer-pair from Bolshe SE shows a mean coherence and standard deviation that are slightly lower than those observed in Chunskey. The highest coherence from sparse forest in the summer is found at Bolshe NW, but here we also find the largest standard deviations.

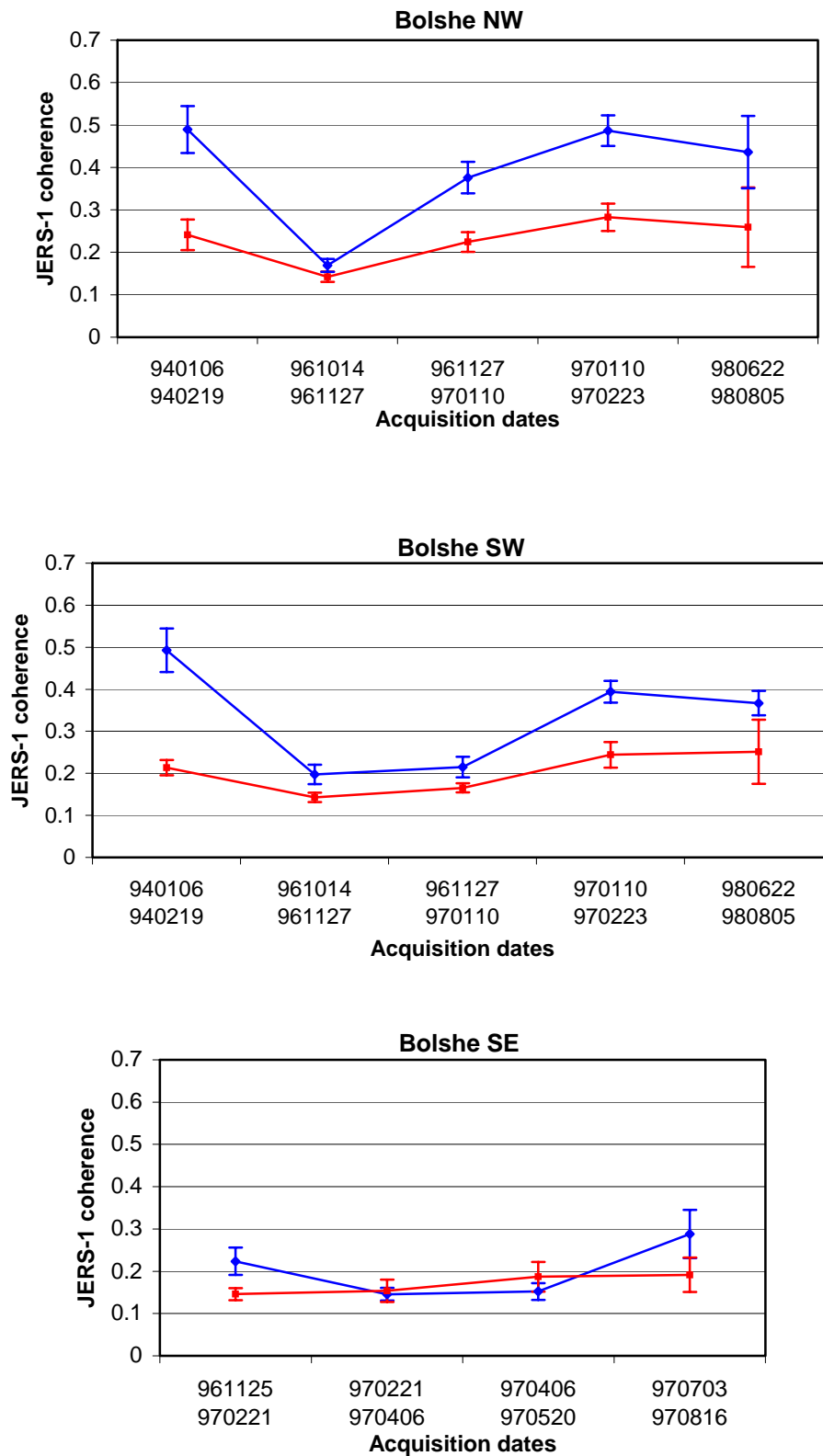


Figure 4.7 Coherence for all acquisition dates from the test areas in Bolshe Murtinsky. The upper curves give the mean coherence values for sparse forest and the lower curves for dense forest. The error bars represent +/- one standard deviation.

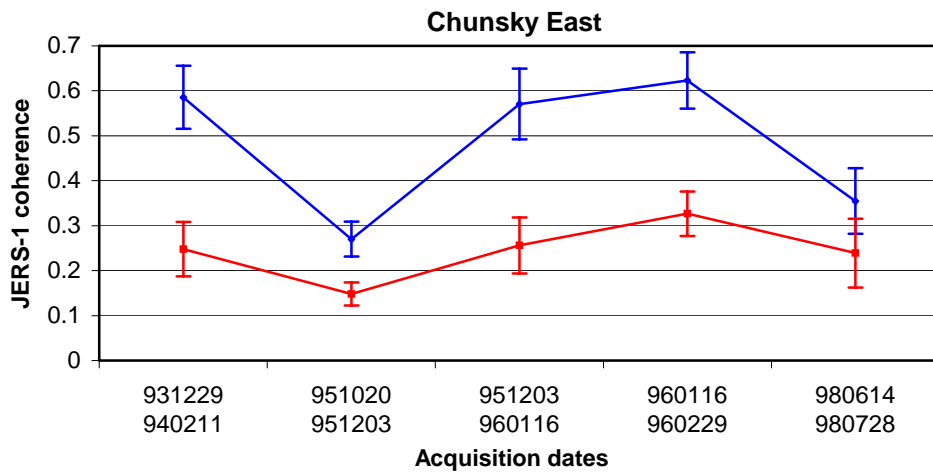
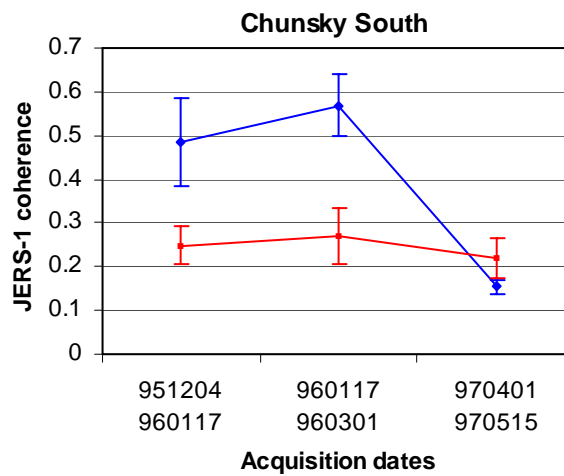
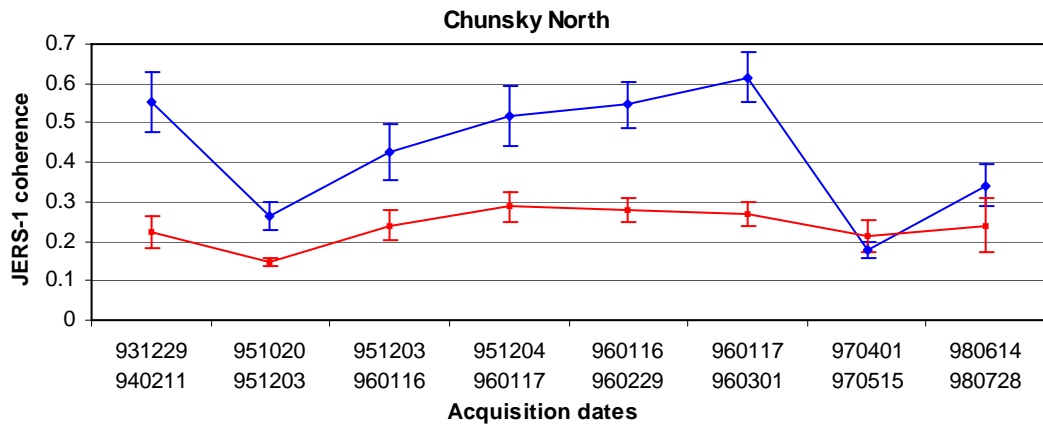


Figure 4.8 Coherence for all acquisition dates from the test areas in Chunsky. The upper curves give the mean coherence values for sparse forest and the lower curves for dense forest. The error bars represent +/- one standard deviation.

The general trend for the winter pairs is that the coherence increases with the time that has past since the freezing, and continues to increase until the thawing period starts. This trend indicate that even though the average daily temperatures in this region go below zero sometime in the beginning of November, the forest, as observed by L-band at HH-polarization, will continue to stabilize with time.

When comparing the curves from Bolshe NW and Bolshe SW we find that in addition to the pair from 27 November 1996- 10 January 1997 the pairs from 10 January - 23 February 1997 and 22 June –5 August 1998 also show lower coherence for sparse forest in Bolshe SW than in Bolshe NW. For Bolshe SE an 88-day pair has been added since no 44-day pairs from the winter were available. Even though the temporal baseline is longer and with rapid temperature changes occurring shortly before both acquisitions, the coherence for sparse forest is still higher than for the pairs that were affected by thawing.

Two adjacent JERS-1 paths covered Chunsy North, so that acquisitions with only one day separation were available. For the winter 1995/1996 it was possible to create two coherence images from path 158 that were shifted one day relative to the corresponding coherence images from path 157. One observation from Figure 4.8 is that the coherence values for sparse forest from path 158 are higher than the ones that originate from path 157 one day earlier. Since there were no significant differences in the environmental conditions this seems to indicate a dependence on look angle, where a smaller look angle gives a higher coherence. For dense forest this behaviour is only found for the December/January pairs.

4.1.6 Interannual consistency

The availability of JERS-1 pairs from two different years, but acquired during the same season, make it possible to check the interannual consistency. A high consistency indicates that the environmental conditions were similar and that the measurements are possible to repeat. This can also be interpreted as a low sensitivity to small differences in the weather parameters during this season and thereby a high stability of the coherence measurements. If the overall consistency is high the same comparison can be used to identify changes in the forest cover. This application will be described in Chapter 6.

Four of the six test areas have been covered by JERS-1 pairs from more than one year. For Bolshe NW and Bolshe SW a pair from January/February 1994 could be compared with a pair from the same months 1997, and for Chunsy North and Chunsy East a pair from the winter 1993/1994 could be compared with a pair acquired in January/February two years later. The results are displayed in four plots in Figure 4.9. For three of the four test areas a correlation coefficient of over 0.95 is obtained. Only at Chunsy North is the correlation reduced to 0.90 by a few outliers. Some of these outliers can be identified as clear-cuts. For Bolshe SW it can be observed that the group with medium to low growing stock volume ($< 130 \text{ m}^3/\text{ha}$) falls slightly under the 1:1 line. This is a result of the smaller coherence for 1997. For our test areas the Siberian inland winter climate seems to give environmental conditions that are stable enough to allow repeated or even annual coherence measurements with comparable results. Unfortunately no JERS-1 pairs were available for an interannual check of other seasons, nonetheless the decorrelation

during freezing, thawing and rain and large standard deviations for summer-coherence make other seasons less appealing for repeated measurements, e.g. for change detection or forest monitoring.

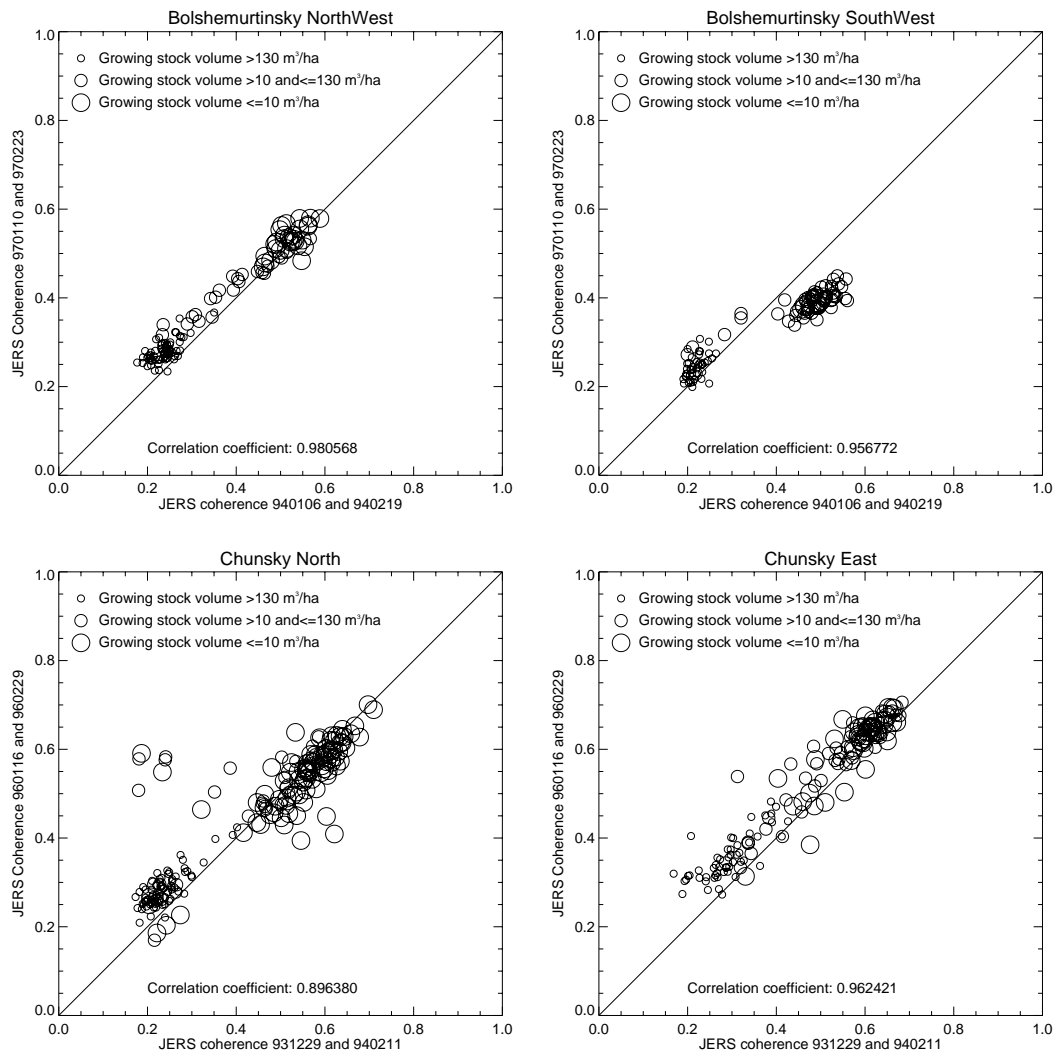


Figure 4.9 JERS repeat-pass coherence from two different dates plotted against each other. All forest stands with more than 50 pixels have been included.

4.2 Temporal baseline

4.2.1 Anthropogenic and natural forest change

In addition to changes in the environmental conditions, anthropogenic and natural changes in the forest cover also cause decorrelation. Natural disturbances can be damage by fire, storm, insect infestation, or forest diseases. To the anthropogenic changes we can count both those originating from forest management and harvesting, e.g. clear-cutting, selective logging, and thinning, but also disturbances caused by pollution or human induced fire. In Siberia vast areas have been affected by fire the last decade. Most of these fires are thought to be caused, directly or indirectly, by humans, and about 80 % of all fires are ground fires. The ground fires do not give as

dramatic changes as the stand replacing fires, but if they are severe enough they will result in the eventual death of many trees. Dead trees will have lower water content, leading to a reduction of the dielectric constant, but they will also experience a reduction of the number of needles/leaves, twigs, and eventually branches. Fire will also consume the ground vegetation and give a drier top soil layer, affecting the scattering.

For SAR systems with a short temporal baseline it is unlikely that disturbances like these will occur between the acquisitions, but for JERS-1 with a 44-day repeat-cycle the probability for this type of decorrelation should not be neglected. However, it must be kept in mind that the anthropogenic and natural disturbances are local events and will not decorrelate the whole image. In the image pairs that have been analysed in this thesis it has not been possible to identify any decorrelation originating from anthropogenic or natural change in the forest cover.

4.2.2 Multiple repeat-cycles

Based on the previous analysis of the temporal decorrelation due to environmental conditions, an increase of the time between the acquisitions can be expected to reduce the possibility to find JERS-1 pairs with high coherence. Longer temporal baseline is never the direct cause for decorrelation, but it allows more changes of the observed objects to occur. To avoid the strong decorrelating effects of freezing or thawing there are two alternatives. The temporal baseline should be 1) short enough to be within one season, or 2) long enough that the temperatures have returned to the same range (frozen or unfrozen) as during the first acquisition. With a repeat-cycle as long as 44 days, a temporal baseline longer than two or three repeat-cycles will result in a change of season between the acquisitions. In Section 4.1 it was shown that the highest level of coherence normally is reached during frozen conditions. With the available JERS-1 scenes it was possible to form several 88-day pairs from the winter season. In addition the availability of a few scenes from the winter 1993/94 allowed the formation of pairs with temporal baselines of two and three years. For path 163 an 88-day pair from the summer 1997 was available, but the shift in orbit that occurred sometime between May and July that year gave a spatial baseline that exceeded the critical value. The following analysis of multiple repeat-cycles will therefore be focused exclusively on coherence from the winter season. The temporal and spatial baselines for the selected pairs are given in Table 4.1.

The coherence values for the selected pairs have been plotted in Figure 4.10. For the three test areas in Bolshe Murtinsky both the 3-year and the 88-day pairs show low coherence and minimal difference between sparse and dense forest. These values are comparable with the ones that were obtained for the 44-day pair from Bolshe SW from November/January, but now the low coherence is found for the whole image and not only locally. The coherence values from the three test areas in Chunksky show a different trend and prove that under favourable conditions it is possible to get a fairly high contrast between sparse and dense forest with 88-day pairs. The pairs with two years temporal baseline have lower coherence for sparse forest, but it is still high enough that it should be possible to separate sparse and dense forest. Spatial baselines or temperatures at the acquisitions cannot explain the differences between Bolshe Murtinsky and Chunksky. A hypothesis is that the high temperatures shortly before the Bolshe Murtinsky acquisitions gave changes large enough to cause

decorrelation when the temporal baseline is longer than 44 days, but this cannot be proved.

Table 4.1 Selected JERS-1 pairs with temporal baselines of 88 days or more.

First date	Second date	GRS Path	Temporal baseline [repeat-cycles]	Spatial baseline perpendicular [m]	Test areas
1994-01-06	1997-01-10	165	25 (3 years)	606	Bolshe NW & SW
1994-02-19	1997-02-23	165	25 (3 years)	3028	Bolshe NW & SW
1996-11-25	1997-02-21	163	2 (88 days)	1012	Bolshe SE
1996-11-27	1997-02-23	165	2 (88 days)	1038	Bolshe NW & SW
1993-12-29	1996-01-16	157	17 (2 years)	2646	Chunsky North & East
1994-02-11	1996-02-29	157	17 (2 years)	2880	Chunsky North & East
1995-12-03	1996-02-29	157	2 (88 days)	314	Chunsky North & East
1995-12-04	1996-03-01	158	2 (88 days)	400	Chunsky North & South

In Figure 4.11 the winter coherence from all test areas and all temporal baselines have been collected in one plot. The values with temporal baselines of 17 and 25 repeat-cycles are from two different test territories. This in combination with the fact that they originate from only four pairs make it impossible to draw any conclusions from a comparison between coherence with temporal baselines of two and three years. However, treated as one group the coherence values give an indication about differences between multi-year baselines and baselines of one or two repeat-cycles. The trend for sparse forest suggests that shorter temporal baselines result in higher coherence. For dense forest the trend is less pronounced, but still visible. Under unfavourable observation conditions there should be no difference if the temporal baseline is 44 days or several years.

4.3 Volume decorrelation

When the perpendicular baselines in Table 3.3 are compared with the critical baselines that were calculated in Section 2.3.3, only the pair from Bolshe Murtinsky that was acquired on 20 May and 3 July 1997 has a baseline that exceeds the critical value. No coherence was processed for this pair. All other pairs have baselines well below the critical value.

In Figure 4.12 the perpendicular baselines have been plotted against the corresponding coherence values. The majority of the baseline values are well distributed over the range between 3 m and 1212 m, and then there is a gap to a smaller group of baselines ranging from 1752 m to 2091 m. As mentioned in Section 4.1.1, for the February-April pair covering Bolshe NW and Bolshe SW the normal coregistration procedure failed so that no coherence estimation could be performed. This has been indicated with a zero coherence value in the figures. For sparse forest, baselines between 0 m and 600 m show coherence values in the whole range between

0.15 and 0.63. For baselines between 600 m and 1200 m no coherence values above 0.38 have been recorded, and in the interval 1700 m to 2100 m the coherence values are spread out between 0.15 and 0.5. However, in general the plots in Figure 4.12 do not reveal any clear correlation between the coherence and the perpendicular baseline for sparse forest. For dense forest there seems to be a weak trend that pairs with short baselines get slightly higher coherence. This could indicate that a shorter baseline gives less volume decorrelation, but we also find a couple of cases where relatively high coherence is found for baselines around 2 km.

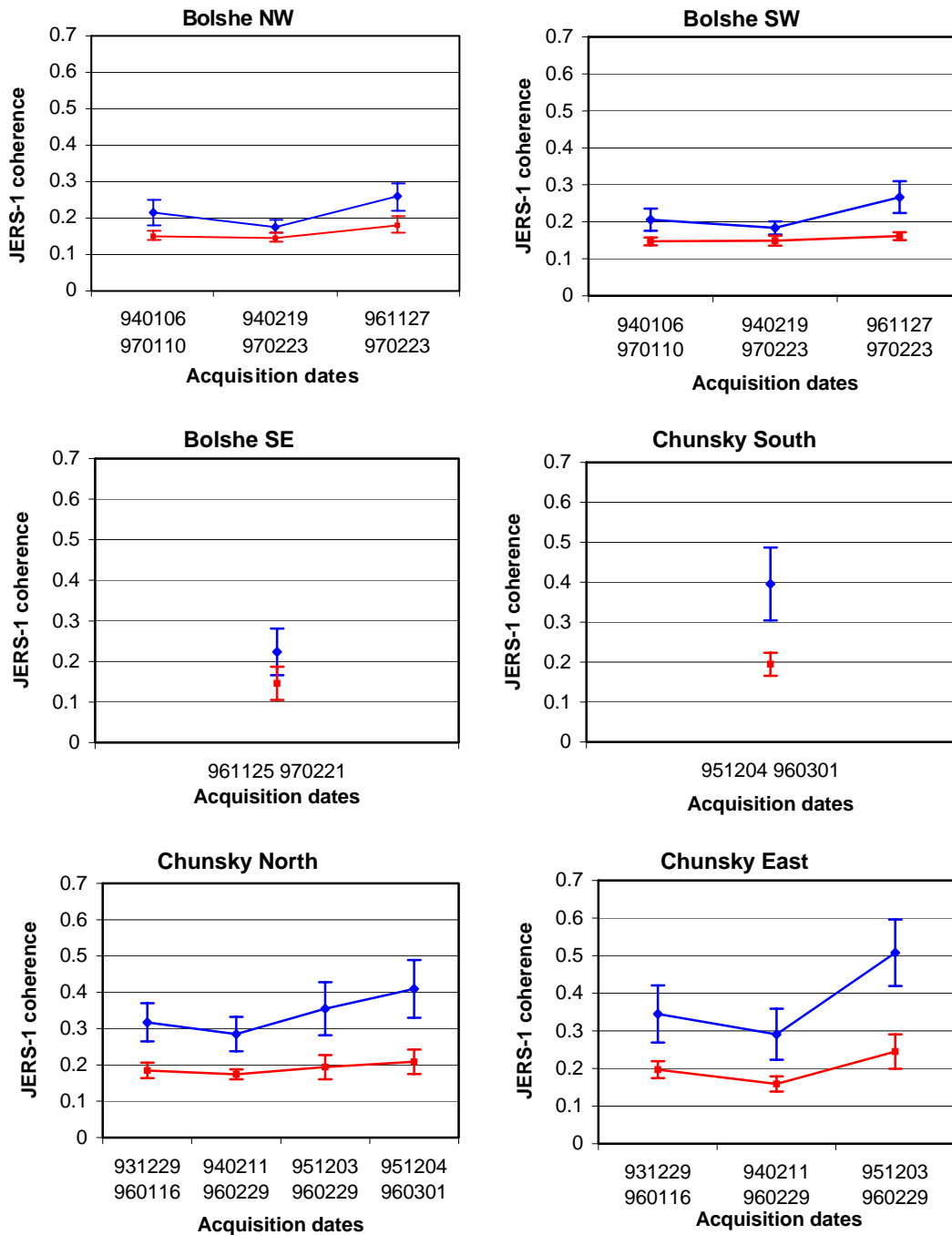


Figure 4.10 Coherence for coherence pairs with temporal baselines longer than 44-days. The upper curves give the mean coherence values for sparse forest and the lower curves for dense forest. The error bars represent +/- one standard deviation.

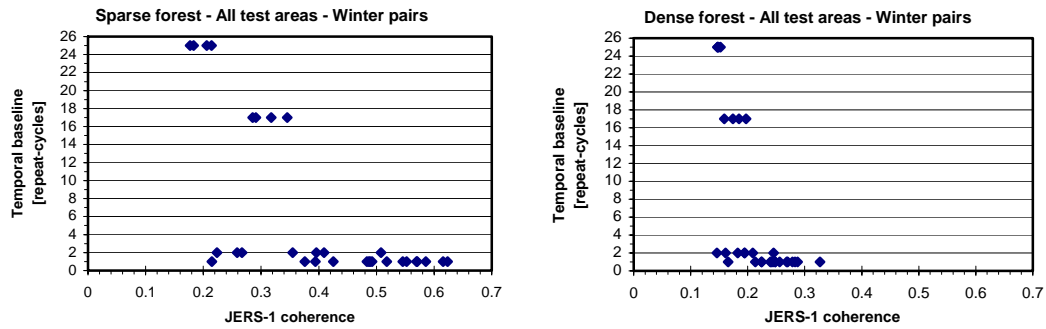


Figure 4.11 The JERS-1 coherence plotted against the temporal baseline.

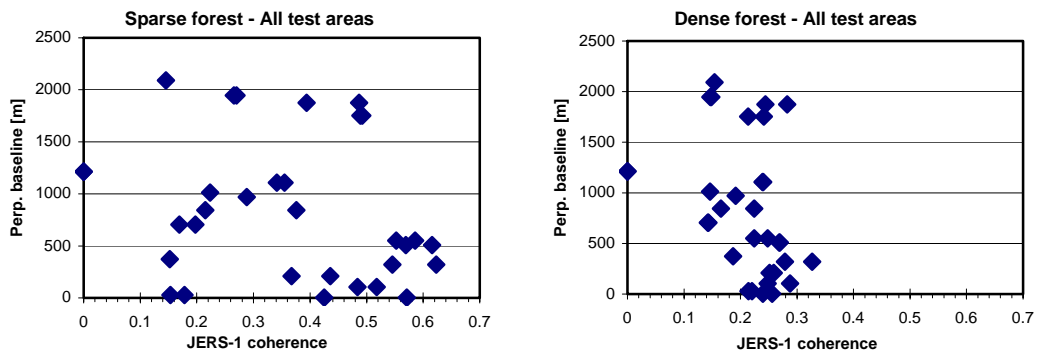


Figure 4.12 The JERS-1 coherence plotted against the spatial baseline.

4.4 Comparison with C-band

A majority of all studies of forest with spaceborne InSAR have been conducted with C-band data. It is therefore motivated to compare the characteristics of L-band coherence with C-band coherence. The data that have been used for this comparison are two ERS-1/2 tandem pairs from Bolshe Murtinsky (track 348) and three tandem pairs from Chunsky (track 491). An analysis of L-band and C-band coherence with comparable temporal baselines was not possible since no repeat-pass pairs from ERS-1/2 or Envisat Advanced SAR (ASAR) were available from the winter season.

The one-day temporal baseline of the ERS-1/2 tandem coherence reduces the risk for temporal decorrelation due to freezing, thawing, differences in snow cover, or anthropogenic or natural changes in the forest cover. The main causes for temporal decorrelation are wind and rain. Compared to L-band, the shorter wavelength makes the C-band coherence sensitive to motion of small scattering elements like twigs and small branches. This increases the importance of the wind as a decorrelating factor.

An overview of the coherence levels for sparse and dense forest from the five studied tandem pairs is given in Figure 4.13. The observed coherence is higher for sparse forest than for dense forest. The comparatively high coherence for the winter pair from Chunsky is in agreement with previous observations done under frozen conditions (KOSKINEN, *et al.*, 2001). For the three test areas in Chunsky the pair from October 1997 shows large differences in coherence level for sparse forest. This inhomogeneous pattern can be observed as a large region of reduced coherence around the centre of the coherence image. The weather station in Boguchany

recorded rainfall between the two acquisitions. It is likely that local rainfall caused the differences in coherence, but with only one weather station this cannot be proved.

An important observation is that the L-band coherence (Figure 4.7 and Figure 4.8) under frozen conditions reaches levels comparable with the C-band coherence from dry unfrozen conditions. In Figure 4.14 the ERS-1/2 coherence has been plotted against the JERS-1 coherence for a few selected pairs. All ground truth polygons containing more than 50 pixels have been included. For Bolshe NW and Bolshe SW, JERS-1 coherence from January/February 1997 is compared with ERS-1/2 coherence from September the same year. For Bolshe NW the polygons follow a straight line where increasing coherence shows the expected decrease in growing stock volume. The correlation coefficient is 0.97. The slope of the line shows a slightly larger dynamic range for the ERS-1/2 coherence; this is likely due to the much shorter interval between the acquisitions. For Bolshe SW the polygons representing growing stock volumes below 10 m³/ha show lower coherence both for ERS-1/2 and JERS-1. This reduction is more pronounced for JERS-1, thereby giving a lower correlation coefficient. For Bolshe SE no 44-day JERS-1 pair from the winter was available. Instead a summer pair acquired only one to two months before the ERS-1/2 pair was selected. Due to the low coherence for the JERS-1 pair, the correlation coefficient is only 0.60.

For Chunksy almost simultaneous ERS-1/2 and JERS-1 pairs from the winter 1996 were available. Results from these pairs have been plotted for Chunksy North and Chunksy South and show correlation coefficients of 0.93 and 0.82. The polygons are spread along a line that shows an offset away from the 1:1 line towards higher ERS-1/2 coherence. The offset is a result of the short temporal baseline of the ERS-1/2 coherence in combination with the stable winter conditions. This gives a higher coherence level for all growing stock volumes. The slope of the line shows that the dynamic range is the same for both the JERS-1 and ERS-1/2 coherence. The polygons that deviate most from the 1:1 line for Chunksy North represent three bogs that are situated along a stream. High coherence for the short temporal baseline and low coherence for the long temporal baseline indicate that these areas are affected by strong temporal decorrelation on a time scale longer than one day. One possible explanation to this decorrelation would be if the bogs were covered by a layer of ice that broke up between the JERS-1 acquisitions. Using the same two pairs, results similar to those displayed for Chunksy North and Chunksy South were observed for Chunksy East. In contrast to these simultaneous acquisitions, Chunksy East is in Figure 4.14 represented by a JERS-1 pair and an ERS-1/2 pair that were separated by almost four years. The ERS-1/2 pair is from October 1997 and do not show the same offset that the January pair has. The polygons are well distributed along a line that covers the coherence range from 0.2 to 0.7 without big deviation from the 1:1 slope. This illustrates the case when both the JERS-1 and the ERS-1/2 coherence have large dynamic ranges. The correlation coefficient is 0.89.

These results suggests that for forestry applications where C-band coherence has been reported to give good results it should in many cases also be possible to use L-band repeat-pass coherence from frozen winter conditions. Some examples of such applications will be shown in Chapter 5 and Chapter 6.

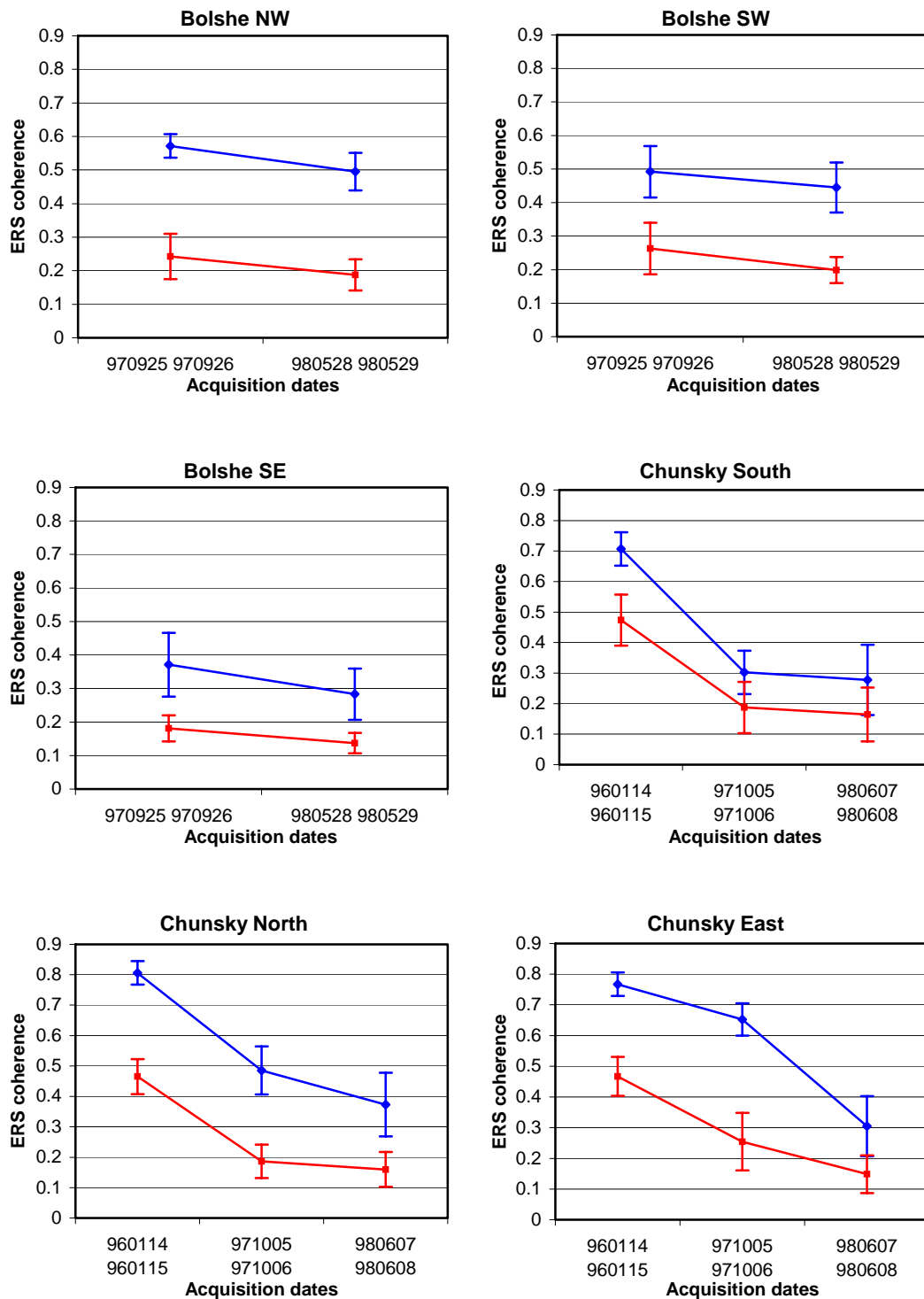


Figure 4.13 Coherence for ERS-1/2 tandem coherence. The upper curves give the mean coherence values for sparse forest and the lower curves for dense forest. The error bars represent +/- one standard deviation.

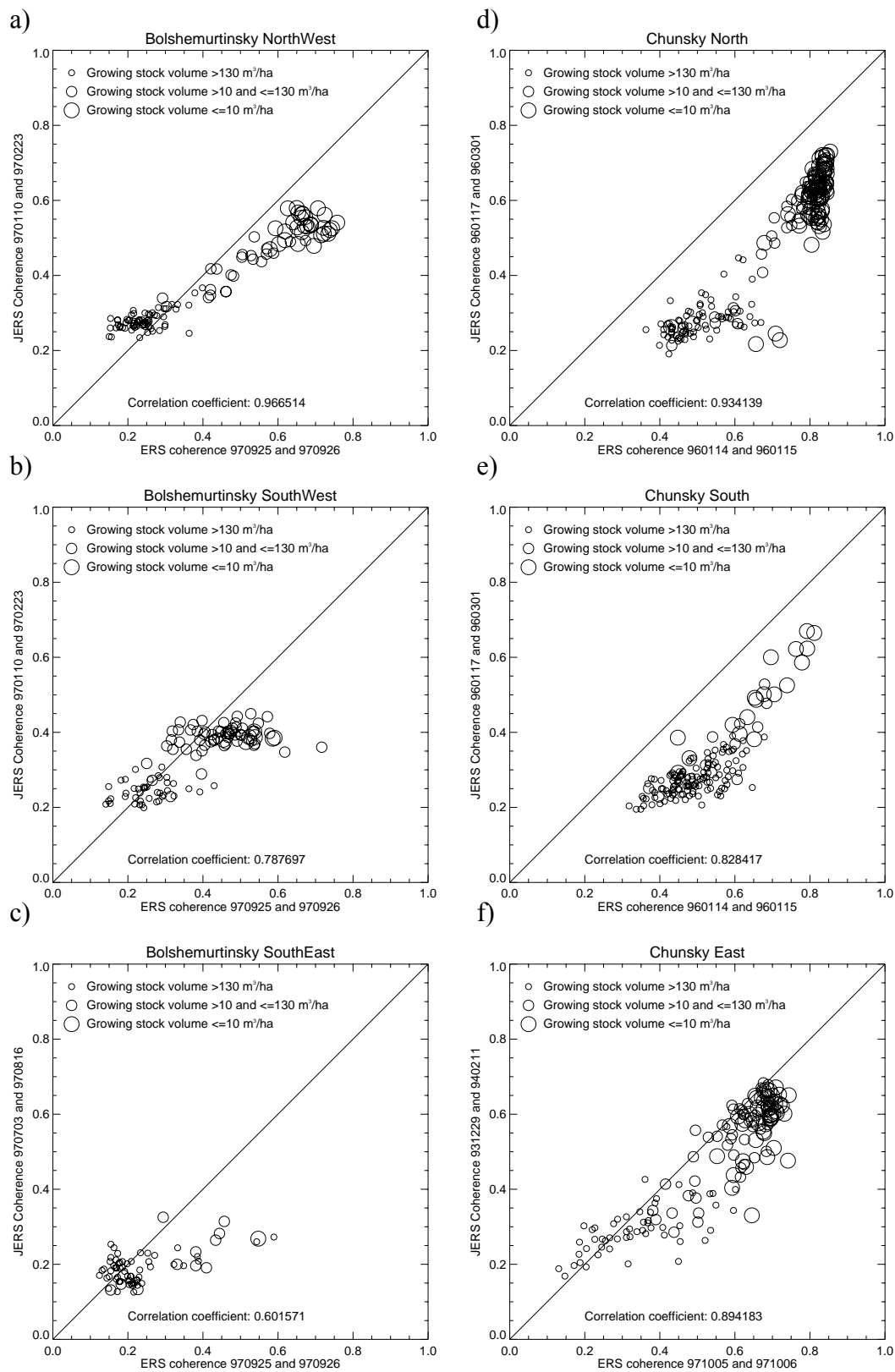


Figure 4.14 ERS-1/2 tandem coherence plotted against the JERS-1 repeat-pass coherence. All forest stands with more than 50 pixels have been included.

4.5 Conclusions

In this chapter a number of possible causes for temporal decorrelation were examined and the effect of the spatial baseline was investigated. A comparison between C-band coherence from ERS-1/2 and L-band coherence from JERS-1 was also conducted.

The analysis of environmental conditions showed that freezing and thawing cause strong decorrelation. This reduction in coherence is likely a combined effect of changing dielectric constant and the occurrence or disappearance of a snow layer. Considering the limited effect a snow layer has on L-band signals, the change in dielectric constant can be assumed to be the main decorrelating factor. Rain was also found to give decorrelation, but for the available image pairs the decorrelating effect was not as strong as for freezing or thawing. The highest coherence was reached for sparse forest when both acquisitions were done under frozen winter conditions. These conditions also gave the largest contrast in coherence between sparse and dense forest. Snowfall did not seem to affect the winter coherence. Due to insufficient measurements, no conclusions could be made about the effect of wind.

To investigate how the coherence depends on time between acquisitions a number of image pairs with temporal baselines longer than 44 days were selected. Following the evaluation of environmental effects, only winter pairs were considered. The available data allowed pairs with temporal baselines of 88 days, two years and three years to be formed. The analysis showed that under favourable conditions 88-day coherence from sparse forest can reach above 0.5, which is in the upper range for 44-day coherence. The coherence for temporal baselines over one year was significantly lower, but at some test areas still showed possibilities to separate sparse and dense forest.

Based on the available data, no clear correlation could be identified between spatial perpendicular baseline and coherence. However, dense forest displays a weak tendency towards higher coherence for baselines shorter than 500 m. Baselines up to 2 km were found to give high coherence for sparse forest.

The comparison with tandem coherence from ERS-1/2 revealed that, even though the repeat-cycle for JERS-1 is considerably longer, the winter coherence reaches levels comparable with those from unfrozen ERS-1/2 acquisitions. For ERS-1/2 coherence from the winter an overall higher coherence was observed.

Chapter 5

Forest parameter retrieval

One of the most important forest parameters is the biomass. Information about forest biomass is crucial for studies of the global carbon cycle and of regional changes in the vegetation, as well as for local forest inventories. One way to quantify the above ground biomass is to estimate the growing stock volume, which is defined as the stem volume per unit area. This chapter presents the results from an evaluation of the possibilities to use JERS-1 repeat-pass coherence for growing stock volume retrieval. A comparison with tandem coherence from ERS-1/2 is included.

5.1 Growing stock volume retrieval

The retrieval process can be divided in four parts: model selection, model training, retrieval and finally error analysis. Based on the results from the analysis of temporal decorrelation in the previous chapter, only 44-day coherence from the winter season will be considered. The test area Bolshe SE has been excluded because no suitable data were available.

To avoid problems with forest types where the growing stock volume is unevenly distributed within a stand or not well defined (e.g. unclosed natural forest and bogs), or where rapid changes would make results from different years difficult to compare (e.g. clear-cuts and burned forest) only natural stands have been included in the analysis. For four of the five studied test areas about 90 % of all stands were marked as natural stands in the ground truth database (see Table 3.1 and Table 3.2). In Chunksy North 81% of all stands were natural stands. Only stands containing at least 5 ha (20 pixels) after the edge erosion of the stands in the digital forest mask have been considered. In Bolshe NW this reduced the fraction of natural stands by a few percent. For the other four test areas edge erosion and removal of small stands did not change the fraction of natural stands. The distributions of growing stock volumes for the different test areas are shown in Figure 5.1. With the exception of Bolshe SW, the distribution of growing stock volume does not change significantly when only eroded natural stands are included. This indicates that the analysis should be representative for the whole test areas. The deviation for Bolshe SW is explained by the fact that the western part of the test area was not covered by satellite data so that these stands had to be removed (see Figure 3.1).

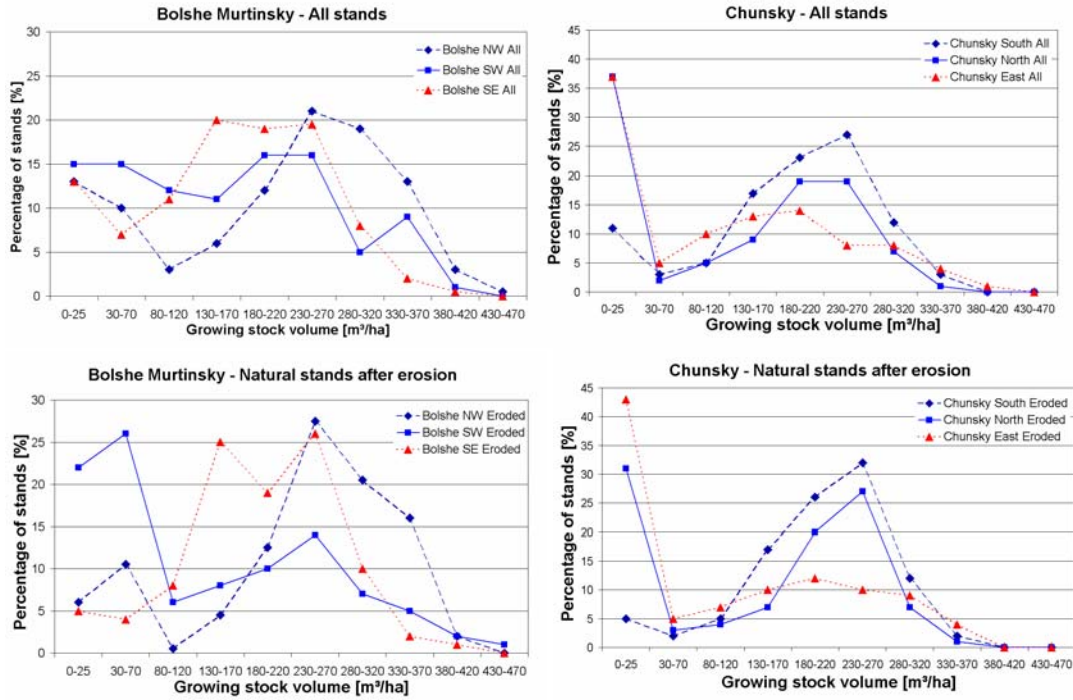


Figure 5.1 Growing stock volume distributions for all test areas. The two upper diagrams show the distribution for all available stands and the two lower ones for natural stands with a size of at least 20 pixels after edge erosion.

5.1.1 Model selection

It is known that there is a correlation between the level of coherence and the growing stock volume. In general the coherence decreases with increasing stock volume. The linear Pearson correlation coefficients between growing stock volume and JERS-1 coherence in Table 5.1 and Table 5.2 confirm that this trend is valid also for the data in this study.

For the retrieval it is necessary to have a model that as correctly as possible describes the relation between the coherence and the growing stock volume. At C-band this relation has in some cases been described as linear (SMITH, *et al.*, 1998; MANNINEN *et al.*, 2000; FRANSSON, *et al.*, 2001) and in other cases as exponential (ASKNE *et al.*, 1997a; KOSKINEN, *et al.*, 2001; SANTORO, *et al.*, 2002b; WAGNER, *et al.*, 2003). For spaceborne L-band coherence all available studies have indicated an exponential relation (LUCKMAN, *et al.*, 2000; ASKNE, *et al.*, 2003b; ERIKSSON, *et al.*, 2003). Scatterplots with coherence against growing stock volume confirmed that an exponential model would be more suitable than a linear model. Two examples of these scatterplots are given in Figure 5.2. An empirical model of the following form can be used to describe the relationship:

$$\gamma(V) = A * e^{B*V} + C \quad (5.1)$$

γ is the coherence, V the growing stock volume, and A , B and C are model parameters. The parameter A represents the span between the minimum and maximum coherence values of the curve, often called the dynamic range. B

corresponds to the slope of the exponential curve and indicates how fast the coherence values decrease toward the minimum value. This minimum value will hereafter be referred to as the offset and is given by the model parameter C . For estimation of growing stock volume, curves with a large dynamic range (large value of A), and a slow decrease in coherence with increasing growing stock volume (small negative value of B) are desired. The coherence offset is less critical, as long as it does not get so high that it reduces the dynamic range. When these conditions are fulfilled, there is a higher probability that a certain coherence value can be connected with the correct growing stock volume through inversion of the model.

Table 5.1 Linear Pearson correlation coefficients for growing stock volume and JERS-1 coherence

Acquisition dates	Bolshe-Murtinsky Northwest	Bolshe-Murtinsky Southwest
1994-01-06 1994-02-19	-0.84	-0.85
1996-10-14 1996-11-27	-0.70	-0.73
1996-11-27 1997-01-10	-0.63	-0.70
1997-01-10 1997-02-23	-0.86	-0.84
1998-06-22 1998-08-05	-0.65	-0.57

Table 5.2 Linear Pearson correlation coefficients for growing stock volume and JERS-1 coherence

Acquisition dates	Chunsky North	Chunsky South	Chunsky East
1993-12-29 1994-02-11	-0.78		-0.87
1995-10-20 1995-12-03	-0.78		-0.78
1995-12-03 1996-01-16	-0.71		-0.79
1995-12-04 1996-01-17	-0.72	-0.60	
1996-01-16 1996-02-29	-0.80		-0.83
1996-01-17 1996-03-01	-0.84	-0.68	
1997-04-01 1997-05-15	0.40	0.47	
1998-06-14 1998-07-28	-0.59		-0.49

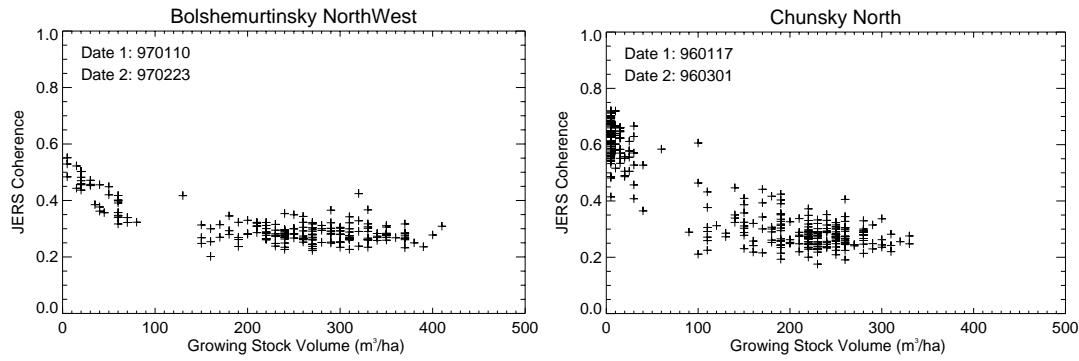


Figure 5.2 Relationship between JERS repeat-pass coherence and growing stock volume for one pair from Bolshe Murtinsky and one pair from Chunsky.

In some models, attempts have been made to connect the parameters A , B and C with the components of the coherence and the backscatter that originate from the ground respectively from the forest canopy and with physical properties like the canopy transmissivity (KOSKINEN, *et al.*, 2001). One of these models, the interferometric water cloud model (IWCM), goes one step further and incorporates terms that make it possible to account for volumetric decorrelation and InSAR geometry effects (ASKNE, *et al.*, 1997b; DAMMERT, 1999; SANTORO, *et al.*, 2002b; ASKNE, *et al.*, 2003b). The IWCM has been successfully applied to C-band data, but some of the simplifications that were made for the retrieval might not apply for L-band data (SANTORO, 2003). For the investigation of the possibility to retrieve growing stock volume from repeat-pass L-band coherence a simple regression model of the form in Equation (5.1) was found to serve the purpose.

5.1.2 Model training

Before the model can be used for retrieval of growing stock volume the three unknown model parameters A , B and C need to be determined. This is done by regression between the coherence and the growing stock volume from a training set. The following procedure was used to select the training set:

1. All forest stands in the ground truth database have a unique number. These numbers are Russia-wide identifiers that combine information about forest district, kvartal and stand, and are thereby related to the geographical location of each stand. For each test area all stands were sorted after their unique number and were given a position number P .
2. The stands were divided in four groups with the following selection scheme:

$$\text{Group 1: } P = 1 + n * 4$$

$$\text{Group 2: } P = 2 + n * 4$$

$$\text{Group 3: } P = 3 + n * 4$$

$$\text{Group 4: } P = 4 + n * 4$$

$$0 \leq n \leq \frac{P_{\max}}{4} - 1$$

where P_{\max} is the largest position number that is exactly divisible by four and n is an integer.

- The stem volume distribution for each group was analysed and the group with the most evenly distributed growing stock volume was selected as training set. The three remaining groups were combined into a test set.

This procedure was repeated for each test area. The number of stands in the training sets varied between 38 and 85 depending on the total number of stands in the test area. An example of the regression curves is shown in Figure 5.3. Corresponding plots for all other 44-day coherence images can be found in Figure B1 to B5 in Appendix B. The stands from the test set have been included in the figures and have been plotted with the growing stock volumes from the ground truth database. If the training set is representative for the whole test area the curve should not deviate from the general trend of the stands in the test set. A visual inspection did not reveal any significant discrepancies, which is an indication that the curve fitting and the selection of the training sets were successful. The model parameters from the curve fitting are listed in Table 5.3 and Table 5.4. The values of the dynamic range (A) and the offset (C) of the regression curves are in most cases in good agreement with the coherence values for sparse and dense forest that can be found in Figure 4.7 and Figure 4.8. It also indicates that there is a close relationship between the offset level and the coherence of dense forest and between the dynamic range and the difference in coherence between sparse and dense forest. The parameter B indicates how fast the coherence decrease when the growing stock volume increases. This is something that cannot be seen in any of the figures in Chapter 4. Using the criteria for successful retrieval (large A and small negative B) that were proposed in the previous section, especially the coherence from 1993/94 from Bolshe SW, Chunksy North and Chunksy East look promising.

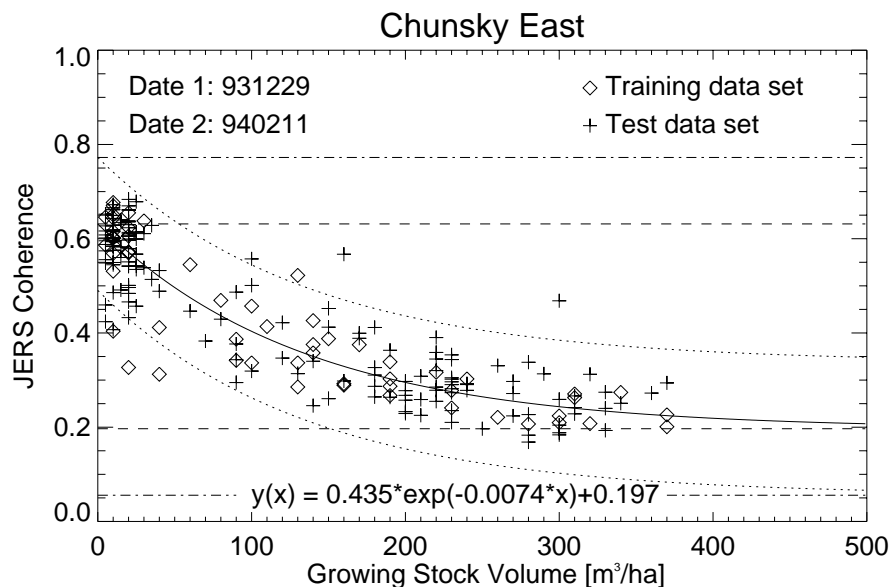


Figure 5.3 Example of regression curve for Chunksy East. The regression parameters are given in the expression at the bottom of the plot. The dashed lines correspond to the upper and lower limits of the regression curve. The dotted lines represent the two standard deviation distances from the curve and the dashed dotted lines are the limits for removal of outliers.

Table 5.3 Values of the regression parameters from the curve fitting of the JERS-1 coherence from the test areas in Bolshe Murtinsky.

Acquisition dates	Bolshe-Murtinsky Northwest		
	<i>A</i>	<i>B</i>	<i>C</i>
1994-01-06 1994-02-19	0.325	-0.0245	0.242
1996-11-27 1997-01-10	0.194	-0.0202	0.222
1997-01-10 1997-02-23	0.240	-0.0198	0.284
	Bolshe-Murtinsky Southwest		
1994-01-06 1994-02-19	0.363	-0.0088	0.182
1996-11-27 1997-01-10	0.056	-0.0342	0.180
1997-01-10 1997-02-23	0.213	-0.0075	0.212

Table 5.4 Values of the regression parameters from the curve fitting of the JERS-1 coherence from the test areas in Chunksky.

Acquisition dates	Chunksky North		
	<i>A</i>	<i>B</i>	<i>C</i>
1993-12-29 1994-02-11	0.410	-0.0083	0.167
1995-12-03 1996-01-16	0.262	-0.0060	0.178
1995-12-04 1996-01-17	0.314	-0.0063	0.219
1996-01-16 1996-02-29	0.326	-0.0096	0.242
1996-01-17 1996-03-01	0.403	-0.0111	0.242
	Chunksky South		
1995-12-04 1996-01-17	0.250	-0.0108	0.234
1996-01-17 1996-03-01	0.397	-0.0134	0.258
	Chunksky East		
1993-12-29 1994-02-11	0.435	-0.0074	0.197
1995-12-03 1996-01-16	0.342	-0.0107	0.255
1996-01-16 1996-02-29	0.344	-0.0115	0.321

5.1.3 Retrieval method

Once the model parameters have been determined, growing stock volume can be retrieved by inversion of the model. The estimated growing stock volume can be expressed as:

$$\hat{V}(\gamma) = \frac{1}{B} \ln\left(\frac{\gamma - C}{A}\right) \quad (5.2)$$

Using Equation (5.2) it is only possible to retrieve growing stock volumes for coherence values that are in the range between the maximum and minimum values of the regression curve. The minimum coherence value corresponds to the offset and is defined by the parameter C . The maximum value is given by the offset plus the dynamic range, i.e. $C+A$. The dashed lines in Figure 5.3 indicate these values. Values outside this range must be removed from the test set or be given new coherence values that are within the allowed limits. The following strategy was adopted:

1. Coherence values that could be identified as outliers were removed (see definition of outliers below).
2. Stands with coherence values above the maximum value were set to the growing stock volume $0 \text{ m}^3/\text{ha}$.
3. Stands with coherence values below the minimum value were given the same growing stock volume as the training stand with the highest growing stock volume.

For each stand in the training set the deviations of the coherence values from the curve were measured. The standard deviation of these distances indicates how large the spread within the training set is. Theoretically, if outliers are defined as stands where the distance between the coherence value and the curve exceeds two standard deviations, they should be removed from the test set. In Figure 5.3 this corresponds to all points outside the region limited by the two dotted lines. In practice, before the retrieval process only the measured coherence value is known. It is therefore necessary to use criteria that only rely on the coherence and not on the growing stock volume. A simple method is to remove all coherence values that are larger than the maximum value of the curve plus two standard deviations, or smaller than the offset value minus two standard deviations (SANTORO, *et al.*, 2002b). The dash dot lines in Figure 5.3 indicate this region. It is inevitable that only the most extreme outliers can be identified. This method has been used for the retrieval that is presented in this thesis.

5.1.4 Retrieval results

To test the selected retrieval method and the accuracy of the estimated growing stock volume, a test set with known growing stock volumes is required. As mentioned in section 5.1.2, 25% of the available stands in the ground truth database were utilized for the model training and the remaining 75 % to test the model. To describe the results of the retrieval procedure the root mean square error, RMSE, and the coefficient of determination, R^2 , have been used. One way to account for inaccuracy

in the ground truth data in the RMSE computation has been proposed by (FRANSSON, *et al.*, 2001):

$$RMSE = \sqrt{\frac{1}{N_{test}} \sum_{i=1}^{N_{test}} (\hat{V}_i - V_i^{gt})^2 - 0.5 \frac{1}{N_{test}} \sum_{i=1}^{N_{test}} (SE_i)^2} \quad (5.3)$$

N_{test} represents the number of samples in the test set, \hat{V}_i is the estimated growing stock volume for stand i and V_i^{gt} the growing stock volume for the corresponding stand in the ground truth database. The sampling error in m^3/ha for stand i is given by SE_i and the factor 0.5 is a correction due to systematic sampling design, in accordance with empirical investigations by (LINDGREN, 1984). This expression requires that the sampling error can be calculated for each stand. Since this is not the case for the test areas in this study a modified version of Equation (5.3) had to be used. According to the inventory standards as described in the Russian Forest Inventory handbook the required inventory accuracy for growing stock volume is 15 % for stands that are ready to be harvested and 20 % for all other stands (SCHMULLIUS, *et al.*, 2001; STOLBOVOI & MCCALLUM, 2002). Based on this, SE was replaced by a fixed value that was calculated as 20 % of the mean growing stock volume of the test set.

The values of R^2 and the RMSE for all analysed coherence images are listed in Table 5.5 and Table 5.6 for Bolshe Murtinsky and Chunsky respectively. Figure 5.4 displays two examples of the retrieved growing stock volume plotted against the ground truth growing stock volume. Both are from the same test areas, but show very different results. For the coherence from 1994 the RMSE of the retrieved growing stock volume is $60 m^3/ha$ and R^2 is 0.75. The values are along the 1:1 line. This can be considered being a relatively successful retrieval. On the other hand, the RMSE for the coherence for the period November 1996 to January 1997 is as high as $174 m^3/ha$ and the values of the retrieved growing stock volumes are grouped at the high and low end of the available range. This is a result of the small dynamic range (see Table 5.3 or Figure B.2) and the fact that the regression curve saturates already below $100 m^3/ha$. Even the slightest deviation from the curve will result in a completely wrong estimation. For this reason it is practically impossible to assign correct growing stock volumes to the coherence values. Stands with ground truth growing stock volumes in the whole range from 5 to $470 m^3/ha$ end up below the regression curve and are therefore given the maximum growing stock volume. The surprisingly high value of R^2 is due to the high proportion of stands with low growing stock volumes. As can be seen in Figure 5.1, about 50 % of all stands in Bolshe SW have growing stock volumes below $80 m^3/ha$. The small dynamic range for this specific coherence image is not typical for the available winter images, but the retrieval results show what can be expected when strong temporal decorrelation occur. This strengthens the assumption that acquisitions during the transition period from fall to winter or from winter to spring should be avoided. In Appendix B, Figure B.6 to Figure B.9, the retrieved growing stock volumes have been plotted against the ground truth growing stock volumes for all available 44-day pairs from the winter.

To allow a comparison between test areas with different distributions of growing stock volume a third statistical measure, the relative RMSE, was included in the analysis. The relative RMSE was calculated as the RMSE divided by the mean of the

growing stock volume in the test set. The value was multiplied by 100 to get it in percent. The relative RMSE for all coherence images are given in Table 5.7 and 5.8 for Bolshe Murtinsky and Chunskey respectively. Apart from the pair November 1996 to January 1997 from Bolshe SW, all relative RMSE are within the range 40 to 80 %. Comparing the values in these two tables with the RMSE in the two previous tables it can be observed that Bolshe NW and Chunskey South, which both have RMSE that are above 99 m³/ha, have relative RMSE that are in the mid to low range (47 – 62 %) compared to the other test areas. The opposite pattern is found for Chunskey East.

Table 5.5 RMSE and R² for the retrieval of growing stock volume from the JERS-1 coherence.

Acquisition dates	Bolshe-Murtinsky Northwest		Bolshe-Murtinsky Southwest	
	RMSE [m ³ /ha]	R ²	RMSE [m ³ /ha]	R ²
1994-01-06 1994-02-19	131.9	0.26	60.2	0.75
1996-11-27 1997-01-10	133.2	0.28	174.7	0.56
1997-01-10 1997-02-23	126.5	0.39	89.9	0.61

Table 5.6 RMSE and R² for the retrieval of growing stock volume from the JERS-1 coherence.

Acquisition dates	Chunskey North		Chunskey South		Chunskey East	
	RMSE [m ³ /ha]	R ²	RMSE [m ³ /ha]	R ²	RMSE [m ³ /ha]	R ²
1993-12-29 1994-02-11	93.5	0.57			62.9	0.72
1995-12-03 1996-01-16	113.3	0.46			79.8	0.66
1995-12-04 1996-01-17	94.7	0.52	130.6	0.06		
1996-01-16 1996-02-29	78.5	0.62			81.1	0.67
1996-01-17 1996-03-01	82.3	0.63	99.9	0.27		

Table 5.7 Relative RMSE for the retrieval of growing stock volume from the JERS-1 coherence.

Acquisition dates	Bolshe-Murtinsky Northwest	Bolshe-Murtinsky Southwest
	RMSE [%]	RMSE [%]
1994-01-06 1994-02-19	55.7	43.1
1996-11-27 1997-01-10	56.2	125.0
1997-01-10 1997-02-23	53.5	64.3

Table 5.8 Relative RMSE for the retrieval of growing stock volume from the JERS-1 coherence.

Acquisition dates	Chunsky North	Chunsky South	Chunsky East
	RMSE[%]	RMSE [%]	RMSE [%]
1993-12-29 1994-02-11	61.7		52.5
1995-12-03 1996-01-16	75.1		68.0
1995-12-04 1996-01-17	62.8	62.0	
1996-01-16 1996-02-29	51.8		69.1
1996-01-17 1996-03-01	54.5	47.7	

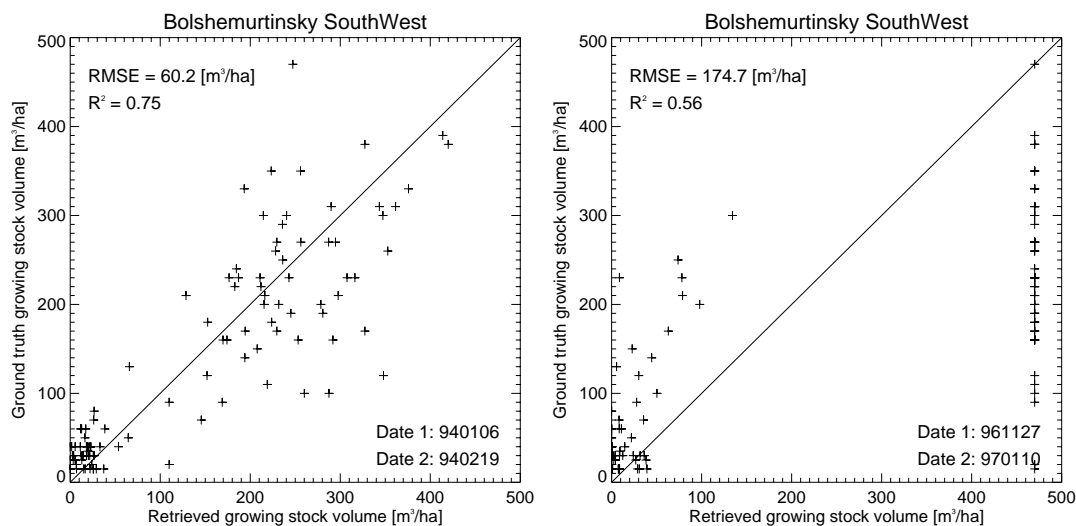


Figure 5.4 Comparison between the retrieved growing stock volumes and the growing stock volumes from the forest inventory. RMSE and R^2 are given in the upper left corner of each plot. The plot to the left shows successful retrieval while the right plot is the result of retrieval from an image with an overall low coherence level.

5.2 Comparison with C-band

C-band coherence from the ERS-1/2 tandem mission has delivered good results for retrieval of growing stock volume for boreal forest at a test site in Sweden. Under frozen conditions a best RMSE as low as 21 m³/ha has been reported for retrieval from a single coherence image using the IWCM (SANTORO, *et al.*, 2002b). The corresponding relative RMSE was 15 % and the value of R^2 0.92. Using linear regression for the same Swedish test site, Kättböle, other authors found a best RMSE of 26 m³/ha (FRANSSON, *et al.*, 2001) and 31 m³/ha (SMITH, *et al.*, 1998). These values all indicate retrieval accuracy higher than the one achieved with L-band coherence for the Siberian test sites. However, C-band studies from other test areas

have reported less accurate retrieval results. The best RMSE here range from 54 m³/ha (MANNINEN, *et al.*, 2000) over 91 m³/ha (HYYPÄ, *et al.*, 2000) and 99 m³/ha (KOSKINEN, *et al.*, 2001) to 130 m³/ha (SMITH, *et al.*, 1998). This stresses how important it is to do the comparison between C-band and L-band coherence at the same test area using the same ground data, retrieval model, training set and test set. The only published study where retrieval of growing stock volume was done with spaceborne L-band coherence was conducted with a JERS-1 pair from Kättböle (ASKNE, *et al.*, 2003b). A best RMSE of 54 m³/ha was reported. This result can be compared with the C-band results reported by (SANTORO, *et al.*, 2002b), but it should be noted that the L-band acquisitions were done in April and May and not during optimal frozen conditions. The relative vicinity to the North Sea and the Gulf Stream make the winter climate in southern Sweden mild in comparison with Siberia. The chances of getting repeat-pass coherence from a 44-day period with temperatures below zero are therefore limited.

Using the same methods as described for the JERS-1 repeat-pass coherence, retrieval was performed for all available ERS-1/2 tandem pairs from track 348 and 491. No retrieval results from track 305 will be presented, since no comparison with L-band was possible. The JERS-1 coherence covering the corresponding test areas, Bolshe NE and Bolshe SE, was not suitable for retrieval. For Chunsky ERS-1/2 tandem data from the winter were available, allowing a comparison with JERS-1 data from the same season. For JERS-1 the stable observation conditions during the Siberian winter reduce the temporal decorrelation for sparse forest. This is a requirement in order to get a dynamic range that is large enough to allow retrieval. For ERS-1/2 tandem the frozen conditions also reduce the decorrelation for dense forest. This is mainly a result of the much shorter repeat-cycle. If the reduction in decorrelation is larger for dense forest than for sparse forest the stable observation conditions will actually lead to a smaller dynamic range, which is a negative effect for the retrieval. The stable observation conditions often lead to a reduction in the spread around the regression curve. For the retrieval process the smaller deviations from the curve can be of greater importance than a reduction in the dynamic range. In Figure 5.5 an example of the curve fitting for an ERS-1/2 pair from the winter is displayed. The test area is the same as the one used for the JERS-1 coherence in Figure 5.3. Both figures show curves that are favourable for growing stock volume retrieval. Images of the regression curves for all remaining ERS-1/2 pairs and test areas are collected in Figure B.10 to Figure B.14 in Appendix B.

For the purpose of describing the characteristics of the regression curves and their suitability for retrieval the tandem pairs can be divided in three groups according to weather condition at and between the acquisitions (see Table 3.4 and Table 3.6): frozen, dry unfrozen, and unfrozen with rain. The group “frozen” corresponds to the same observation conditions that were found suitable for the JERS-1 coherence. This group shows an offset level that is considerably higher than for the other groups, as well as compared to the L-band coherence. This is a result of the above-mentioned reduction in decorrelation for dense forest. For the available winter-pair the dynamic ranges and slope of the curves are of the same order as for the JERS-1 coherence. The coherence in the group “dry unfrozen” display offset levels and curve slopes similar to those observed for L-band, but seems to result in slightly larger dynamic ranges. Rain reduces the dynamic range and makes the coherence decrease faster with increasing growing stock volume. As discussed in Chapter 4.4, the pair acquired in October 1997 over Chunsky displays large differences between the three test areas

covered. The characteristics of the regression curves suggest that Chunsy South was more affected by rain than Chunsy North and Chunsy East. Regardless of which group the C-band coherence belong to, the standard deviations of the distances from the curves are in most cases larger than in Figure 6.5. The spread also appears to be slightly larger than that observed for the JERS-1 curves.

The values of the chosen retrieval accuracy indicators, the RMSE, R^2 and relative RMSE, are listed in Table 5.9 to Table 5.12. Plots showing how well the estimated growing stock volumes correspond to the ground truth growing stock volumes have been included in Appendix B, Figure B.15 to Figure B.18. Comparing the relative RMSE for all ERS-1/2 pairs it can be noted that there are large differences between the test areas even when the measurements originate from the same acquisition dates. This stresses the influence that the structure and composition of the test areas has on the retrieval results. The previously presented retrieval results for the JERS-1 coherence are in many cases as good as, or better than the C-band results. Even though the C-band coherence from dry unfrozen conditions presents a larger dynamic range, the larger deviations from the curve decrease the retrieval accuracy to the same levels as for the L-band coherence.

Table 5.9 RMSE and R^2 for the retrieval of growing stock volume from ERS-1/2 coherence.

Acquisition dates	Bolshe-Murtinsky Northwest		Bolshe-Murtinsky Southwest	
	RMSE [m ³ /ha]	R ²	RMSE [m ³ /ha]	R ²
1997-09-25 1997-09-26	113.7	0.43	109.0	0.44
1998-05-28 1998-05-29	137.9	0.24	121.7	0.37

Table 5.10 RMSE and R^2 for the retrieval of growing stock volume from ERS-1/2 coherence.

Acquisition dates	Chunsy North		Chunsy South		Chunsy East	
	RMSE [m ³ /ha]	R ²	RMSE [m ³ /ha]	R ²	RMSE [m ³ /ha]	R ²
1996-01-14 1996-01-15	87.3	0.58	119.4	0.17	91.1	0.70
1997-10-05 1997-10-06	57.0	0.73	143.3	0.07	139.8	0.53
1998-06-07 1998-06-08	125.5	0.32	149.6	0.08	130.0	0.48

Table 5.11 Relative RMSE for the retrieval of growing stock volume from ERS-1/2 coherence.

Acquisition dates	Bolshe-Murtinsky Northwest	Bolshe-Murtinsky Southwest
	RMSE [%]	RMSE [%]
1997-09-25 1997-09-26	48.0	77.3
1998-05-28 1998-05-29	58.2	87.1

Table 5.12 Relative RMSE for the retrieval of growing stock volume from ERS-1/2 coherence.

Acquisition dates	Chunsky North	Chunsky South	Chunsky East
	RMSE [%]	RMSE [%]	RMSE [%]
1996-01-14 1996-01-15	57.9	57.2	77.5
1997-10-05 1997-10-06	37.3	68.4	119.0
1998-06-07 1998-06-08	83.2	71.3	108.2

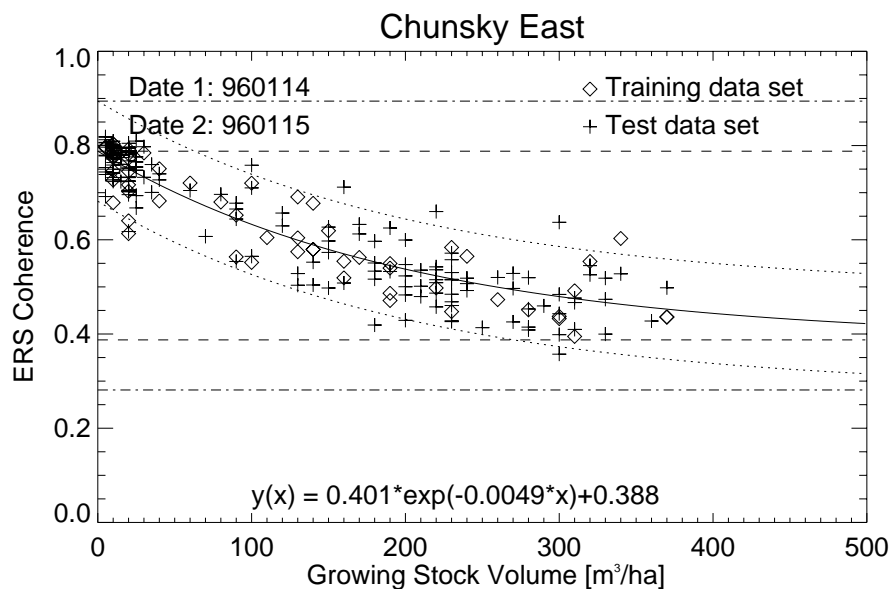


Figure 5.5 Example of regression curve for ERS-1/2 coherence from Chunsky East. The regression parameters are given in the expression at the bottom of the plot. The dashed lines correspond to the upper and lower limits of the regression curve. The dotted lines represent the two standard deviation distances from the curve and the dashed dotted lines are the limits for removal of outliers.

5.3 Conclusions

In this chapter retrieval of growing stock volume from JERS-1 repeat-pass coherence has been demonstrated. A model was chosen and methods for selection of training data and removal of outliers were defined. The accuracy of the retrieval was analysed and finally a comparison with retrieval from ERS-1/2 tandem coherence was conducted.

In a first step the correlation between coherence and growing stock volume was tested. For winter pairs the linear Pearson correlation coefficient was found to range from -0.60 to -0.87. In half of these cases the coefficient was -0.8, or better. This proved that there is a correlation between JERS-1 repeat-pass coherence and growing stock volume. An exponential model was selected to describe the relationship. After training of the model with curve fitting, the regression curves were compared with test sets, and in all cases it was found that the curves were in good agreement with the test data.

As indicators for the retrieval accuracy the RMSE, the relative RMSE and the coefficient of determination R^2 were chosen. A best RMSE of 60 m³/ha was obtained and in most cases the RMSE was smaller than 100 m³/ha. With one exception the relative RMSE stayed within the range 43 to 76 %. R^2 showed large variations, partly depending on the distribution of growing stock volumes for the respective test area. The best R^2 was observed to be 0.75.

The same model was used for the retrieval from ERS-1/2 tandem coherence. The best obtained values of RMSE, relative RMSE and R^2 were 57 m³/ha, 37 % and 0.73 respectively. However, for over 70% of the studied pairs the RMSE was over 100 m³/ha. The results are far from the best ones reported by other authors for test areas in Northern Europe. This might be explained by different structure of the forests, with more mixed, unmanaged forests in Siberia, and by larger uncertainties in the ground data. This can result in larger spread in the data, which will inevitably lead to larger uncertainties in the retrieval. The obtained retrieval accuracy for JERS-1 coherence is in many cases as high as, or better than for the ERS-1/2 coherence. This indicates that under frozen winter conditions L-band repeat-pass coherence can be an alternative to C-band coherence with shorter temporal baselines for growing stock volume retrieval.

Chapter 6

Forest mapping and monitoring

The purpose of this chapter is to investigate if it is possible to use spaceborne L-band repeat-pass coherence for mapping and monitoring of forest and to give a preview of two potential forestry applications. The term mapping will be used to denote applications where only one temporal coverage of a large geographical area is required. For monitoring, at least two coverages are needed to determine if any changes have occurred. The suitable time span between these acquisitions depends on the processes or changes that should be detected or observed. For most forestry applications annual observations are sufficient, but forest fire is one example where frequent data acquisitions and rapid response is desirable. It has not been the intention to give a full analysis of the topic or to develop new methods for mapping or monitoring. This is left for future work.

6.1 Growing stock volume mapping

As an example of a mapping application the mapping of growing stock volume has been selected. Two approaches have been evaluated. The first one is based on retrieval using the regression model presented in Chapter 5 and the second is a version of the adaptive classification algorithms introduced in the SIBERIA project (SCHMULLIUS, *et al.*, 2001; WAGNER, *et al.*, 2003). Both methods use JERS-1 coherence and JERS backscatter as inputs. The results are compared with forest inventory data and with the output from the SIBERIA algorithm using the ERS-1/2 tandem coherence and JERS-1 backscatter it was designed for. To allow a comparison, the same growing stock volume classes as in the SIBERIA project have been used. These forest classes were chosen after analysis of the information content in the available satellite data and of its correlation with the growing stock volume in the forest inventory database. In addition, two non-forest land cover classes were included in the SIBERIA classification legend (Table 6.1).

The first approach used the regression model given in Equation 5.1 to describe the relationship between the JERS-1 coherence and the growing stock volume. Training of the model was done as described in Chapter 5. Coherence from frozen conditions was used. Compared to the coherence, the JERS-1 backscatter contains partly complementary information, and was in the SIBERIA project found to provide separation between the forest classes and the non-forest classes, something that was not possible with the ERS-1/2 coherence. The most convenient procedure would be

to use the backscatter from one of the winter acquisitions that were used for the coherence estimation. However, since JERS-1 backscatter in general gives a larger dynamic range for unfrozen conditions (SANTORO, *et al.*, 2003), and because water surfaces cannot always be separated from other classes when the surface is frozen, it is preferable to combine the winter coherence with a backscatter image acquired under unfrozen conditions. For the JERS-1 backscatter an expression of the following form was used:

$$\sigma^0(V) = \sigma_\infty + (\sigma_0 - \sigma_\infty) \cdot e^{-\frac{V}{V_\sigma}} \quad (6.1)$$

where σ_0 and σ_∞ are respectively the backscatter coefficients at $V = 0 \text{ m}^3/\text{ha}$ (non-forest) and for asymptotic values of V (dense forest), and V_σ is the value of V at which the exponential function has increased by e . After determination of the unknown model parameters, the coherence and backscatter expressions were used to calculate class means for each growing stock volume class. These mean values were used for a Maximum Likelihood classification of the whole image. The resulting growing stock volume map for the test area Chunsy North is displayed in Figure 6.1 a). For the test areas the map could be compared with forest inventory data. In Table 6.2 the results of the accuracy assessment are listed.

One problem with mapping of large geographical areas is that there are not always forest inventory data available for the whole region. Without training data from all satellite scenes there is a high risk that growing stock volume maps that originate from several scenes will be inhomogeneous and contain visible boarder effects. This can be a result of changing environmental conditions that give coherence and backscatter levels that fluctuate from one scene to the other. These effects are more severe between scenes in the across track direction than along track. To reduce this problem, a classification method that adapts to the coherence and backscatter levels, with only limited use of training data, was developed in the SIBERIA project. Empirical models similar to those utilized in the first classification approach were used. Some model parameters were given fixed values, but the most sensitive parameters were estimated from the coherence and backscatter histograms of each scene. After the model parameters were determined, the same Maximum Likelihood classifier as in the first approach was used. The methods were developed for the use of ERS-1/2 tandem coherence together with JERS- backscatter, but have here been tested with JERS repeat-pass coherence instead of the ERS-1/2 coherence. A more detailed description of the SIBERIA classification procedures and the involved empirical models are given in (WAGNER, *et al.*, 2003) and of obtained accuracy levels in (BALZTER *et al.*, 2002).

Table 6.1 Classes used in the SIBERIA project

SIBERIA classes	Land cover type
Water	River, lake, inland water
Smooth open areas	Agricultural fields, river sand bar
Open areas (< 20 m ³ /ha)	Bogs, meadows, hayfields, pasture, clear-cut, burnt forest (stand replacing), young regrowth
Forest 20 - 50 m ³ /ha	Forest 20 - 50 m ³ /ha
Forest 50 - 80 m ³ /ha	Forest 50 - 80 m ³ /ha
Forest > 80 m ³ /ha	Forest > 80 m ³ /ha

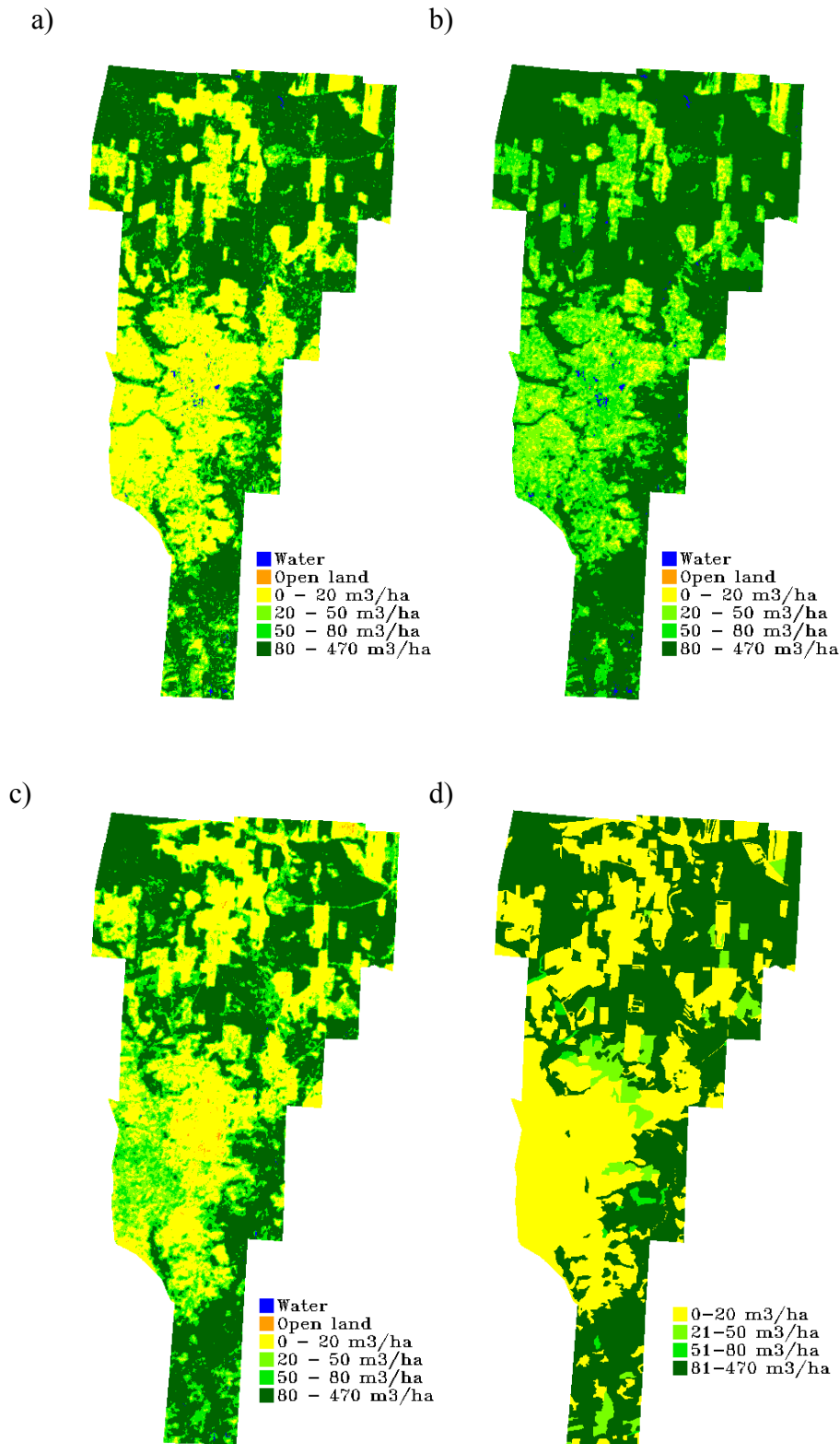


Figure 6.1 Growing stock volume maps for Chunsky North produced with a) JERS-1 coherence and backscatter using the regression model from Chapter 5, b) JERS-1 coherence and backscatter and the SIBERIA algorithm, c) ERS-1/2 tandem coherence and JERS-1 backscatter and the SIBERIA algorithm. Forest inventory data are shown in d). The JERS-1 coherence is from January/February 1996, the JERS-1 backscatter from August 1998, the ERS coherence from October 1997 and the forest inventory data from 1998.

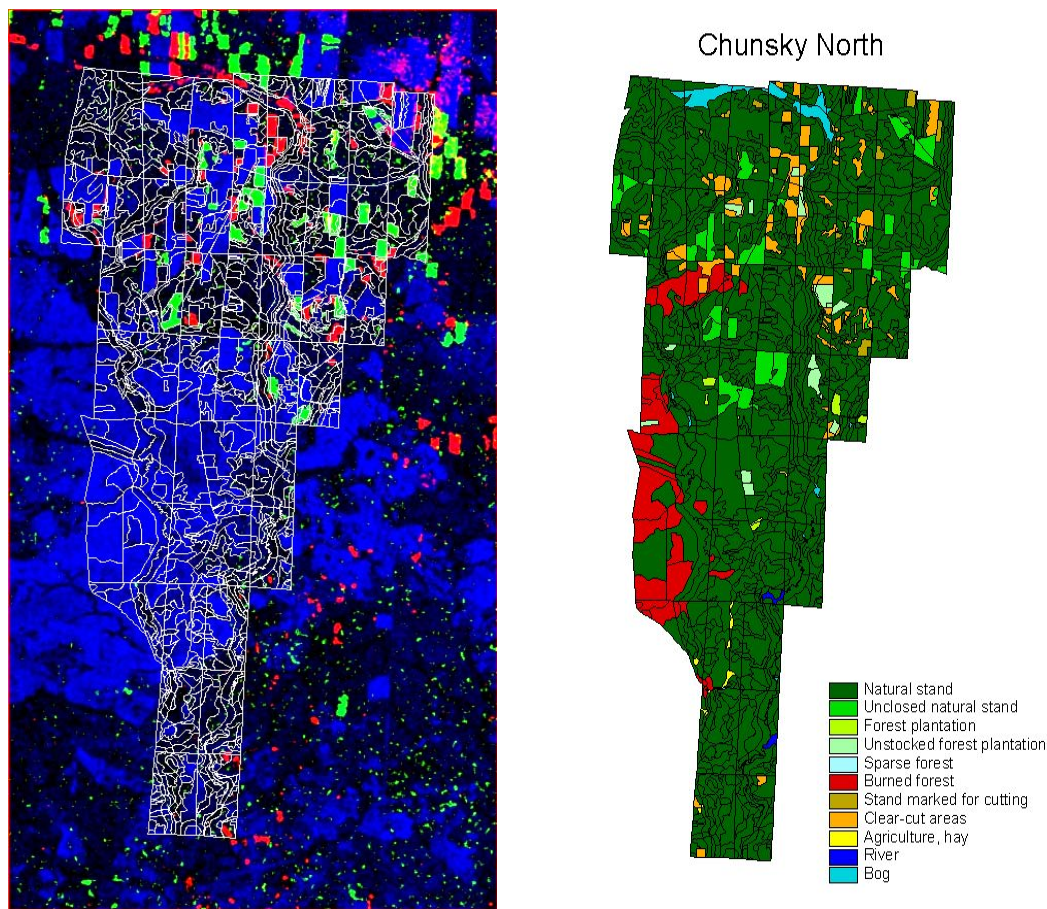


Figure 6.2 Change detection map for Chunsky North (left figure) and land cover classes according to the forest inventory database (right figure). The change detection map is an RGB-composite with the following bands:
Blue: JERS-1 coherence from December 1993/February 1994
Green: Difference between JERS-1 coherence from January/February 1996 and JERS-1 coherence from December 1993/February 1994
Red: Difference between ERS-1/2 coherence from October 1997 and ERS-1/2 coherence from January 1996.

Interpretation:

- Blue**=Open areas or sparse forest before December 1993
- Green**=Changes that occurred between February 1994 and January 1996
- Red**=Changes that occurred between January 1996 and October 1997.

The classification results for Chunsky North using the second approach are given in Figure 6.1 b) and Table 6.3. It can be seen that the growing stock volumes for sparse forest classes are overestimated. This is a result of the model assumption that the dynamic range increase with increasing offset level. That this can lead to misclassification has been demonstrated for ERS-1/2 tandem data from the winter season (ERIKSSON *et al.*, 2002a), but the effect is the same for JERS-1 data. A comparison with ERS-1/2 tandem coherence from October 1997 is given in Figure 6.1 c) and Table 6.4. The accuracy assessment shows values comparable with those from the JERS-1 coherence with the first classification approach. It is also possible to identify clear-cuts that have occurred between the acquisition of the JERS-data and the ERS-1/2 data.

Table 6.2 Classification accuracy for Chunsky North using JERS-1 coherence and backscatter and “normal” training of a regression model.

Class [m ³ /ha]	Prod. Acc. [%]	User Acc. [%]	Prod. Acc. [pixels]	User Acc. [pixels]
< 20	65.68	88.41	43507/66240	43507/49208
20 – 50	19.39	10.12	1299/6699	1299/12841
50 – 80	26.53	1.63	334/1259	334/20528
> 80	79.32	88.48	64217/80959	64217/72580

Table 6.3 Classification accuracy for Chunsky North using JERS-1 coherence and backscatter and the SIBERIA algorithm.

Class [m ³ /ha]	Prod. Acc. [%]	User Acc. [%]	Prod. Acc. [pixels]	User Acc. [pixels]
< 20	10.64	90.89	7027/66040	7027/7731
20 – 50	31.45	7.94	2106/6697	2106/26531
50 – 80	27.42	1.11	345/1258	345/31137
> 80	92.82	83.91	75111/80917	75111/89513

Table 6.4 Classification accuracy for Chunsky North using ERS-1/2 tandem coherence and JERS-1 backscatter and the SIBERIA algorithm.

Class [m ³ /ha]	Prod. Acc. [%]	User Acc. [%]	Prod. Acc. [pixels]	User Acc. [pixels]
< 20	61.16	87.18	40511/66236	40511/46470
20 – 50	20.20	7.19	1353/6699	1353/18809
50 – 80	30.42	1.56	383/1259	383/24613
> 80	75.31	93.43	60982/80971	60982/65273

6.2 Change detection

When a time series of high quality data is available it should be possible to detect and monitor changes in the forest cover. For Chunsky North two image pairs from December 1993 / February 1994 and January / February 1996 made it possible to evaluate the possibility to use JERS-1 repeat-pass coherence for change detection.

Unfortunately, forest inventory data were only available from 1998, and did not come with any information about when clear-cutting or fires occurred. However, due to their regular shapes and strong contrast to surrounding dense forest, new clear-cuts are often easy to identify visually.

In addition to the JERS-1 pairs from 1993/1994 and 1996, two ERS-1/2 tandem pairs were available, the first from the same period as the last JERS-1 pair, and the second from October 1997. Combining these four pairs it was possible to create a change detection map where the identified changes could be divided in two groups depending on if they occurred in the period February 1994 to January 1996 or between January 1996 and October 1997. This map is shown in Figure 6.2. It was created by calculating the difference in coherence over the two periods and then using strong thresholding of the histograms of the resulting difference images to filter out the strongest changes. A comparison with the forest inventory data in the same figure reveals that the forest fires either occurred before December 1993 or after October 1997, or the changes in forest cover were not strong enough to remain after the threshold filtering.

6.3 Conclusions

The two evaluated forestry applications show that spaceborne L-band repeat-pass coherence has a potential for forest mapping and monitoring. The growing stock volume classification was tested with two different methods that require one coherence image and one backscatter image. The results show a high accuracy for classification of the class with growing stock volumes above 80 m³/ha, but with the current version of the SIBERIA algorithm, the growing stock volume is overestimated for sparse and young forest. A modification of the algorithm that allows automatic adaptation to the dynamic range of each coherence image would be desirable and can be expected to improve the results.

Using histogram thresholds for a time series of at least two coherence images it was possible to identify larger changes like clear-cuts that occurred in the period between the acquisitions for the two images. For identification of smaller changes, e.g. selective logging or thinning, refined methods will be needed. A corresponding time series of ground data is vital for the validation. Lack of validation data prevented a more thorough study for the available test areas.

Chapter 7

Conclusions

7.1 Summary of results

The main goal of this thesis was to answer some of the open questions regarding characteristics and usefulness of L-band coherence for forestry applications. Based on the availability of ground and satellite data the work was limited to the study of boreal forest with JERS-1 repeat-pass coherence. Six test areas located at the Central Siberian Plateau were selected and 19 JERS-1 44-day pairs were evaluated. Five ERS-1/2 tandem pairs were included in the study to allow a comparison between L-band and C-band coherence.

The first part of the analysis was focused on finding the main causes for decorrelation of the available JERS-1 repeat pass coherence. Based on available meteorological data, the effects of different environmental conditions at or between the acquisitions were studied. It was found that that freeze and thaw cause strong decorrelation. Rain was also found to give decorrelation, but for the available image pairs the decorrelating effect was not as strong as for freeze or thaw. The highest coherence was reached for sparse forest when both acquisitions were done under frozen winter conditions. These conditions also gave the largest contrast in coherence between sparse and dense forest. Snowfall did not seem to affect the winter coherence. Due to insufficient measurements, no conclusions could be made about the effect of wind.

The influence of temporal and spatial baseline on the coherence was also investigated. Coherence from winter pairs with temporal baselines of 88 days, two years and three years was compared with the 44-day coherence. The analysis showed that under favourable conditions 88-day coherence from sparse forest could reach above 0.5. For images that were separated by over one year, the coherence was significantly lower, but at some test areas still showed possibilities to separate sparse and dense forest. No clear correlation could be identified between perpendicular baseline and coherence, even though dense forest displays a weak tendency towards higher coherence for baselines shorter than 500 m. Baselines up to 2 km were found to give high coherence for sparse forest.

A comparison between JERS-1 repeat-pass coherence and ERS-1/2 tandem coherence showed that under frozen conditions L-band coherence could reach levels comparable to C-band coherence acquired under unfrozen conditions.

In the second part of the study it was evaluated if JERS-1 repeat-pass coherence can be used to retrieve growing stock volume. Based on the results from the analysis of temporal decorrelation, only 44-day coherence from the winter season was considered. An exponential model was selected to describe the relationship between coherence and growing stock volume. As indicators for the retrieval accuracy the RMSE, the relative RMSE and the coefficient of determination R^2 were chosen. A best RMSE of 60 m³/ha was obtained and in most cases the RMSE was smaller than 100 m³/ha. With one exception the relative RMSE stayed within the range 43 to 76 %. R^2 showed large variations, partly depending on the distribution of growing stock volumes for the respective test area. The best R^2 was observed to be 0.75.

The same model was used for growing stock volume retrieval from ERS-1/2 tandem coherence. The best obtained values of RMSE, relative RMSE and R^2 were 57 m³/ha, 37 % and 0.73 respectively. For over 70% of the studied pairs the RMSE was over 100 m³/ha. The obtained retrieval accuracy for JERS-1 coherence is in many cases as good as, or better than for the ERS-1/2 coherence. This indicates that under frozen winter conditions L-band repeat-pass coherence can be an alternative to C-band coherence for growing stock volume retrieval.

In the final part of the study the aim was to make a first evaluation of potential forestry applications with JERS-1 repeat-pass coherence. Two applications were selected for the evaluation, one representing forest mapping and the other forest monitoring. To investigate the mapping potential, a simple growing stock volume classification was done. The classification was done with a method that requires one coherence image and one backscatter image. The results show a high accuracy for classification of the class with growing stock volumes above 80 m³/ha, but with the current version of the SIBERIA algorithm, the growing stock volume is overestimated for sparse and young forest.

As an example of forest monitoring with JERS-1 repeat-pass coherence, a simple method for change detection was tested. Using histogram thresholds for a time series of at least two coherence images it was possible to identify larger changes like clear-cuts that occurred in the period between the acquisitions for the two images. For identification of smaller changes, e.g. selective logging or thinning, refined methods will be needed. The possibility to combine L-band and C-band coherence was demonstrated with a time series consisting of coherence images from JERS-1 (1994 and 1996) and one from ERS-1/2 (1997).

7.2 Discussion

The presented results show that as long as the acquisitions are made under frozen conditions, satellite-borne L-band interferometric coherence can provide information for forestry applications. This is a positive result, but it is also connected with geographical and temporal limitations. Only in boreal forest can we expect to find frozen conditions at two acquisitions separated by 44 days or more. Compared to the continental climate in Siberia, the more coastal climate in Northern Europe also

reduce the probability to find image pairs acquired under frozen conditions. However, the vast majority of the boreal forests in the world are located far enough from the coasts to provide a climate suitable for winter acquisitions. Temporally the acquisition period is limited to a few months per year. With a repeat-cycle as long as 44 days this reduce the number of possible acquisitions so that only two, or in extreme cases three, coherence images can be produced annually. For most types of forest monitoring this should be enough.

It should be noted that no JERS-1 pairs with dry unfrozen conditions at both acquisition dates were available for evaluation. Test areas where data from both frozen and dry unfrozen conditions are available need to be analysed to fill this gap.

The methods and models that have been used in this thesis for retrieval, mapping and monitoring are not the most advanced, but were found to be sufficient for the purpose of demonstrating the capacity of L-band repeat-pass coherence. For operational use, or for increased accuracy, improvements might be needed, or more sophisticated methods and models should be selected.

7.3 Future outlook

Currently there are no satellites in orbit with an L-band SAR onboard, but this will change within a near future. During the second half of 2005 JAXA plans to launch the Advanced Land Observing Satellite (ALOS), which will carry the Phased Array type L-band SAR (PALSAR). PALSAR will have the capability of acquiring fully polarimetric data and electronically steering the look angle within a wide range (See Table A.1 in Appendix A), but most of the time it will be operating with only one or two polarizations at a fixed look angle. The nominal look angle will be 34.3° (ITO *et al.*, 2001) and the polarizations HH or HH+HV. This will provide continuity with the acquisition characteristics of its predecessor JERS-1 SAR. ALOS will have an orbit with a repeat-cycle of 46 days, which should result in repeat-pass coherence with properties and limitations similar to those reported in this thesis. The advantages with PALSAR compared to JERS-1 will be the possibility to acquire simultaneous data in two or four polarizations, or when operated in single polarization mode, a higher spatial resolution. An improved orbit control can also be expected.

Over the years many satellite concepts incorporating an L-band SAR have been proposed. Two of the proposals that currently are under evaluation are the TerraSAR-L and the MAPSAR satellites (ZINK, 2003, SCHRÖDER *et al.*, 2003). As can be seen in Appendix A, these two have a lot in common. Both plan to use a bandwidth that fills the whole 85 MHz that have been allocated by the World Administrative Radio Conference (WARC). This would give a significantly higher spatial resolution than previous and current SAR satellites can offer. With a shorter repeat-cycle, like the 14 days of TerraSAR-L, the possibility to obtain image pairs with high coherence will be greatly increased and the geographical and temporal limitations that were mentioned in the previous discussion will be relaxed. Both of these satellites should be suitable for the polarimetric interferometric SAR (PolInSAR) methods that have been developed for estimation of forest parameters (TREUHAFT *et al.*, 1996; CLOUDE & PPATHANASSIOU, 1998; TREUHAFT & SIQUEIRA, 2000; PPATHANASSIOU & CLOUDE, 2001).

Another innovative idea is the interferometric cartwheel, where a constellation of passive radar micro-satellites flies in formation with a conventional SAR (MASSONNET, 2001; ZINK *et al.*, 2003). The quasi-simultaneous radar acquisitions by the micro-satellites can be used as a single-pass InSAR system. In this way there will be no temporal decorrelation affecting the coherence. This would make it easier to estimate forest parameters like the forest height. It has been proposed to fly a cartwheel constellation together with ALOS or TerraSAR-L.

Chapter 8

Acknowledgements

First of all I would like to thank Prof. Christiane Schmullius. Without her support this thesis would never have been written, and I do not think that I would have gotten the same freedom to work on my own ideas anywhere else. From her I also learnt the importance of having visions and seeing opportunities instead of difficulties. There is no project that is too small or too large, and with hard work even the most impossible proposal deadlines can be managed. When I moved to Germany I had a contract for five months, but Christiane had already promised trying to find financing for an extension. Well, she really did a good job on that! Uncountable contract changes and extensions later I now leave Jena after having spent four intense and unforgettable years in Germany.

Apart from Christiane, there are three persons who have had a great influence on decisions and “coincidences” that eventually gave me the possibility to write this PhD thesis. These three are Lars-Arne Ekerstig, Prof. Jan Askne, and Åke Rosenqvist. I have had very few teachers or professors who have shown as much passion for their subject as Lars-Arne Ekerstig in Kiruna. One of his lectures was on remote sensing. After that I knew what I wanted to work with. A few years later I had finished my university studies and was looking for a job. Jan Askne informed me about a free position at the Joint Research Centre of the European Commission (JRC) and offered me a project position in his group so I could wait for their decision. Without his support and encouragement I would probably not be working with remote sensing today. Even though Åke Rosenqvist was not the one who made the decisions, in different ways he was involved both when I got the job at JRC in Italy and at DLR in Germany. Thanks to his advice and support I also got access to most of the JERS-1 data on which the results in this thesis are based. He is a good friend and an inspiring colleague. If there is one person who can compete with Christiane in having great visions and, even more important, the energy and enthusiasm to make these visions come true, it is Åke.

Other people who deserve to be mentioned for giving me the opportunity to earn experience in the field of radar remote sensing are John Curlander and Richard Carande at Vexcel Corporation in Bolder, USA, Ben Holt and Mark Drinkwater at the National Aeronautics and Space Administration (NASA) Jet Propulsion Laboratory (JPL) in Pasadena, USA, and Alan Belward and Gianfranco DeGrandi in the Global Vegetation Monitoring Unit at JRC in Ispra, Italy. These experiences have been invaluable, and I would not be where I am today without them.

Large parts of this work were funded by the German Ministry for Education and Research (BMBF) through the projects FKZ 50 EE 9725 SIBERIA and 50EE0035 TerraDew, and by the European Commission through the SIBERIA-II project. Preparation of the ground database, creation of the DEMs for Bolshe Murtinsky and processing of the JERS-1 data from 1998 was done within the project SIBERIA (Contract No. ENV4-CT97-0743-SIBERIA), which was financed through the 4th Framework Programme of the European Commission.

Many of the programs and scripts that have been used for the work presented in this thesis are based on programs that were developed within the SIBERIA project, and special acknowledgements here goes to Wolfgang Wagner and Jan Vietmeier at DLR in Oberpfaffenhofen, Germany, Adrian Luckman and Kevin Tansey at the University of Wales in Swansea, UK, Malcolm Davidson at Centre d'Etudes Spatiales de la Biosphere (CESBIO) in Toulouse, France, Shaun Quegan at Sheffield Centre for Earth Observation Science (SCEOS), Sheffield, UK, and Heiko Balzter at the Centre for Ecology and Hydrology (CEH), Monks Wood, UK. The processing of all JERS-1 data from level 0 to SLC-format was done by Andreas Wiesmann at Gamma RS in Bern, Switzerland. All InSAR processing, geocoding and image co-registration was done in Jena with software from Gamma RS. Many thanks go to Urs Wegmüller and Andreas Wiesmann from Gamma RS for their excellent and fast support on all questions regarding the processing. Sergey Maximov is acknowledged for writing the section of the processing script that handles the ERS-1/2 precision orbit vectors.

JERS-1 SAR data were acquired and provided to FSU by the Japan Aerospace Exploration Agency (JAXA) Earth Observation Research and application Centre (EORC) within the framework of the GBFM project. ERS-1/2 data were made available through ESA's 3rd ERS Announcement of Opportunity (Project Number AO3.120 SIBERIA). JERS-1 data from 1998 and ERS-1/2 data from September and October 1997 and from the summer 1998 were received by a mobile receiving station of the DLR. Meteorological data were supplied by the DWD. Supplementary weather data were downloaded from <http://www.wunderground.com/>.

During my years in the Institute of Geography at FSU in Jena I got to know a lot of people. I would like to thank Martin König and Kevin Tansey for helping me getting started in Jena, Frau Mendler with whom I shared the office for over a year, and the whole Geoinformatics group with whom I always had lunch during the first two years. Special thanks goes to Rainer "Hoffi" Hoffmann for keeping the systems and programs running, even though some of us wanted to work on three different operating systems at the same time, and to Bettina Böhm for letting me use her private library, which included the most important scientific journal in my field of research.

The Remote Sensing Group has been in constant growth since I got to Jena. Although we were divided in different projects and buildings it was always easy to talk to people. I must admit it feels sad to leave such a dynamic group and I will miss our coffee meetings and "Kneipenabende", even though they only occurred on an irregular basis. I wish we would have had more trips together, like the one to Frascati. I would also like to thank our "HiWis", in particular Oliver Cartus, Ulli Poppe, and Klarissa Kornhass for help with endless and boring tasks like data processing, data archiving, burning of backup-DVDs and copying of literature.

The person who has been most important for me, as a friend, colleague, and co-author on several papers, is Maurizio Santoro. The importance of having someone in the group working on the same topics, someone to learn from and to discuss problems with can not be overestimated. Sorry that I never learnt Italian properly, otherwise we could have had those discussions in four different languages. A night in the office, waiting for the launch of Envisat, our two-day trip around Thüringen and three “Schwarzbiernächte” are some of the things that will help me remember that it was not only work.

I’m also grateful we got such a great driver for the “Siberia Bus”. Christian Beer was the one who kept the bus green and always tried to keep the passengers in a good mood. Christian, you should write a book with German proverbs. I promise I will buy it. Christian is also the one who had the misfortune to have to correct all my written German.

There are also a large number of people outside the institute who made me feel at home in Jena. Rike, I’m very happy that I met you already after one month in Jena. Thank you for teaching me German and for inviting me to all your parties. Thanks to you I got to know Jena from the students’ point of view. I would also like to thank the “first” Swedish group I met in Jena, (Ingemar, David, Lennart, Mats, Kent, Marie, Sara and Karolina), the “second” Swedish group (Håkan, Henrik, Annette, Anna, Susanna, Erik, Gustav, Bert and Emilie), the “Nordischer Stammtisch” (Annett, Stan, Vero, Julia,) and the FSU Unihockey Team (Fritz & Co.) for a lot of fun and for keeping up some of the Scandinavian traditions and sports.

Last, but not least I must thank my family for always being there for me when I needed them, and never questioning my decisions to move from one end of the world to the other.

“Work all night on a thesis script
Daylight come and me wan’ go home”

Modified from “The Banana Boat Song”
Harry Belafonte, Lord Burgess and William Attaway

References

- Anonymous, "Weather Underground", online: <http://www.wunderground.com/>, The Weather Underground, Inc. Date of access: 29 November 2002.
- ARNAUD, A., ADAM, N., HANSEN, R., INGLADA, J., DURO, J., CLOSA, J., and EINEDER, M., "ASAR ERS Interferometric Phase Continuity", *Proceedings of IGARSS'03*, Toulouse, France, 21-25 July, 2003.
- ASKNE, J., DAMMERT, P. B. G., and SMITH, G., "Interferometric SAR observations of forested areas", *Proceedings of Third ERS Symposium on Space at the service of our Environment*, Florence, 14-21 March, pp. 337-344, 1997a.
- ASKNE, J., DAMMERT, P. B. G., ULANDER, L. M. H., and SMITH, G., "C-band repeat-pass interferometric SAR observations of the forest," *IEEE Transactions on Geoscience and Remote Sensing*, vol. 35, 1, pp. 25-35, 1997b.
- ASKNE, J., WEGMÜLLER, U., SMITH, G., SANTORO, M., and DAMMERT, P., "JERS-1 interferometry of boreal forest," in *JERS-1 Science Program '99 PI Reports*, Shimada, M., Ed.: EORC, National Space Development Agency of Japan, pp. 144-148, 1999.
- ASKNE, J., SANTORO, M., SMITH, G., and FRANSSON, J., "L-band observations of boreal forest stem volume", *Proceedings of 23rd EARSeL Annual Symposium*, Gent, 2-5 June, pp. 159-166, 2003a.
- ASKNE, J., SANTORO, M., SMITH, G., and FRANSSON, J. E. S., "Multitemporal repeat-pass SAR interferometry of boreal forests," *IEEE Transactions on Geoscience and Remote Sensing*, vol. 41, 7, pp. 1540-1550, 2003b.
- BALZTER, H., TALMON, E., WAGNER, W., GAVEAU, D., PLUMMER, S., YU, J. J., QUEGAN, S., DAVIDSON, M., LE TOAN, T., GLUCK, M., SHVIDENKO, A., NILSSON, S., TANSEY, K., LUCKMAN, A., and SCHMULLIUS, C., "Accuracy assessment of a large-scale forest cover map of central Siberia from synthetic aperture radar," *Canadian Journal of Remote Sensing*, vol. 28, 6, pp. 719-737, 2002.
- BAMLER, R., and HARTL, P., "Synthetic aperture radar interferometry," *Inverse Problems*, vol. 14, 4, pp. R1-R54, 1998.
- BERGEN, K., DOBSON, M. C., PIERCE, L., and ULABY, F., "Effects of within-season dielectric variations on terrain classification using SIR-C/X-SAR", *Proceedings of IGARSS'97*, Singapore, 3-8 August, 1997.
- BORN, M., and WOLF, E., *Principles of Optics*, 6 ed, Pergamon Press, 1980.

- CLOUDE, S. R., and PAPATHANASSIOU, K. P., "Polarimetric SAR interferometry," *IEEE Transaction on Geoscience and Remote Sensing*, vol. 36, 5, pp. 1551-1565, 1998.
- CURLANDER, J. C., and MCDONOUGH, R. N., *Synthetic Aperture Radar: Systems and Signal Processing*, Kong, J. A., John Wiley & Sons, Inc., New York, 647 pp., 1991.
- DAMMERT, P. B. G., "Accuracy of INSAR measurements in forested areas", *Proceedings of 'Fringe 96' Workshop on ERS SAR Interferometry*, Zürich, 30 September - 2 October, pp. 37-49, 1996.
- DAMMERT, P. B. G., "Spaceborne SAR Interferometry: Theory and Applications", Ph.D. thesis, *Technical Report 382*, Department of Radio and Space Science, Chalmers University of Technology, Göteborg, Sweden, 1999.
- ERIKSSON, L., SANTORO, M., WIESMANN, A., and SCHMULLIUS, C., "Multi-seasonal study of the SIBERIA classification procedure", *Proceedings of ForestSAT Symposium*, Edinburgh, 5-9 August, CD-ROM, 2002a.
- ERIKSSON, L., WIESMANN, A., and SCHMULLIUS, C., "JERS repeat pass coherence for observation of Siberian forest", *Proceedings of 3rd International Symposium 'Retrieval of Bio- and Geophysical Parameters from SAR Data for Land Applications'*, Sheffield, UK, 11-14 September 2001, ESA SP-475, pp. 33-38, 2002b.
- ERIKSSON, L. E. B., SANTORO, M., WIESMANN, A., and SCHMULLIUS, C., "Multi-temporal JERS repeat-pass coherence for growing stock volume estimation of Siberian forest," *IEEE Transactions on Geoscience and Remote Sensing*, vol. 41, 7, pp. 1561-1570, 2003.
- ESA, "New views of the Earth - Engineering achievements of ERS-1", SP-1176/III, pp. 1-124, ESA ESTEC, Noordwijk, The Netherlands, 1997.
- FAO, "Global Forest Resources Assessment 2000 - Main Report", Forestry Paper 140, pp. 479, FAO, Rome, Italy, 2001.
- FRANSSON, J. E. S., SMITH, G., ASKNE, J., and OLSSON, H., "Stem volume estimation in boreal forests using ERS-1/2 coherence and SPOT XS optical data," *International Journal of Remote Sensing*, vol. 22, 14, pp. 2777-2791, 2001.
- GABRIEL, A. K., and GOLDSTEIN, R. M., "Crossed orbit interferometry: theory and experimental results from SIR-B," *International Journal of Remote Sensing*, vol. 9, 5, pp. 857-872, 1988.
- GATELLI, F., MONTI GUARNIERI, A., PARIZZI, F., PASQUALI, P., PRATI, C., and ROCCA, F., "The wavenumber shift in SAR interferometry," *IEEE Transactions on Geoscience and Remote Sensing*, vol. 32, 4, pp. 855-865, 1994.
- GATES, D. M., "Water relations of forest trees," *IEEE Transaction on Geoscience and Remote Sensing*, vol. 29, 6, pp. 836-842, 1991.
- GOLDSTEIN, R. M., and ZEBKER, H. A., "Interferometric radar measurement of ocean surface current," *Nature*, vol. 328, pp. 707-709, 1987.
- GOLDSTEIN, R. M., ZEBKER, H. A., and WERNER, C. L., "Satellite radar interferometry: Two-dimensional phase unwrapping," *Radio Science*, vol. 23, 4, pp. 713-720, 1988.
- GRAHAM, L. C., "Synthetic interferometer radar for topographic mapping," *Proceedings of the IEEE*, vol. 62, 6, pp. 763-768, 1974.

- GUNERIUSSEN, T., HØGDA, K. A., JOHNSEN, H., and LAUKNES, I., "InSAR for estimation of changes in Snow Water Equivalent of dry snow," *IEEE Transactions on Geoscience and Remote Sensing*, vol. 39, 10, pp. 2101-2108, 2001.
- HAGBERG, J. O., ULANDER, L. M. H., and ASKNE, J., "Repeat-pass SAR interferometry over forested terrain," *IEEE Transactions on Geoscience and Remote Sensing*, vol. 33, 2, pp. 331-340, 1995.
- HALLDIN, S., GRYNING, S.-E., GOTTSCHALK, L., JOCHUM, A., LUNDIN, L.-C., and VAN DE GRIEND, A. A., "Energy, water and carbon exchange in a boreal forest landscape - NOPEX experiences," *Agricultural and Forest Meteorology*, vol. 98-99, pp. 5-29, 1999.
- HARRELL, P. A., BOURGEOU-CHAVEZ, L. L., KASISCHKE, E. S., FRENCH, N. H. F., and CHRISTENSEN JR., N. L., "Sensitivity of ERS-1 and JERS-1 radar data to biomass and stand structure in Alaskan boreal forest," *Remote Sensing of Environment*, vol. 54, pp. 247-260, 1995.
- HESS, L., MELACK, J. M., and SIMONETT, D. S., "Radar detection of flooding beneath the forest canopy: a review," *International Journal of Remote Sensing*, vol. 11, 7, pp. 1313-1325, 1990.
- HYYPPÄ, J., HYYPPÄ, H., INKINEN, M., ENGDAHL, M., LINKO, S., and ZHU, Y.-H., "Accuracy comparison of various remote sensing data sources in the retrieval of forest stand attributes," *Forest Ecology and Management*, vol. 128, 1-2, pp. 109-120, 2000.
- ISRAELSSON, H., ASKNE, J., FRANSSON, J., and SYLVANDER, R., "JERS-1 SAR analysis of boreal forest biomass", in Final report of JERS-1/ERS-1 System Verification Program, Volume II, pp. 38-45, Ministry of International Trade and Industry, National Space Development Agency of Japan, Tokyo, 1995.
- ITO, N., HAMAZAKI, T., and TOMIOKA, K., "ALOS/PALSAR characteristics and status", *Proceedings of CEOS SAR Workshop*, Tokyo, Japan, 2-5 April, 2001.
- JENSEN, J. R., *Remote sensing of the environment - An earth resource perspective*, Prentice Hall, Upper Saddle River, New Jersey, USA, 544 pp., 2000.
- KINGSLEY, S., and QUEGAN, S., *Understanding radar systems*, McGraw-Hill Book Company, Berkshire, England, 375 pp., 1992.
- KOSKINEN, J., "Snow monitoring using microwave radars", Ph.D. thesis, Laboratory of Space Technology, Helsinki University of Technology, Espoo, Finland, 2001.
- KOSKINEN, J. T., PULLIAINEN, J. T., HYYPPÄ, J. M., ENGDAHL, M. E., and HALLIKAINEN, M. T., "The seasonal behavior of interferometric coherence in boreal forest," *IEEE Transactions on Geoscience and Remote Sensing*, vol. 39, 4, pp. 820-829, 2001.
- KRAMER, H. J., *Observation of the Earth and Its Environment - Survey of Missions and Sensors*, 4th ed, Springer Verlag, Berlin, Germany, 1982 pp., 2002.
- KRAVKA, M., KREJZAR, T., and CERMÁK, J., "Water content in stem wood of large pine and spruce trees in natural forests in central Sweden," *Agricultural and Forest Meteorology*, vol. 98-99, pp. 555-562, 1999.
- KURVONEN, L., PULLIAINEN, J., and HALLIKAINEN, M., "Retrieval of biomass in boreal forests from multitemporal ERS-1 and JERS-1 SAR images," *IEEE Transactions on Geoscience and Remote Sensing*, vol. 37, 1, pp. 198-205, 1999.

- LI, F. K., and GOLDSTEIN, R. M., "Studies of multibaseline spaceborne interferometric synthetic aperture radars," *IEEE Transactions on Geoscience and Remote Sensing*, vol. 28, 1, pp. 88-97, 1990.
- LI, S., and STURM, M., "Patterns of wind-drifted snow on Alaskan arctic slope, detected with ERS-1 interferometric SAR," *Journal of Glaciology*, vol. 48, 163, pp. 495-504, 2002.
- LIN, R. T., "Review of the dielectric properties of wood and cellulose," *Forest Products Journal*, vol. 17, 7, pp. 61-66, 1967.
- LINDGREN, O., "A study on circular plot sampling of Swedish forest compartments", *Report 11*, Department of Biometry and Forest Management, Swedish University of Agricultural Sciences, Umeå, Sweden, 1984.
- LUCKMAN, A., BAKER, J., and WEGMÜLLER, U., "Repeat-pass interferometric coherence measurements of disturbed tropical forest from JERS and ERS satellites," *Remote Sensing of Environment*, vol. 73, pp. 350-360, 2000.
- MANNINEN, T., PARMES, E., HÄME, T., SEPHTON, A., BACH, H., and BORGEAUD, M., "ERS coherence and SLC images in forest characterisation", *Proceedings of ERS-Envisat Symposium*, Gothenburg, 16-20 October, 2000.
- MASSONNET, D., "Capabilities and limitations of the interferometric cartwheel," *IEEE Transaction on Geoscience and Remote Sensing*, vol. 39, 3, 2001.
- MCDONALD, K. C., ZIMMERMANN, R., WAY, J., and CHUN, W., "Automated instrumentation for continuous monitoring of the dielectric properties of woody vegetation: system design, implementation, and selected in situ measurements," *IEEE Transactions on Geoscience and Remote Sensing*, vol. 37, 4, pp. 1880-1894, 1999.
- OLMSTED, C., "Alaska SAR facility scientific SAR user's guide", *ASF-SD-003*, pp. 1-53, Alaska SAR facility, Fairbanks, Alaska, USA, 1993.
- PAPATHANASSIOU, K. P., and CLOUDE, S. R., "Single-baseline polarimetric SAR interferometry," *IEEE Transaction on Geoscience and Remote Sensing*, vol. 39, 11, pp. 2352-2363, 2001.
- PULLIAINEN, J. T., KURVONEN, L., and HALLIKAINEN, M. T., "Multitemporal behavior of L- and C-band SAR observations of boreal forests," *IEEE Transactions on Geoscience and Remote Sensing*, vol. 37, 2, pp. 927-937, 1999.
- RANSON, K. J., and SUN, G., "Effects of environmental conditions on boreal forest classification and biomass estimates with SAR," *IEEE Transactions on Geoscience and Remote Sensing*, vol. 38, 3, pp. 1242-1252, 2000.
- RIGNOT, E., "Dual-frequency interferometric SAR observations of a tropical rain-forest," *Geophysical Research Letters*, vol. 23, 9, pp. 993-996, 1996.
- ROGERS, A. E. E., and INGALLS, R. P., "Venus: Mapping the surface reflectivity by radar interferometry," *Science*, vol. 165, 3895, pp. 797-799, 1969.
- ROSEN, P. A., HENSLEY, S., PELTZER, G., RIGNOT, E., and WERNER, C., "JERS-1 synthetic aperture radar interferometry applications: mapping of rain forest environments and crustal deformation studies," in *JERS-1 Science Program '99 PI Reports*, Shimada, M., Ed.: EORC, National Space Development Agency of Japan, pp. 179-184, 1999.

- ROSENQVIST, Å., FORSBERG, B. R., PIMENTEL, T., RAUSTE, Y. A., and RICHEY, J. E., "The use of spaceborne radar data to model inundation patterns and trace gas emission in the central Amazon floodplain," *International Journal of Remote Sensing*, vol. 23, 7, pp. 1303-1328, 2002.
- ROTH, A., KNÖPFLE, W., HUBIG, M., and ADAM, N., "Operational interferometric SAR products", *Proceedings of IGARSS'98*, Seattle, USA, 6-10 July, 1998.
- ROTH, A., KNÖPFLE, W., RABUS, B., GEBHARDT, S., and SCALES, D., "GeMoS - A system for the geocoding and mosaicking of interferometric digital elevation models", *Proceedings of IGARSS'99*, Hamburg, Germany, 28 June - 2 July, 1999.
- RUMSEY, H. C., MORRIS, G. A., GREEN, R. R., and GOLDSTEIN, R. M., "A radar brightness and altitude image of a portion of Venus," *Icarus*, vol. 23, pp. 1-7, 1974.
- SALAS, W. A., RANSON, K. J., ROCK, B. N., and SMITH, K. T., "Temporal and spatial variations in dielectric constant and water status of dominant forest species from New England," *Remote Sensing of Environment*, vol. 47, pp. 109-119, 1994.
- SANTORO, M., ASKNE, J., ERIKSSON, L., SCHMULLIUS, C., WIESMANN, A., and FRANSSON, J. E. S., "Seasonal dynamics and stem volume retrieval in boreal forests using JERS-1 backscatter", *Proceedings of SPIE 9th International Symposium on Remote Sensing*, Agia Pelagia, Crete, 22-27 September, 4879 - Remote Sensing for Agriculture, Ecosystems, and Hydrology IV, pp. 231-242, 2002a.
- SANTORO, M., ASKNE, J., SMITH, G., and FRANSSON, J. E. S., "Stem Volume Retrieval in Boreal Forests with ERS-1/2 Interferometry," *Remote Sensing of Environment*, vol. 81, 1, pp. 19-35, 2002b.
- SANTORO, M., "Estimation of Biophysical Parameters in Boreal Forests from ERS and JERS SAR Interferometry", Ph.D. thesis, Department of Geoinformatics and Remote Sensing, Friedrich-Schiller-University, Jena, Germany, 2003.
- SANTORO, M., ERIKSSON, L., SCHMULLIUS, C., and WIESMANN, A., "Seasonal and topographic effects on growing stock volume estimates from JERS-1 backscatter in Siberian forests", *Proceedings of 23rd EARSeL Annual Symposium*, Gent, 2-5 June, pp. 151-158, 2003.
- SANTORO, M., ASKNE, J., and DAMMERT, P. B. G., "Tree height retrieval from ERS interferometric phase in boreal forest," *IEEE Transactions on Geoscience and Remote Sensing*, submitted.
- SCHMULLIUS, C., ED., BAKER, J., BALZTER, H., DAVIDSON, M., ERIKSSON, L., GAVEAU, D., GLUCK, M., HOLZ, A., LETOAN, T., LUCKMAN, A., MARSCHALK, U., MC CALLUM, I., NILSSON, S., ORRMALM, S., QUEGAN, S., RAUSTE, Y., ROTH, A., ROZHKOVA, V., SOKOLOV, V., SHVIDENKO, A., SIRRO, L., SKUDING, V., STROZZI, T., TANSEY, K., UTSI, R., VIETMEIER, J., VOLOSHUK, L., WAGNER, W., WEGMÜLLER, U., WESTIN, T., WIESMANN, A., and YU, J. J., "SIBERIA - SAR Imaging for Boreal Ecology and Radar Interferometry Applications", Final Report, EU Contract ENV4-CT97-0743-SIBERIA, Friedrich-Schiller-University, Jena, Germany, 2001.
- SCHRÖDER, R., PULS, J., HAJNSEK, I., JOCHIM, F., NEFF, T., KONO, J., PARADELLA, W. R., DA SILVA, M. M. Q., DE MORISSON VALERIANO, D., and COSTA, M. P. F., "MAPSAR: A small L-band SAR mission for land observation", *Proceedings of IAA*, B3, 2003

SCHWÄBISCH, M., and GEUDTNER, D., "Improvement of phase and coherence map using azimuth prefiltering: Examples from ERS-1 and X-SAR", *Proceedings of IGARSS'95*, Florence, 10-14 July, 1, pp. 205-207, 1995.

SELLERS, P. J., HALL, F. G., KELLY, R. D., BLACK, A., BALDOCCHI, D., BERRY, J., RYAN, M., RANSON, K. J., CRILL, P. M., LETTENMAIER, D. P., MARGOLIS, H., CIHLAR, J., NEWCOMER, J., FITZJARRALD, D., JARVIS, P. G., GOWER, S. T., HALLIWELL, D., WILLIAMS, D., GOODISON, B., WICKLAND, D. E., and GUERTIN, F. E., "BOREAS in 1997: Experiment overview, scientific results, and future directions," *Journal of Geophysical Research*, vol. 102, D24, pp. 28731-28769, 1997.

SEYMOUR, M. S., and CUMMING, I. G., "Maximum Likelihood estimation for SAR interferometry", *Proceedings of IGARSS'94*, Pasadena, 8-12 August, pp. 2272-2275, 1994.

SHI, J., HENSLEY, S., and DOZIER, J., "Mapping snow cover with repeat pass synthetic aperture radar", *Proceedings of IGARSS'97*, Singapore, 3-8 August, 1997.

SHI, J., and DOZIER, J., "Estimation of Snow Water Equivalence Using SIR-C/X-SAR - Part I: Inferring Dry Snow Density and Subsurface Properties," *IEEE Transactions on Geoscience and Remote Sensing*, vol. 38, 6, pp. 2465-2474, 2000.

SMITH, G., DAMMERT, P. B. G., and ASKNE, J., "Decorrelation mechanisms in C-Band SAR interferometry over boreal forest," in *Microwave Sensing and Synthetic Aperture Radar*, Franceschetti, G., Oliver, C. J., Rubertone, F. S., and Tajbakhsh, S., Eds.: Proc. SPIE 2958, pp. 300-310, 1996.

SMITH, G., DAMMERT, P. B. G., SANTORO, M., FRANSSON, J. E. S., WEGMÜLLER, U., and ASKNE, J., "Biomass retrieval in boreal forest using ERS and JERS SAR", *Proceedings of Second International Workshop on Retrieval of Bio- and Geophysical Parameters from SAR data for Land Applications*, ESTEC Noordwijk, 21-23 October, pp. 293-300, 1998.

STOLBOVOI, V., and MCCALLUM, I., "Land Resources of Russia", International Institute for Applied Systems Analysis and the Russian Academy of Science, Laxenburg, Austria, CD-ROM, 2002.

STROZZI, T., WEGMÜLLER, U., and MÄTZLER, C., "Mapping wet snowcovers with SAR interferometry," *International Journal of Remote Sensing*, vol. 20, 12, pp. 2395-2403, 1999.

SUGA, Y., and TAKEUCHI, S., "Application of JERS-1 InSAR for monitoring deforestation of tropical rain forest", *Proceedings of IGARSS 2000*, Honolulu, 24-28 July 2000, 1, pp. 432-434, 2000.

TAKEUCHI, S., and YONEZAWA, C., "Utilization of coherence information from JERS-1/SAR for forest type discrimination", *Proceedings of IGARSS'97*, Singapore, 3-8 August, 1997.

TAKEUCHI, S., YONEZAWA, C., and SUGA, Y., "Extraction of land cover information using JERS-1/SAR interferometry", *Proceedings of EUSAR '98 - European Conference on Synthetic Aperture Radar*, Friedrichshafen, Germany, May 25-27, 1998, A98-43151 12-32, pp. 503-506, 1998.

TAKEUCHI, S., and YAMADA, S., "Monitoring of forest fire damage by using JERS-1 InSAR", *Proceedings of IGARSS 2002*, Toronto, Canada, 24-28 June, 2002.

- TAKEUCHI, S., and OGURO, Y., "A comparative study of coherence patterns in C-band and L-band interferometric SAR from tropical rain forest areas," *Advances in Space Research*, vol. 32, 11, pp. 2305-2310, 2003.
- TRETER, U., *Die borealen Waldländer*, 1 ed, Westermann Schulbuchverlag GmbH, Braunschweig, Germany, 210 pp., 1993.
- TREUHAF, R. N., MADSEN, S. N., MOGHADDAM, M., and VAN ZYL, J. J., "Vegetation characteristics and underlying topography from interferometric radar," *Radio Science*, vol. 31, 6, pp. 1449-1485, 1996.
- TREUHAF, R. N., and SIQUEIRA, P. R., "Vertical structure of vegetated land surfaces from interferometric and polarimetric radar," *Radio Science*, vol. 35, 1, pp. 141-177, 2000.
- ULABY, F., and STILES, W., "Microwave Response of Snow," *Advances in Space Research*, vol. 1, 10, pp. 131-149, 1981.
- ULABY, F. T., MOORE, R. K., and FUNG, A. K., *Microwave Remote Sensing, Active and Passive*, vol. II, Dedham, MA: Artech House, 1986a.
- ULABY, F. T., MOORE, R. K., and FUNG, A. K., *Microwave Remote Sensing, Active and Passive*, vol. III, Artech House, Dedham, MA, 1986b.
- ULANDER, L. M. H., DAMMERT, P. B. G., and HAGBERG, J. O., "Measuring tree height using ERS-1 SAR interferometry", *Proceedings of IGARSS'95*, Florence, 10-14 July, pp. 2189-2191, 1995.
- ULANDER, L. M. H., and HAGBERG, J. O., "Radiometric and Interferometric Calibration of ENVISAT-1 ASAR", Research Report, 172, Department of Radio and Space Science, Chalmers University of Technology, Göteborg, Sweden, 1995.
- UNEP, "Convention on biological diversity", online: www.biodiv.org, Secretariat of the Convention on Biological Diversity - United Nations Environment Programme, Web site. Date of access: 1 April 2004.
- WAGNER, W., LUCKMAN, A., VIETMEIER, J., TANSEY, K., BALZTER, H., SCHMULLIUS, C., DAVIDSON, M., GAVEAU, D., GLUCK, M., LE TOAN, T., QUEGAN, S., SHVIDENKO, A., WIESMANN, A., and YU, J. J., "Large-scale mapping of boreal forest in SIBERIA using ERS tandem coherence and JERS backscatter data," *Remote Sensing of Environment*, vol. 85, pp. 125-144, 2003.
- WAY, J., PARIS, J., KASISCHKE, E., SLAUGHTER, C., VIERECK, L., CHRISTENSEN, N., DOBSON, M. C., ULABY, F., RICHARDS, J., MILNE, A., SIEBER, A., AHERN, F. J., SIMONETT, D., HOFFER, R., IMHOFF, M., and WEBER, J., "The effect of changing environmental conditions on microwave signatures of forest ecosystems: preliminary results of the March 1988 Alaskan aircraft SAR experiment," *International Journal of Remote Sensing*, vol. 11, 7, pp. 1119-1144, 1990.
- WEGMÜLLER, U., and WERNER, C. L., "Land applications using ERS-1/2 tandem data", *Proceedings of Fringe 96 Workshop: ERS SAR Interferometry*, Zürich, 30 September-2 October 1996, pp. 97-112, 1996.
- WEGMÜLLER, U., STROZZI, T., and WERNER, C., "Forest applications of ERS, JERS and SIR-C SAR interferometry", *Proceedings of IGARSS'97*, Singapore, 3-8 August, 1997.
- WEGMÜLLER, U., "Automated terrain corrected SAR geocoding", *Proceedings of IGARSS'99*, Hamburg, Germany, 28 June - 2 July, 1999.

WEGMÜLLER, U., WERNER, C., STROZZI, T., and WIESMANN, A., "Automated and precise image registration procedures", *Proceedings of 1st International Workshop on the Analysis of Multitemporal Remote Sensing Images*, Trento, Italy, 13-14 Sept., 2001.

WERNER, C., WEGMÜLLER, U., STROZZI, T., and WIESMANN, A., "Gamma SAR and interferometric processing software", *Proceedings of ERS-Envisat Symposium*, Gothenburg, Sweden, 16-20 October 2000, ESA SP-461, 2000.

WIESMANN, A., WEGMÜLLER, U., and STROZZI, T., "JERS SAR processing for the boreal forest mapping project SIBERIA", *Proceedings of CEOS SAR Workshop*, Toulouse, France, 26-29 October 1999, ESA SP-450, pp. 19-23, 2000a.

WIESMANN, A., WEGMÜLLER, U., STROZZI, T., and WERNER, C., "JERS InSAR coherence over Siberian boreal forest", *Proceedings of ERS-Envisat Symposium*, Gothenburg, 16-20 October, 2000b.

YONEYAMA, K., KOIZUMI, T., SUZUKI, T., KURAMASU, R., ARAKI, T., ISHIDA, C., KOBAYASHI, M., and KAKUICHI, O., "JERS-1 development status," *Acta Astronautica*, vol. 21, 11/12, pp. 783-794, 1990.

ZEBKER, H. A., and VILLASENOR, J., "Decorrelation in interferometric radar echoes," *IEEE Transactions on Geoscience and Remote Sensing*, vol. 30, 5, pp. 950-959, 1992.

ZINK, M., "The TerraSAR-L interferometric mission objective", *Proceedings of Fringe'03*, Frascati, Italy, 1-5 December, 2003.

ZINK, M., KRIEGER, G., and AMIOT, T., "Interferometric performance of a cartwheel constellation for TerraSAR-L", *Proceedings of Fringe'03*, Frascati, Italy, 1-5 December, 2003.

ZISK, S. H., "A new Earth-based radar technique for the measurement of lunar topography," *Moon*, vol. 4, 3-4, pp. 296-300, 1972a.

ZISK, S. H., "Lunar topography: First radar-interferometer measurements of the Alphonsus-Ptolemaeus-Arzachel region," *Science*, vol. 178, pp. 977-980, 1972b.

Appendix A

Table of space-borne L-band SAR sensors

Table A.1 Previous, planned and proposed satellite-borne L-band SAR sensors (ITO *et al.*, 2001; KRAMER, 2002; SCHRÖDER *et al.*, 2003; ZINK, 2003) and (www.eorc.nasda.go.jp/ALOS/).

Mission	SEASAT	JERS-1	ALOS	TerraSAR-L	MAPSAR
Sensor	SAR	SAR	PALSAR	SAR	SAR
Duration	27 June – 10 Oct. 1978 70 days data generation	11 Feb. 1992 – Oct. 1998	Second half of 2005	2008??	2008??
Altitude [km]	769-799 km	568	692	630	620
Repeat cycle [days]	3	44	46	14	37
Frequency [GHz]	1.275	1.275	1.270	1.2575	1.2575
Wavelength [cm]	23.5	23.5	23.6	23.9	23.9
Band width [MHz]	19	15	28 (single pol. relay sat) 14 (all other modes)	80	85
Polarization	HH	HH	HH, VV, HV, VH	HH, VV, HV, VH	HH, VV, HV, VH
Look angle	20°	35.21° (right looking)	9.9°-50.8° (Fine mode) 9.7°-26.2° (Pol.) 20.1°-36.5° (ScanSAR)	20°-45°	20°-42°
Swath width [km]	100	75	40-70 (Fine mode) 20-65 (Polarimetric mode) 250-350 (ScanSAR mode)	40-70 (Stripmap) >200 (ScanSAR)	20-55
Spatial resolution [m]: azimuth	25 (4 looks)	18 (3 looks)	10 / 20 (Fine and Pol.) 94-100 (ScanSAR 2 look)	5 (Stripmap) 50 (ScanSAR dual pol.)	3.1 / 10 / 20 (1 / 3.3 / 6.6 looks)
range	25	18	7-44 / 14-88 (Fine mode) 24-89 (Polarimetric mode) 70-157 (ScanSAR 4 look)	9 (Stripmap) 50 (ScanSAR dual pol.)	3.1-4.7 / 10 / 20

Table A.2 L-band SAR sensors on the NASA Space Shuttle and Russian MIR space station (JORDAN *et al.*, 1995; KRAMER, 2002) and (<http://southport.jpl.nasa.gov/scienceapps/sirb.html>)

Mission	SIR-A	SIR-B	SIR-C	PRIRODA
Sensor	SAR	SAR	L-SAR	Travers
Duration	12-15 Nov. 1981	5-13 October 1984	9-20 April 1994 30 Sept.-11 Oct. 1994	23 April 1996 - 23 March 2001
Altitude [km]	260	224	225	300-400
Repeat cycle [days]	?	1	1	6
Frequency [GHz]	1.28	1.275	1.250	1.28
Wavelength [cm]	23	23.5	23.5	23
Band width [MHz]	?	12	10 / 20	5
Polarization	HH	HH	VV, HH, HV, VH	HH or VV
Look angle	47°	15°-65°	20°-55°	35°
Swath width [km]	50	20-40	15-90	50 (400 km altitude)
Spatial resolution [m]:				
azimuth	40	20-30 (4 looks)	27	20
range	40	16-58	8.3 / 14.9	100

References:

ITO, N., HAMAZAKI, T., and TOMIOKA, K., "ALOS/PALSAR characteristics and status", *Proceedings of CEOS SAR Workshop*, Tokyo, Japan, 2-5 April, 2001.

JORDAN, R. L., HUNEYCUTT, B. L., and WERNER, M., "The SIR-C/X-SAR synthetic aperture radar system," *IEEE Transactions on Geoscience and Remote Sensing*, vol. 33, 4, pp. 829-839, 1995.

KRAMER, H. J., *Observation of the Earth and Its Environment - Survey of Missions and Sensors*, 4th ed, Springer Verlag, Berlin, Germany, 1982 pp., 2002.

SCHRÖDER, R., PULS, J., HAJNSEK, I., JOCHIM, F., NEFF, T., KONO, J., PARADELLA, W. R., DA SILVA, M. M. Q., DE MORISSON VALERIANO, D., and COSTA, M. P. F., "MAPSAR: A small L-band SAR mission for land observation", *Proceedings of IAA*, B3, 2003

ZINK, M., "The TerraSAR-L interferometric mission objective", *Proceedings of Fringe'03*, Frascati, Italy, 1-5 December, 2003.

Appendix B

Results from the model fitting and growing stock volume retrieval

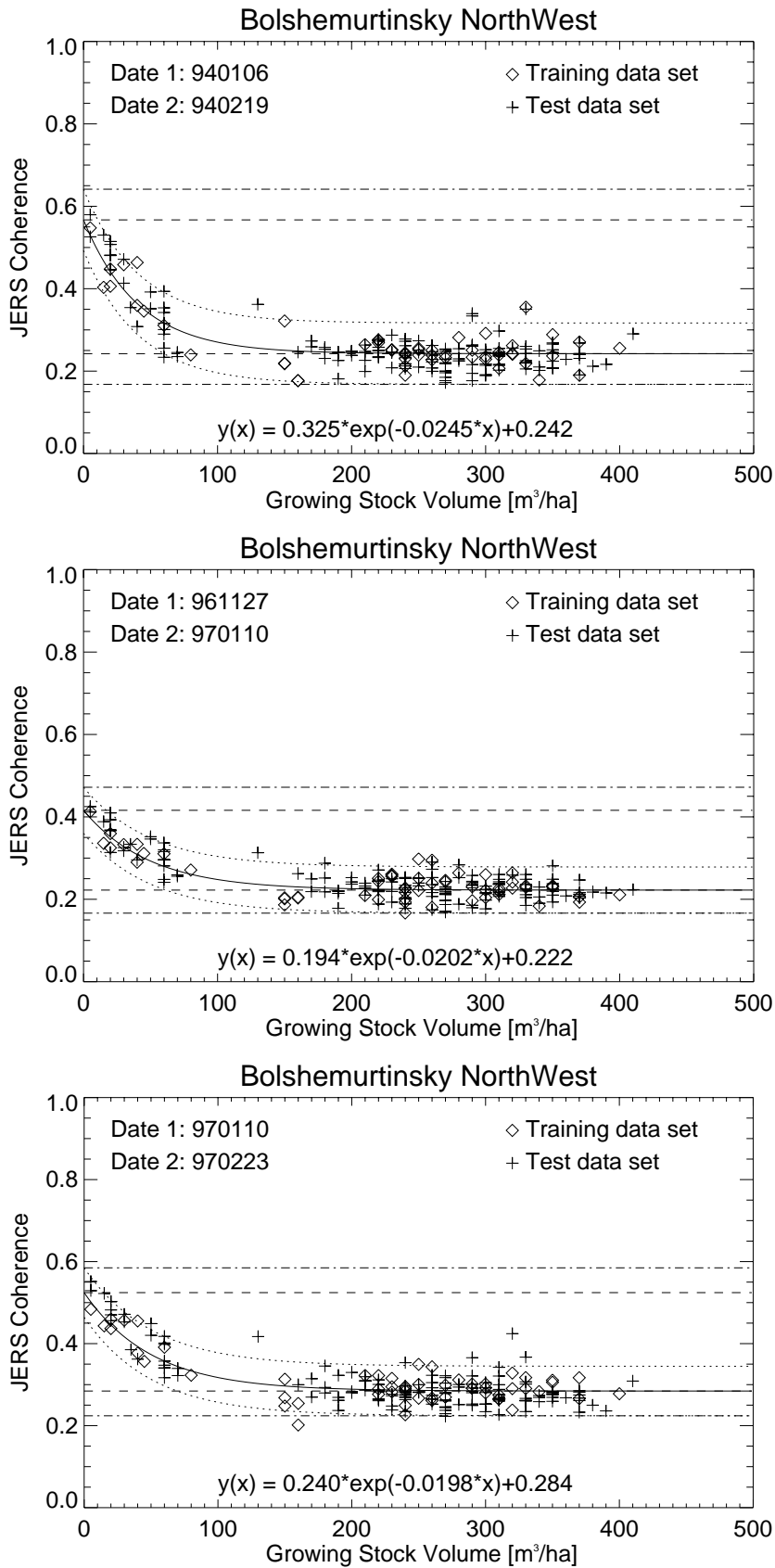


Figure B.1 Regression curves for JERS coherence of Bolshe Murtinsky Northwest. The regression parameters are given in the expressions at the bottom of each plot. The dashed lines correspond to the upper and lower limits of the regression curves. The dotted lines represent the two standard deviation distances from the curve and the dashed dotted lines are the limits that were used for removal of outliers.

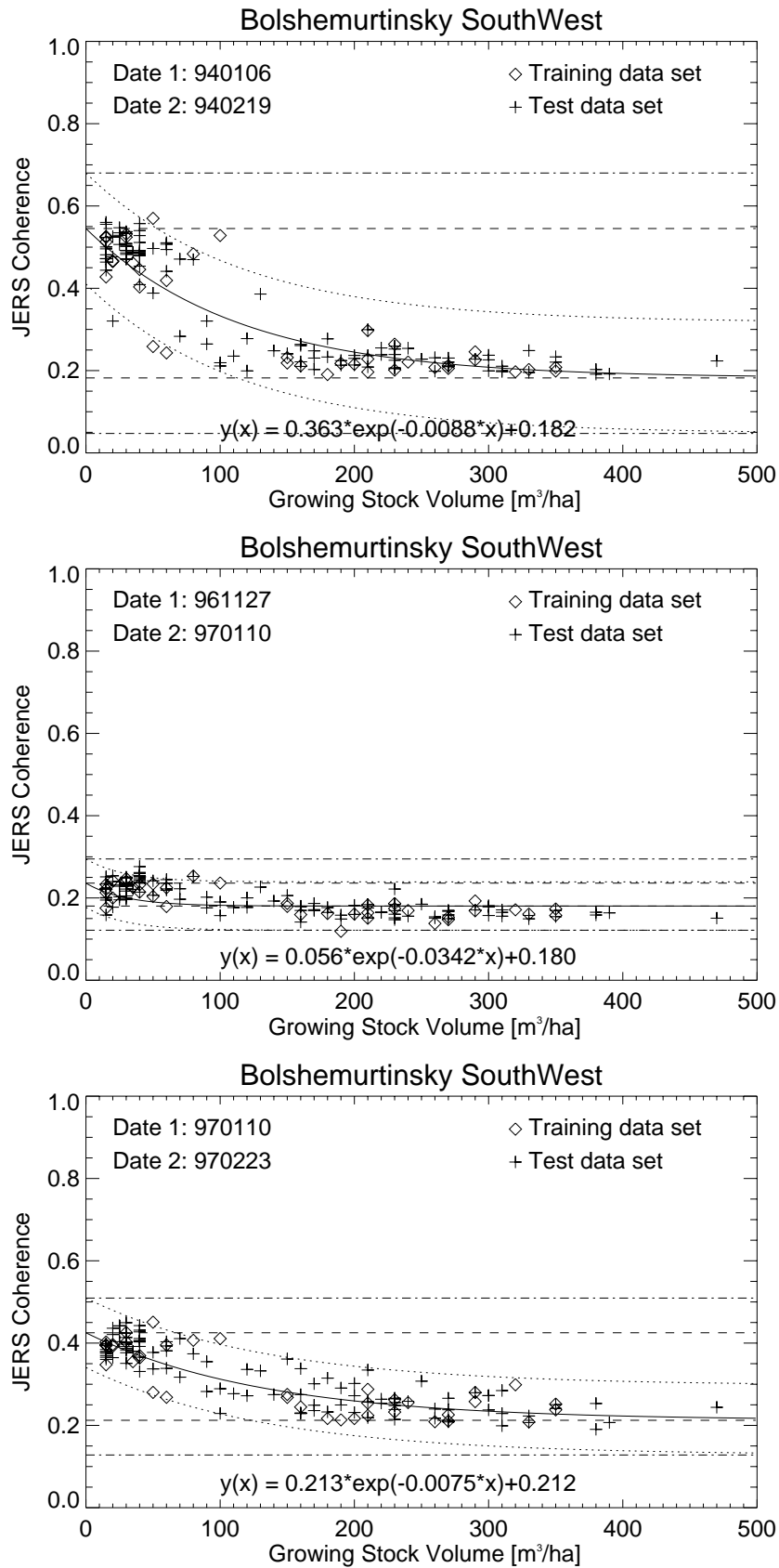


Figure B.2 Regression curves for JERS coherence of Bolshe Murtinsky Southwest. The regression parameters are given in the expressions at the bottom of each plot. The dashed lines correspond to the upper and lower limits of the regression curves. The dotted lines represent the two standard deviation distances from the curve and the dashed dotted lines are the limits that were used for removal of outliers.

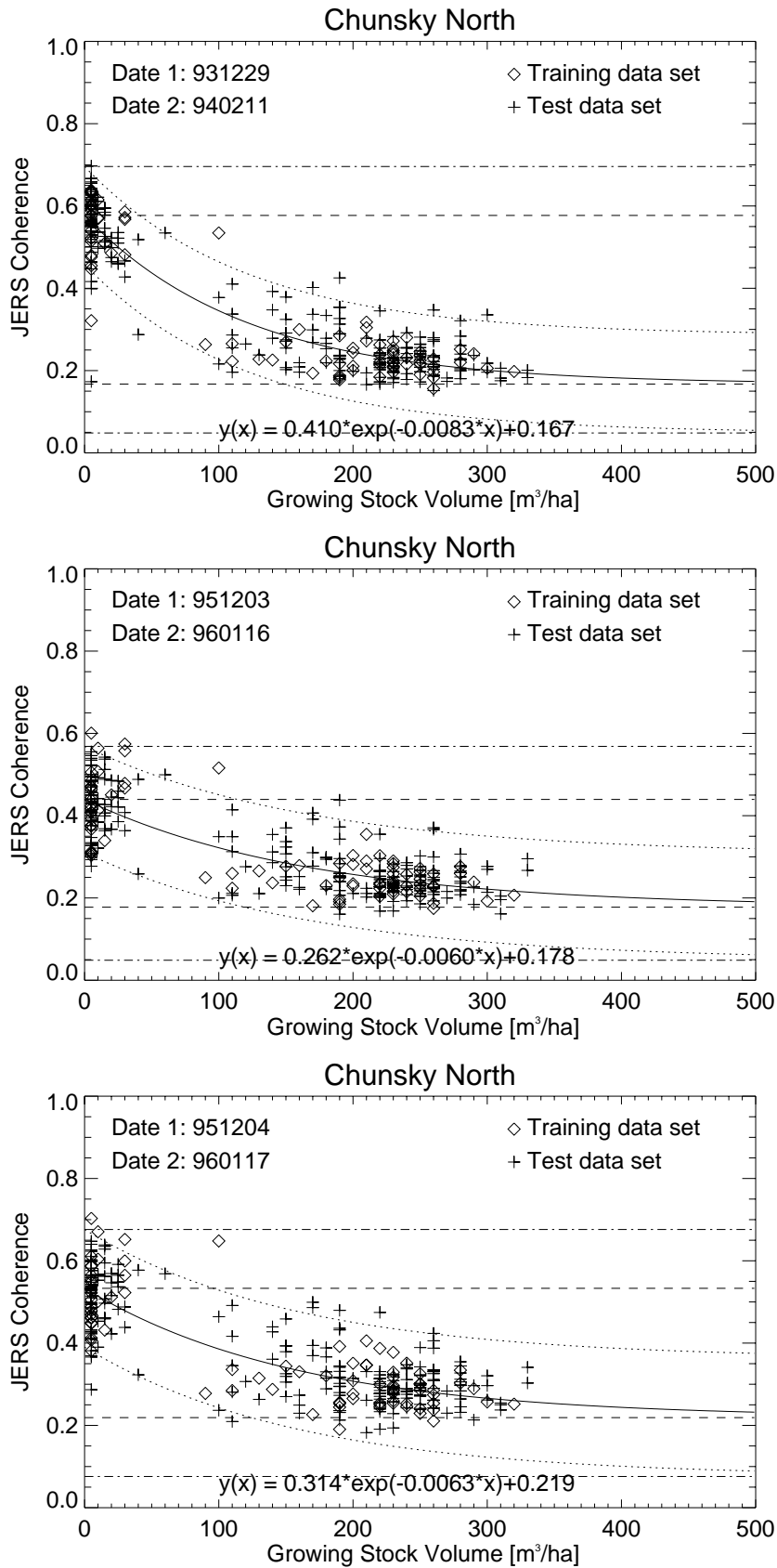


Figure B.3a Regression curves for JERS coherence of Chunsky North. The regression parameters are given in the expressions at the bottom of each plot. The dashed lines correspond to the upper and lower limits of the regression curves. The dotted lines represent the two standard deviation distances from the curve and the dashed dotted lines are the limits that were used for removal of outliers.

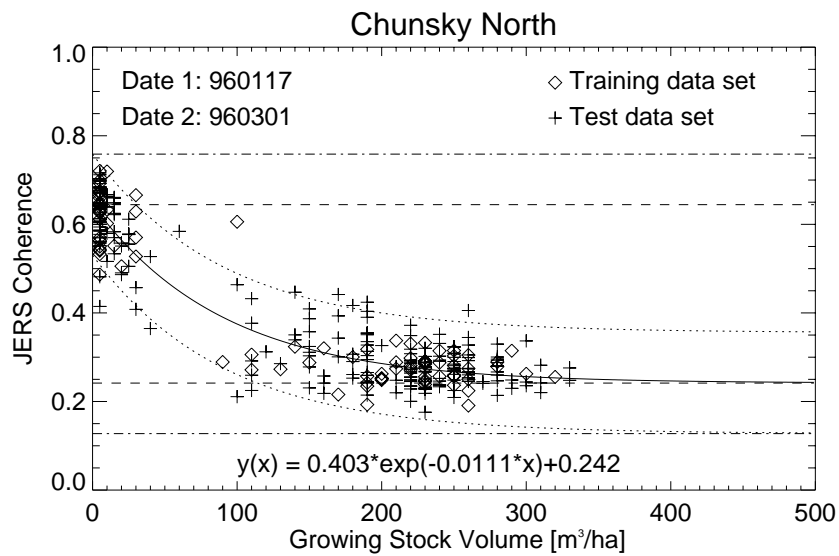
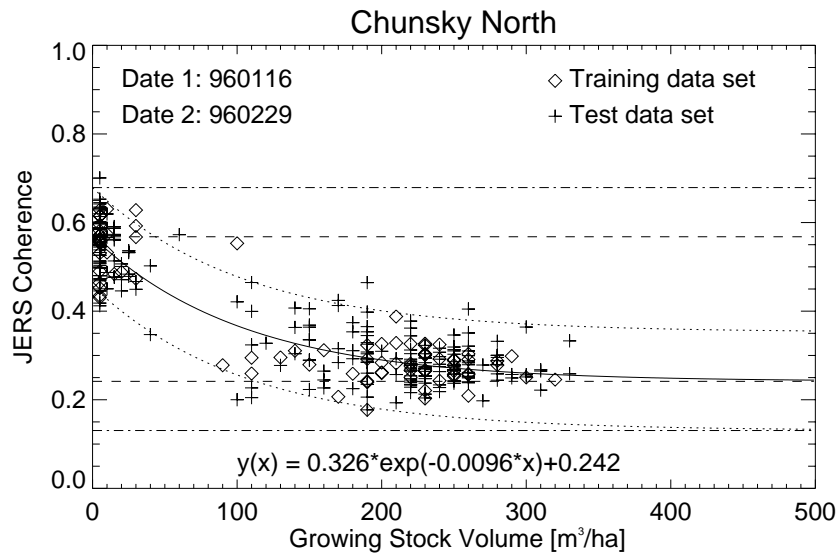


Figure B.3b Regression curves for JERS coherence of Chunsky North. The regression parameters are given in the expressions at the bottom of each plot. The dashed lines correspond to the upper and lower limits of the regression curves. The dotted lines represent the two standard deviation distances from the curve and the dashed dotted lines are the limits that were used for removal of outliers.

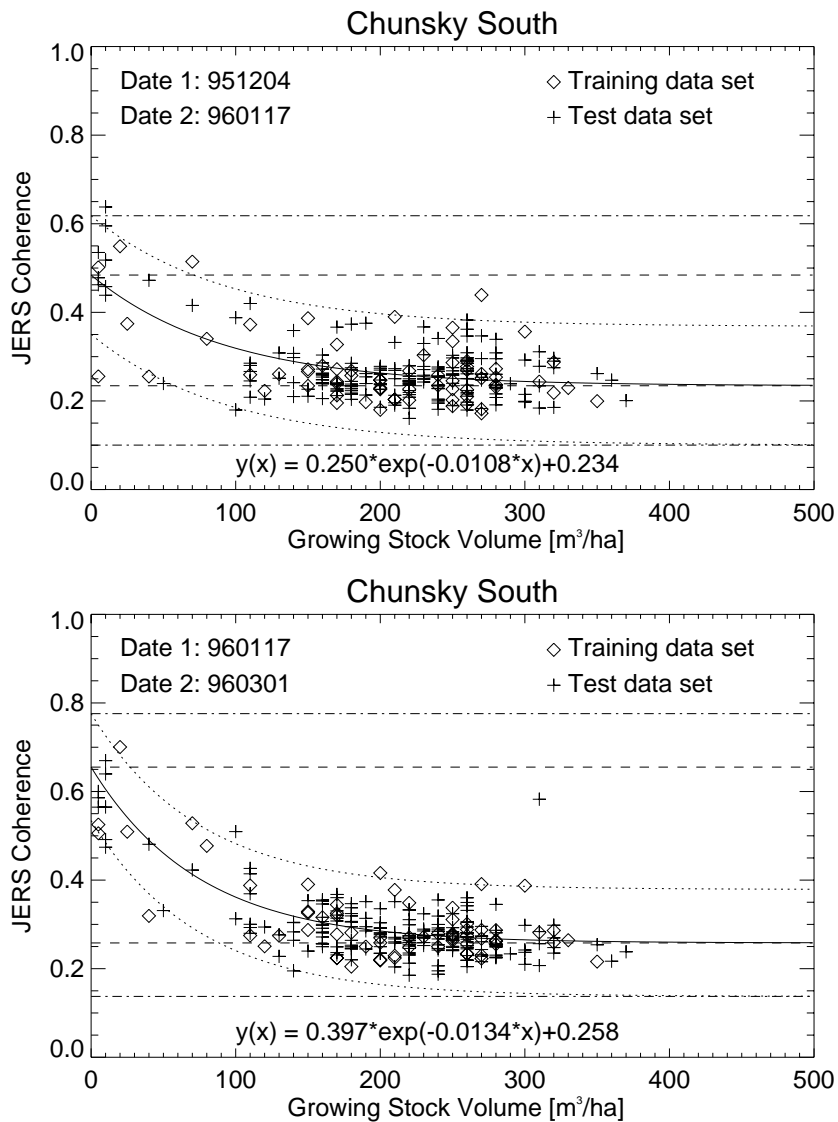


Figure B.4 Regression curves for JERS coherence of Chunsky South. The regression parameters are given in the expressions at the bottom of each plot. The dashed lines correspond to the upper and lower limits of the regression curves. The dotted lines represent the two standard deviation distances from the curve and the dashed dotted lines are the limits that were used for removal of outliers.

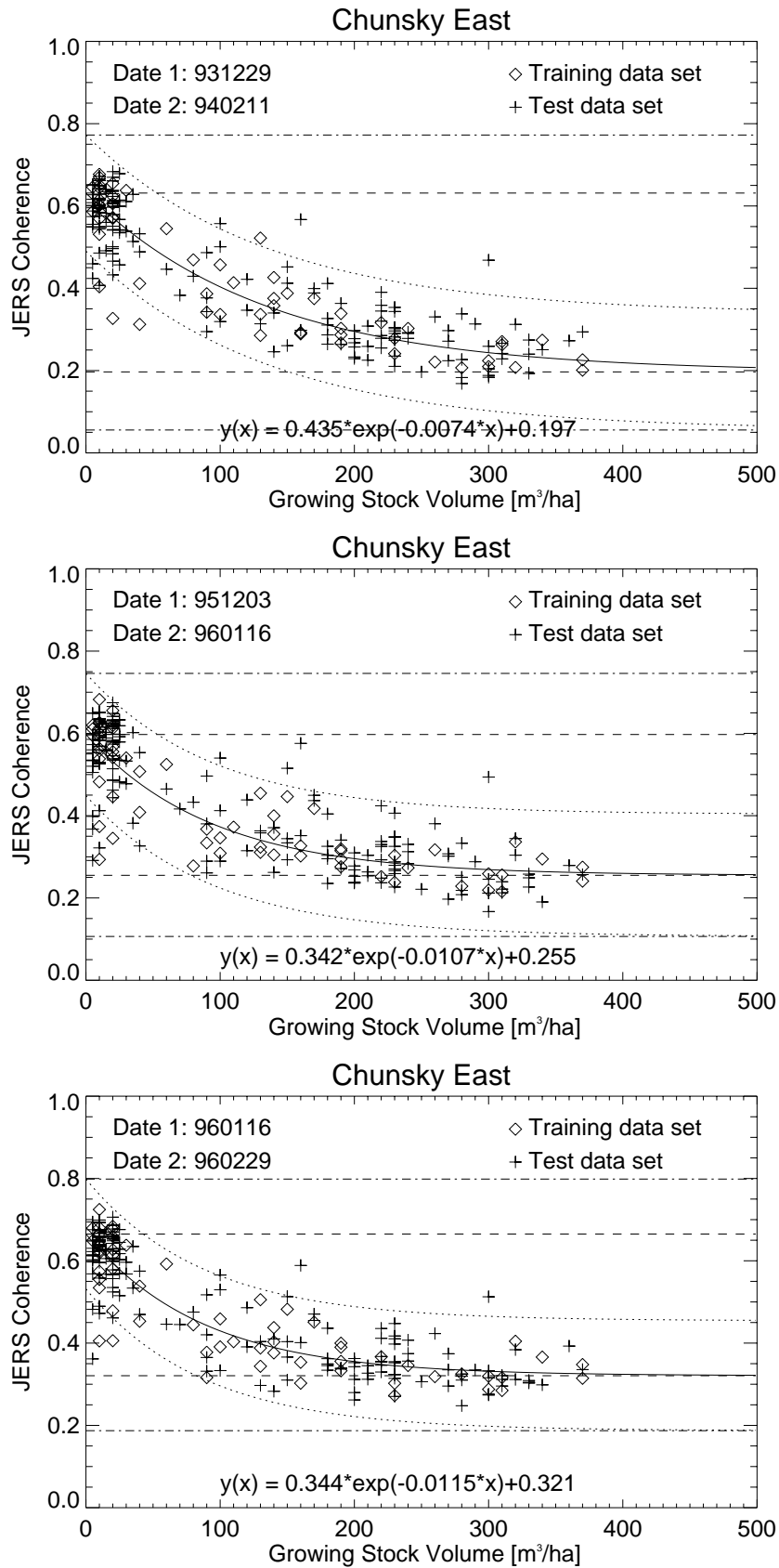


Figure B.5 Regression curves for JERS coherence of Chunsky East. The regression parameters are given in the expressions at the bottom of each plot. The dashed lines correspond to the upper and lower limits of the regression curves. The dotted lines represent the two standard deviation distances from the curve and the dashed dotted lines are the limits that were used for removal of outliers.

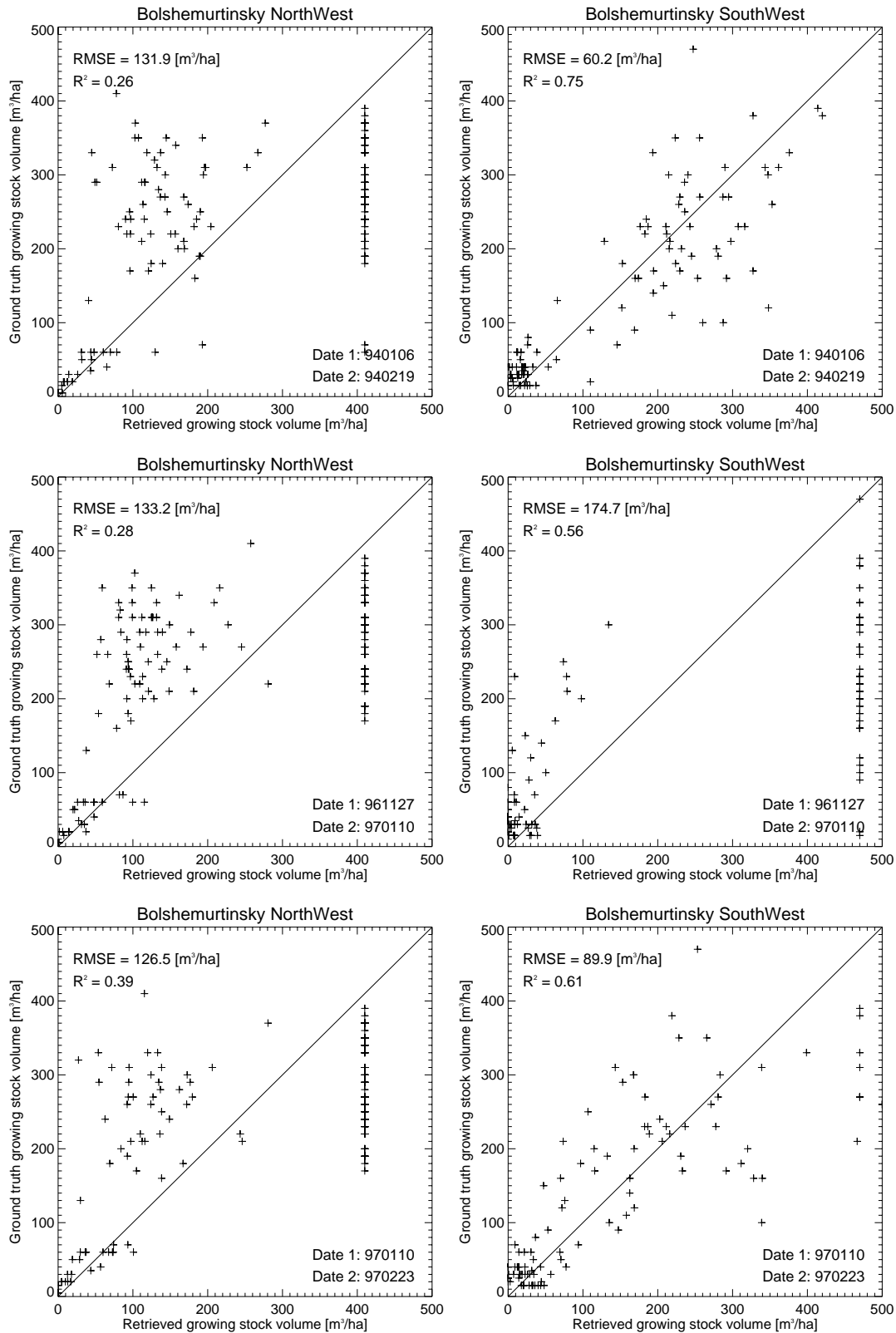


Figure B.6 Comparison between growing stock volumes retrieved from JERS coherence and growing stock volumes from the forest inventory.

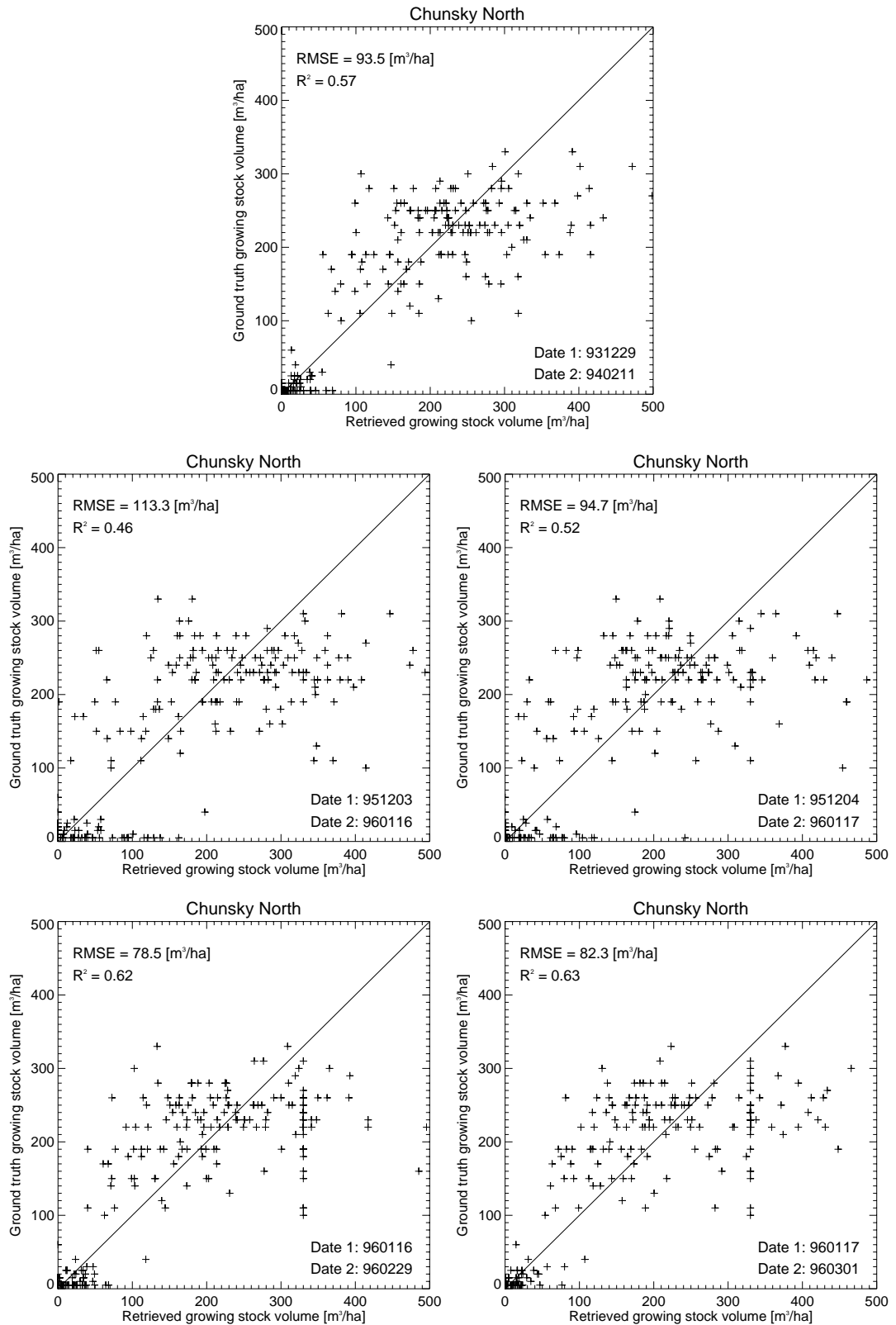


Figure B.7 Comparison between growing stock volumes retrieved from JERS coherence and growing stock volumes from the forest inventory.

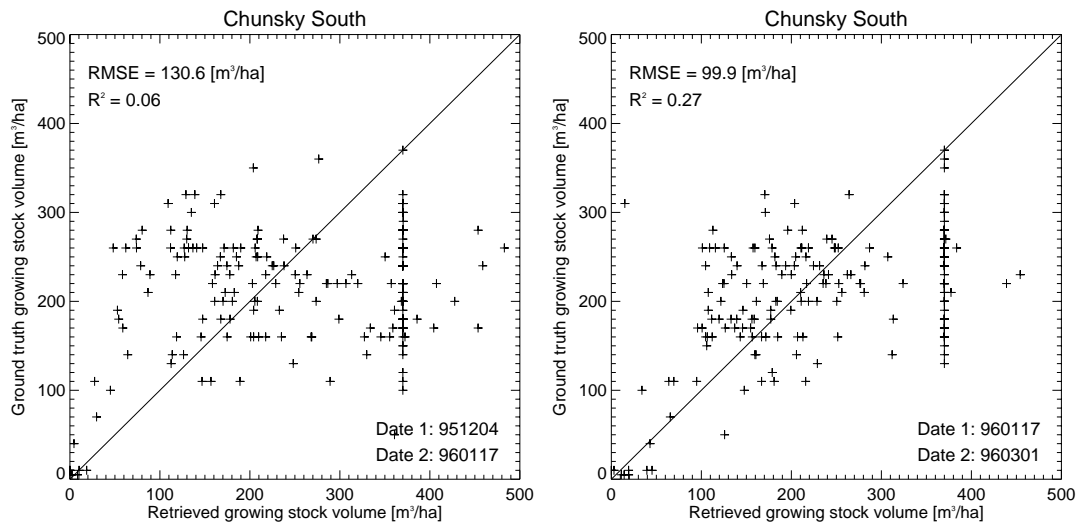


Figure B.8 Comparison between growing stock volumes retrieved from JERS coherence and growing stock volumes from the forest inventory.

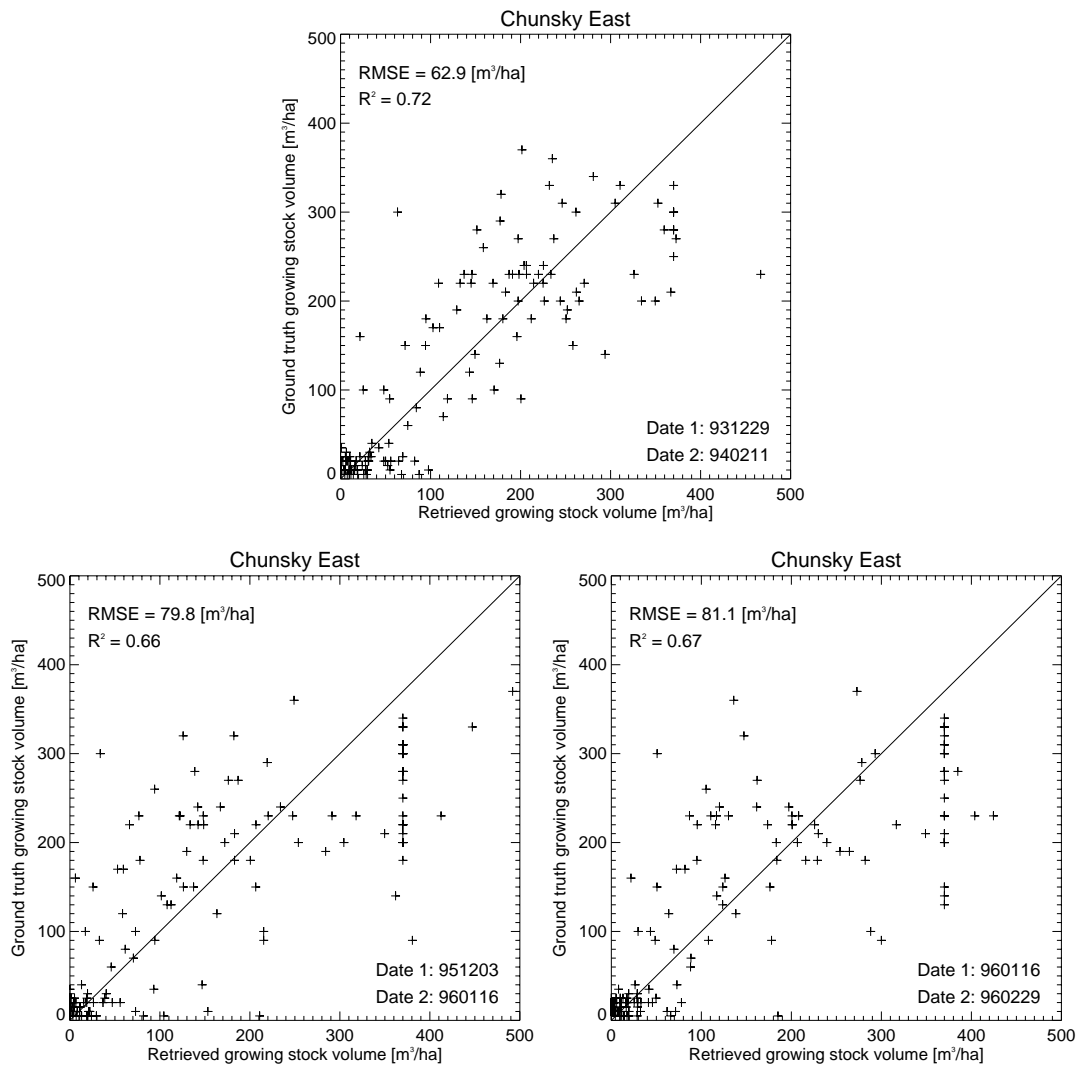


Figure B.9 Comparison between growing stock volumes retrieved from JERS coherence and growing stock volumes from the forest inventory.

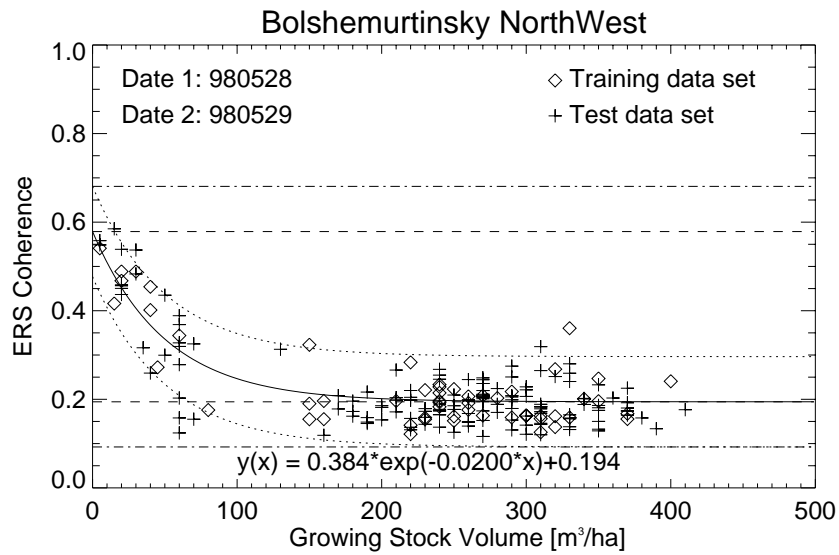
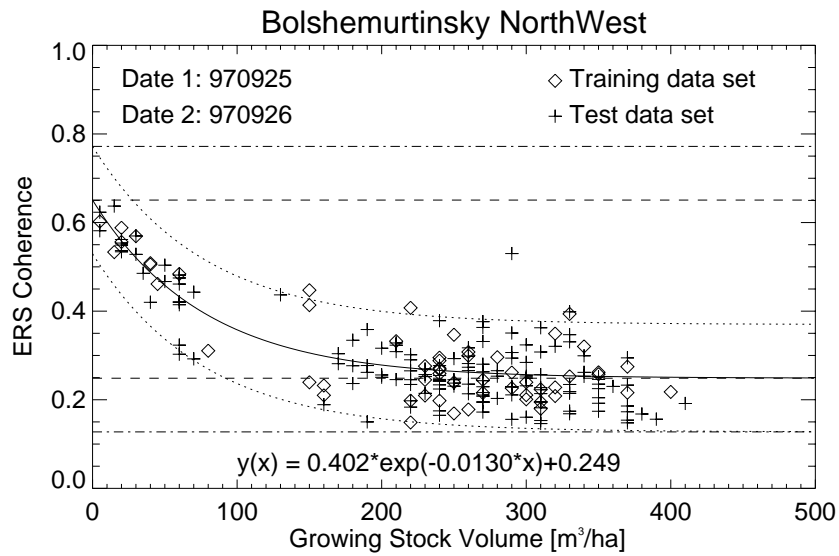


Figure B.10 Regression curves for ERS coherence of Bolshe Murtinsky Northwest. The regression parameters are given in the expressions at the bottom of each plot. The dashed lines correspond to the upper and lower limits of the regression curves. The dotted lines represent the two standard deviation distances from the curve and the dashed dotted lines are the limits that were used for removal of outliers.

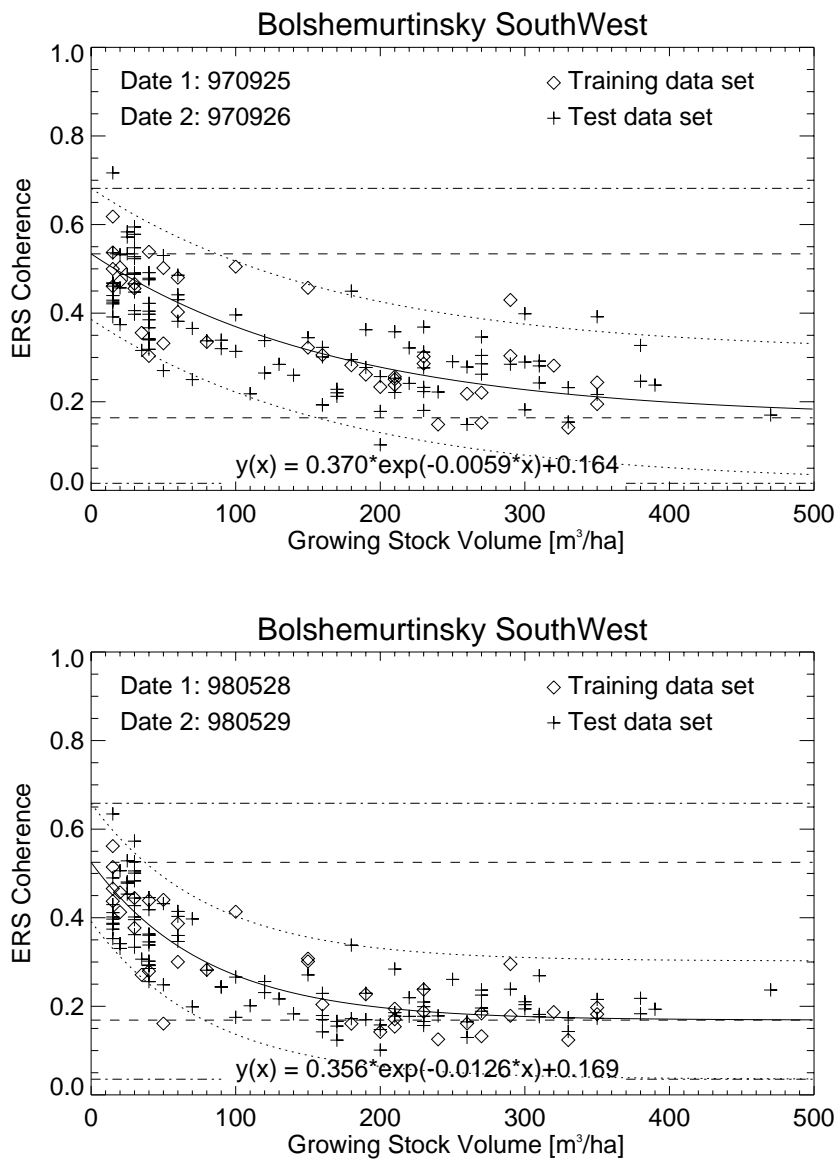


Figure B.11 Regression curves for ERS coherence of Bolshe Murtinsky Southwest. The regression parameters are given in the expressions at the bottom of each plot. The dashed lines correspond to the upper and lower limits of the regression curves. The dotted lines represent the two standard deviation distances from the curve and the dashed dotted lines are the limits that were used for removal of outliers.

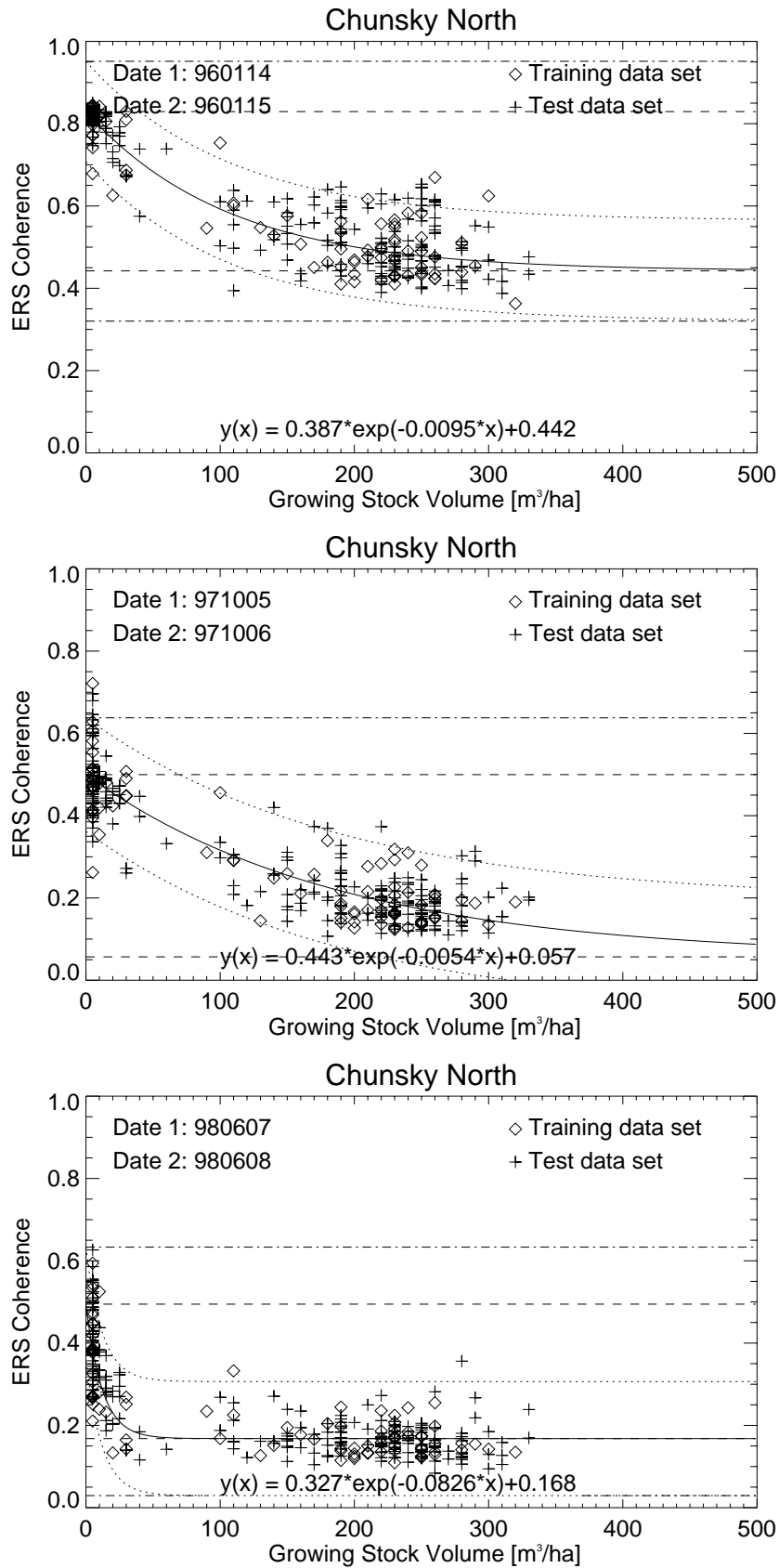


Figure B.12 Regression curves for ERS coherence of Chunsky North. The regression parameters are given in the expressions at the bottom of each plot. The dashed lines correspond to the upper and lower limits of the regression curves. The dotted lines represent the two standard deviation distances from the curve and the dashed dotted lines are the limits that were used for removal of outliers.

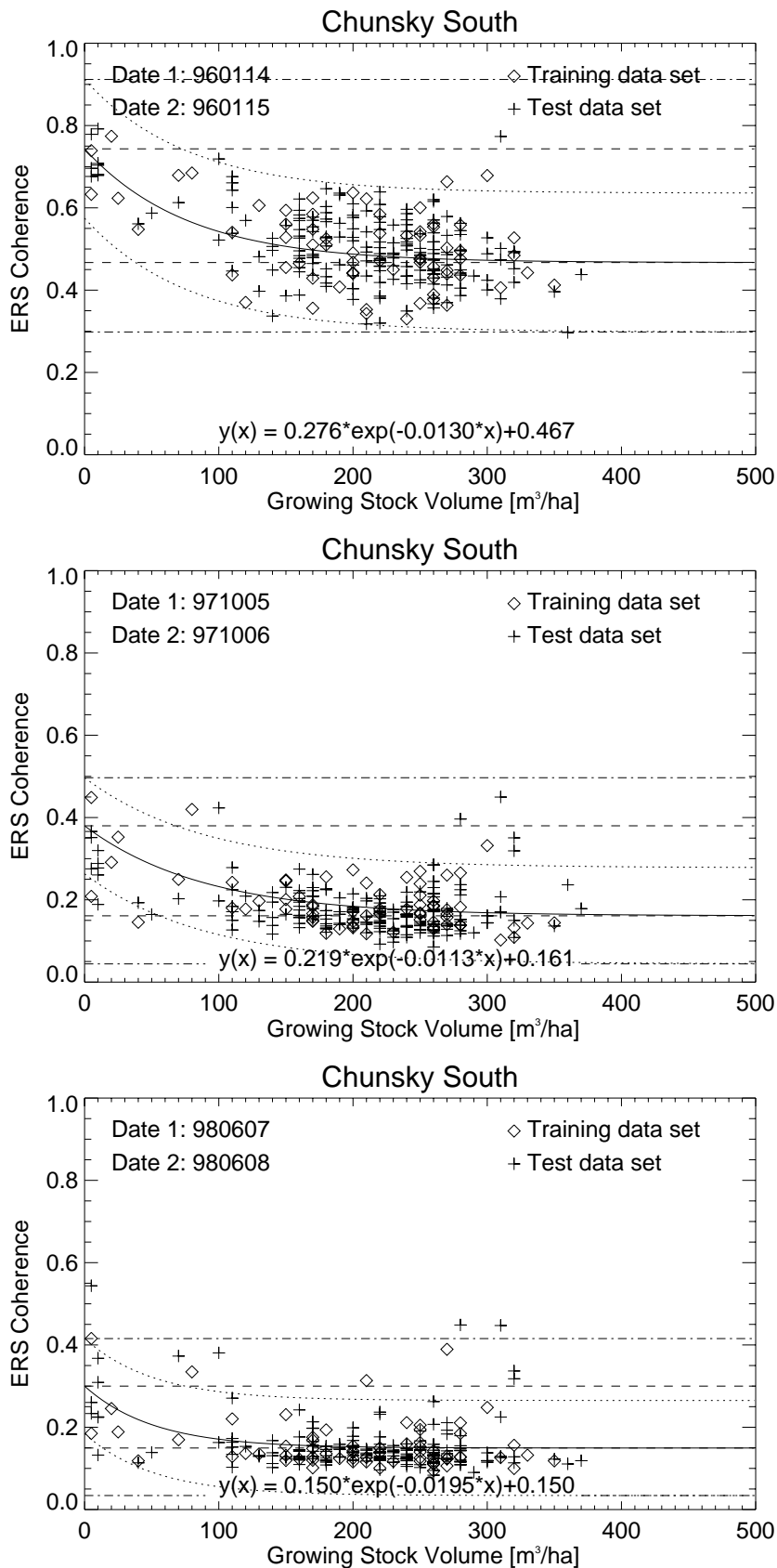


Figure B.13 Regression curves for ERS coherence of Chunsky South. The regression parameters are given in the expressions at the bottom of each plot. The dashed lines correspond to the upper and lower limits of the regression curves. The dotted lines represent the two standard deviation distances from the curve and the dashed dotted lines are the limits that were used for removal of outliers.

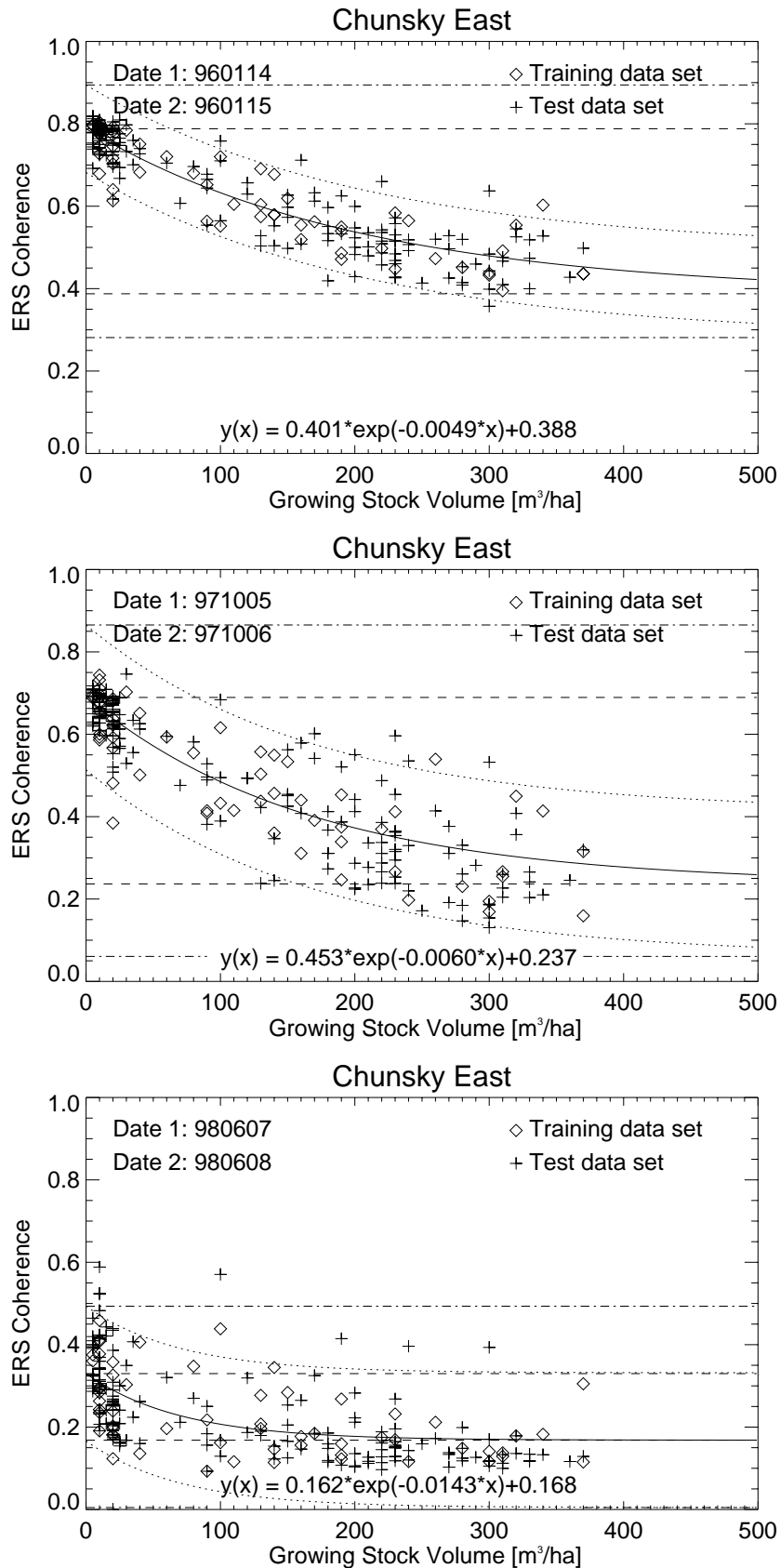


Figure B.14 Regression curves for ERS coherence of Chunsky East. The regression parameters are given in the expressions at the bottom of each plot. The dashed lines correspond to the upper and lower limits of the regression curves. The dotted lines represent the two standard deviation distances from the curve and the dashed dotted lines are the limits that were used for removal of outliers.

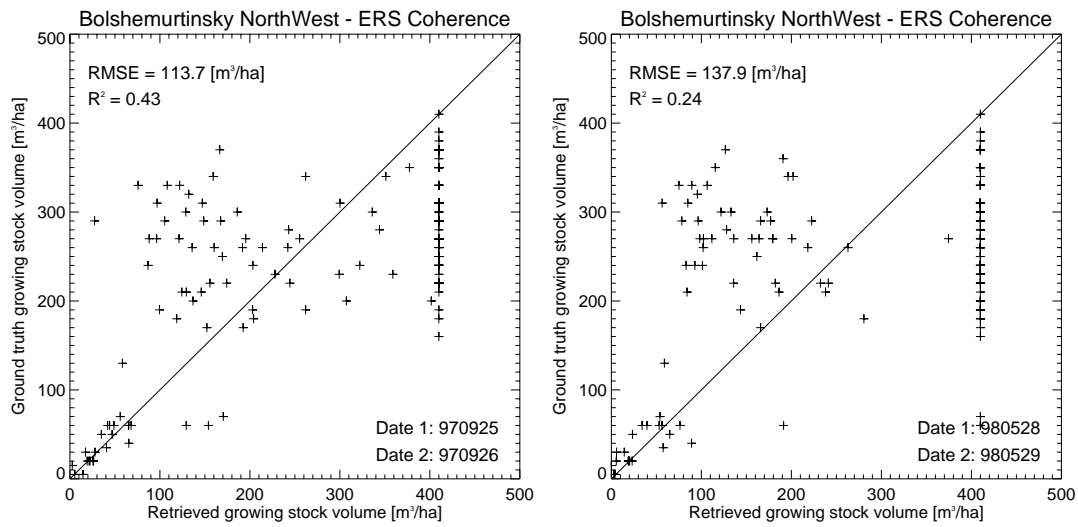


Figure B.15 Comparison between growing stock volumes retrieved from ERS coherence and growing stock volumes from the forest inventory.

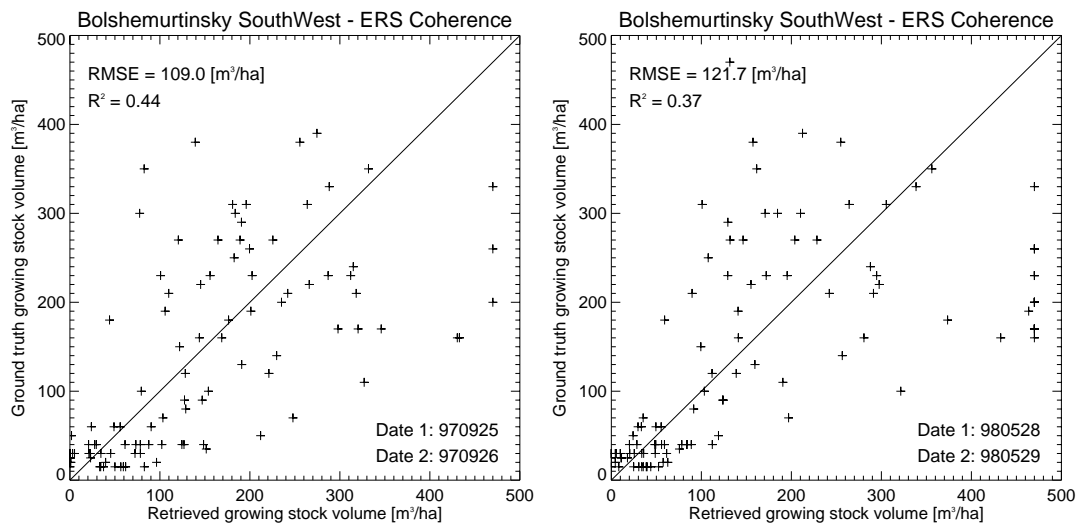


Figure B.16 Comparison between growing stock volumes retrieved from ERS coherence and growing stock volumes from the forest inventory.

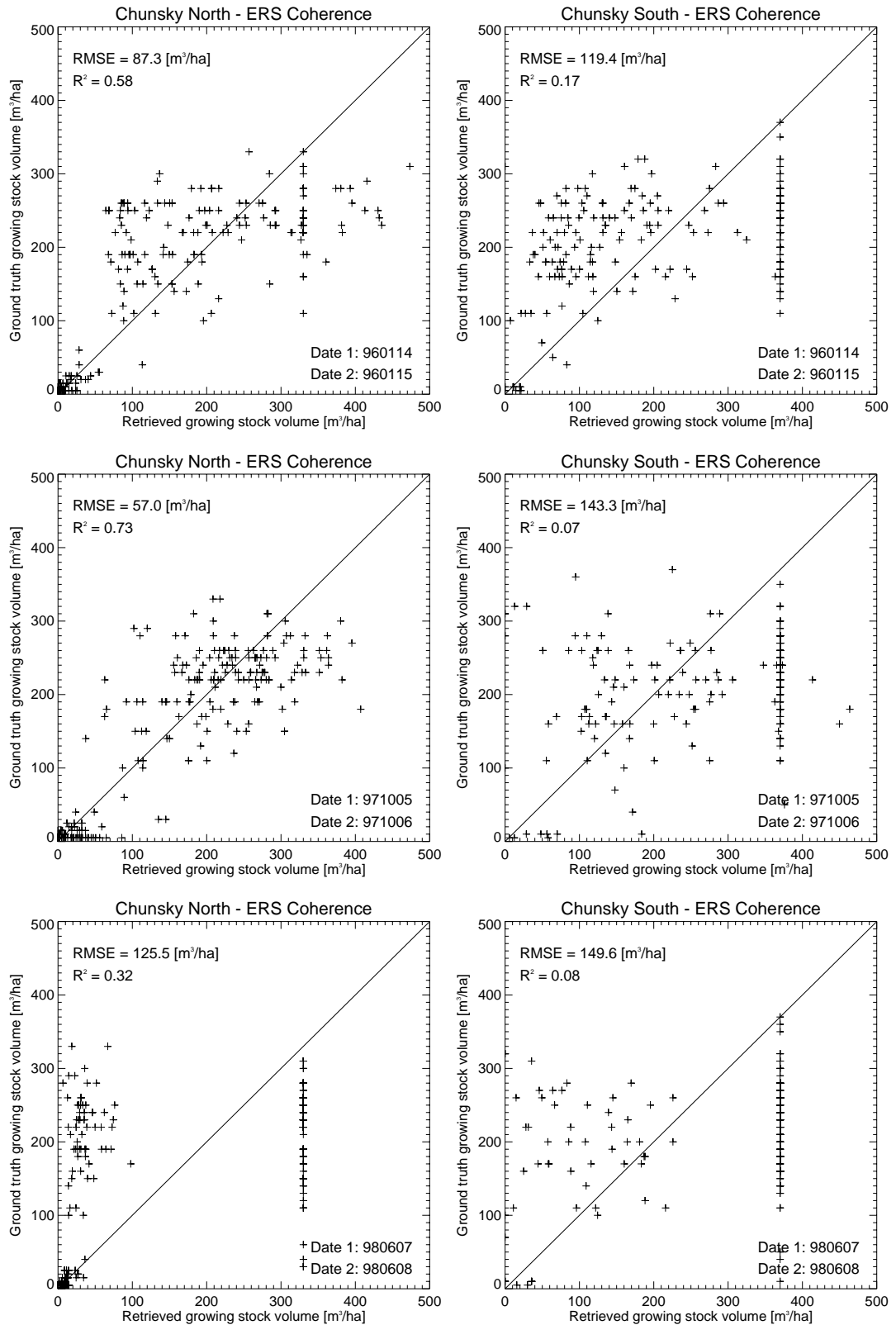


Figure B.17 Comparison between growing stock volumes retrieved from ERS coherence and growing stock volumes from the forest inventory.

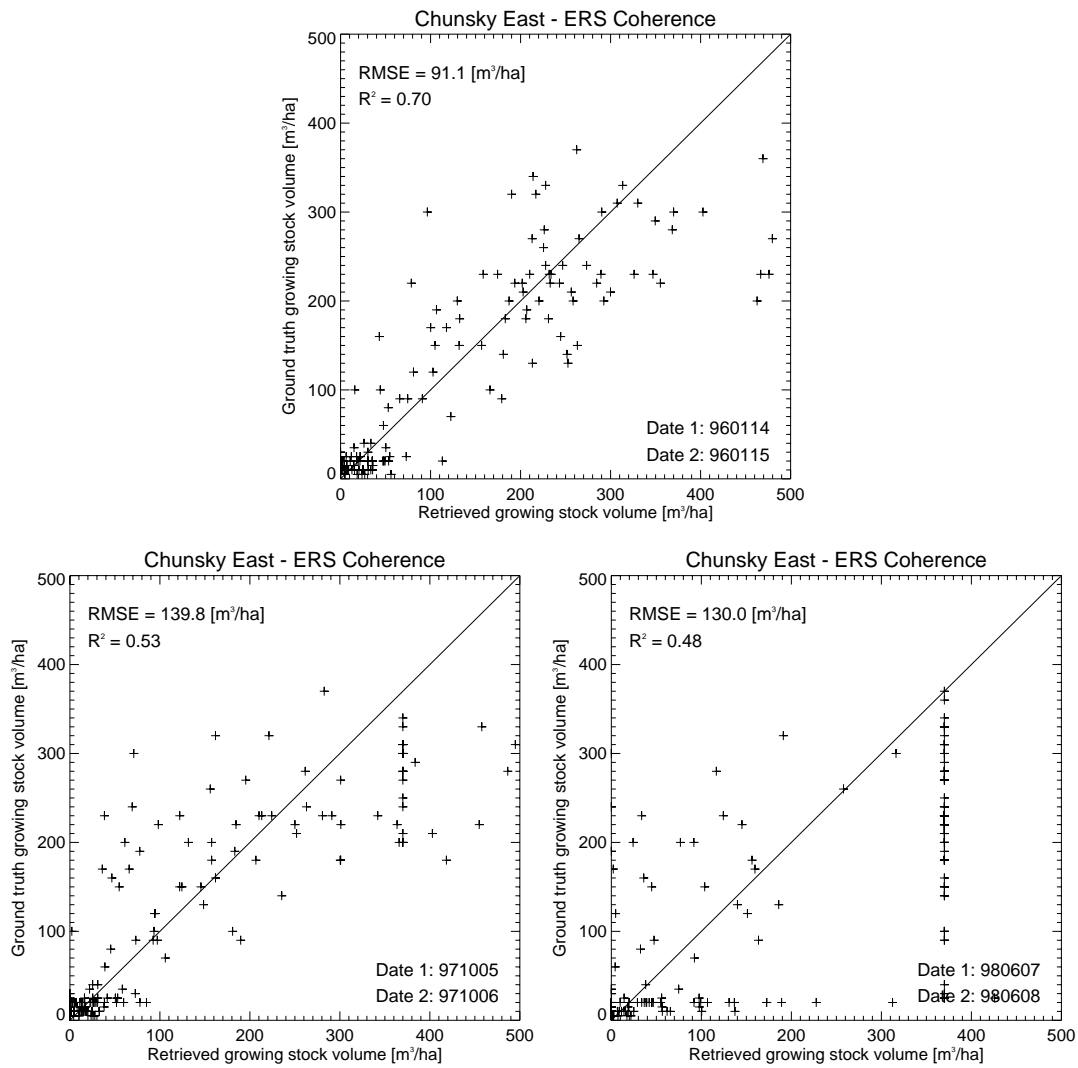


Figure B.18 Comparison between growing stock volumes retrieved from ERS coherence and growing stock volumes from the forest inventory.

SHORT FORM CURRICULUM VITAE

May 2004

Name	Leif Erik Bertil Eriksson
Date of birth	11 June 1970
Place of birth	Bolstad, Sweden
Nationality	Swedish
Marital status	Single
Education:	
Sept. '92 - Feb. '93 & March '94 - Aug. '98	Master of Science in Electrical Engineering Chalmers Univ. of Technology, Göteborg, Sweden
Sept. '90 – June '92	University Certificate in Space Technology Umeå University, Kiruna, Sweden
Aug. '86 – June '90	High School Diploma in Electrical Engineering Nils Ericsonskolan, Trollhättan, Sweden
Relevant working experience:	
Nov. '00 – May '04	Doctoral student position Friedrich-Schiller-University Jena, Germany Institute of Geography, Department of Geoinformatics and Remote Sensing
June '00 – Oct. '00	Took part in the finalising of the SIBERIA project German Aerospace Centre (DLR-DFD-AN), Oberpfaffenhofen, Germany
May '99 – April '00	Worked with ERS & JERS SAR-Data from Siberia Joint Research Centre of the EC (JRC-SAI-GVM), Ispra, Italy
Sept. '97 – Dec. '97	Master thesis project: Analysis of SIR-C polarimetric SAR-data of sea-ice. NASA JPL, Pasadena, California, USA
June '96 – Oct. 96	Software development for visualisation of polarimetric AIRSAR-Data Vexcel Corporation, Boulder, Colorado, USA
Language skills:	
Languages	Swedish (mother tongue), English (fluent), German (good), Italian (poor)

List of publications

Peer-reviewed journal articles

ERIKSSON, L. E. B., SANTORO, M., WIESMANN, A., and SCHMULLIUS, C., "Multi-temporal JERS repeat-pass coherence for growing stock volume estimation of Siberian forest," *IEEE Transactions on Geoscience and Remote Sensing*, vol. 41, 7, pp. 1561-1570, 2003.

SANTORO, M., ERIKSSON, L. E. B., ASKNE, J., and SCHMULLIUS, C., "Assessment of stand-wise stem volume retrieval in boreal forest from JERS-1 L-band SAR backscatter," *International Journal of Remote Sensing*, Submitted, 2004.

Conference proceedings

ERIKSSON, L. E. B., LE TOAN, T., WIESMANN, A., GRIPPA, M., WEGMÜLLER, U., and SCHMULLIUS, C., "SAR repeat-pass coherence in winter for boreal forest applications. A first comparison of ASAR and JERS-1 SAR", *Proceedings of 'Fringe 03' Workshop on ERS SAR and ASAR Interferometry*, ESA-ESRIN, Frascati, 1-5 December, 2003.

ERIKSSON, L. E. B., WIESMANN, A., SCHMULLIUS, C., and SANTORO, M., "The potential of ALOS single polarization InSAR for estimation of growing stock volume in Boreal Forest", *Proceedings of IGARSS 2003*, Toulouse, 21-25 July, 3, pp. 1939-1941, 2003.

ERIKSSON, L. E. B., SANTORO, M., WIESMANN, A., and SCHMULLIUS, C., "Multi-seasonal study of the SIBERIA classification procedure", *Proceedings of ForestSAT Symposium*, Edinburgh, 5-9 August, CD-ROM, 2002.

ERIKSSON, L. E. B., WIESMANN, A., and SCHMULLIUS, C., "JERS repeat pass coherence for observation of Siberian forest", *Proceedings of 3rd International Symposium 'Retrieval of Bio- and Geophysical Parameters from SAR Data for Land Applications'*, Sheffield, UK, 11-14 September 2001, ESA SP-475, pp. 33-38, 2002.

ERIKSSON, L. E. B., WIESMANN, A., SCHMULLIUS, C., and RIEDEL, T., "Multi-temporal JERS coherence for observation of Siberian forest", *Proceedings of IGARSS 2002*, Toronto, 24-28 June, 5, pp. 2896-2898, 2002.

ERIKSSON, L. E. B., DRINKWATER, M., HOLT, B., VALJAVEK, E., and NORTIER, O., "SIR-C Polarimetric Radar Results from the Weddell Sea, Antarctica", *Proceedings of IGARSS'98*, Seattle, USA, 6-10 July 1998, 4, pp. 2222-2224, 1998.

SANTORO, M., ERIKSSON, L. E. B., SCHMULLIUS, C., and WIESMANN, A., "Seasonal and topographic effects on growing stock volume estimates from JERS-1 backscatter in Siberian forests", *Proceedings of 23rd EARSeL Annual Symposium*, Gent, 2-5 June, pp. 151-158, 2003.

SANTORO, M., ASKNE, J., ERIKSSON, L. E. B., SCHMULLIUS, C., WIESMANN, A., and FRANSSON, J. E. S., "Seasonal dynamics and stem volume retrieval in boreal forests using JERS-1 backscatter", *Proceedings of SPIE 9th International Symposium on Remote Sensing*, Agia Pelagia, Crete, 22-27 September, 4879 - Remote Sensing for Agriculture, Ecosystems, and Hydrology IV, pp. 231-242, 2002.

SANTORO, M., SCHMULLIUS, C., ERIKSSON, L. E. B., and HESE, S., "The SIBERIA and SIBERIA-II projects: an overview", *Proceedings of SPIE 9th International Symposium on Remote Sensing*, Agia Pelagia, Crete, 22-27 September, 4886, Remote Sensing for Environmental Monitoring, GIS Application, and Geology II, pp. 247-256, 2002.

Theses and reports

ERIKSSON, L. E. B., "Analysis of SIR-C Dual-frequency Polarimetric Radar Signatures of Sea Ice in the Weddell Sea", Master of Science Thesis, Department of Radio and Space Science, Chalmers University of Technology, Gothenburg, Sweden, 1998.

SCHMULLIUS, C., ED., BAKER, J., BALZTER, H., DAVIDSON, M., ERIKSSON, L. E. B., GAVEAU, D., GLUCK, M., HOLZ, A., LETOAN, T., LUCKMAN, A., MARSCHALK, U., MC CALLUM, I., NILSSON, S., ORRMALM, S., QUEGAN, S., RAUSTE, Y., ROTH, A., ROZHKOVA, V., SOKOLOV, V., SHVIDENKO, A., SIRRO, L., SKUDING, V., STROZZI, T., TANSEY, K., UTSI, R., VIETMEIER, J., VOLOSHUK, L., WAGNER, W., WEGMÜLLER, U., WESTIN, T., WIESMANN, A., and YU, J. J., "SIBERIA - SAR Imaging for Boreal Ecology and Radar Interferometry Applications", Final Report, EU Contract ENV4-CT97-0743-SIBERIA, Friedrich-Schiller-University, Jena, Germany, 2001.

ZIMMERMANN, R., ED., SCHMULLIUS, C., ETZRODT, N., and ERIKSSON, L. E. B., "SIBERIA - SAR Imaging for Boreal Ecology and Radar Interferometry Applications", Final Report, BMBF Contract FKZ 50 EE 9725 SIBERIA, pp. 172, Max-Planck Institute für Biogeochemie, Jena, Germany, 2003.